UC Davis
UC Davis Electronic Theses and Dissertations

Title

High-Throughput Phenotyping Methods in Processing Solanaceae

Permalink

https://escholarship.org/uc/item/4dn88512

Author

Vuong, Vivian

Publication Date

2024

Peer reviewed|Thesis/dissertation

eScholarship.org Powered by the California Digital Library
University of California

High-Throughput Phenotyping Methods in Processing Solanaceae

By

VIVIAN VUONG

DISSTERTATION

Submitted in partial satisfaction of the requirements for the degree of

DOCTOR OF PHILOSOPHY

in

Biological Systems Engineering

in the

OFFICE OF GRADUATE STUDIES

of the

UNIVERSITY OF CALIFORNIA

DAVIS

Approved:

_____

David Slaughter, Chair

_____

Mason Earles

_____

Stavros Vougioukas

Committee in Charge
2024

=

Acknowledgements

First, I would like to thank my Dissertation Committee, Dr. David Slaughter, Dr. Stavros Vougioukas, and Dr. Mason Earles, for helping guide me through this process and for reading this dissertation. I want to extend a thank you to Dr. David Slaughter, for believing in me as an undergraduate student in 2015 and allowing me to join the BAESIL Lab. Throughout my time at UC Davis he has continued to support me and given me so many opportunities that have made me a better engineer. I will never forget that current is the killer.

Next, I want to thank my former lab-mates Dr. Thuy Nguyen, Leland Neilson, and Burt Vannucci for helping me complete this project from start to finish. I also want to think my wonderful undergrad students Earl Ranario, Simon Coelho, Jennifer Medina, Janaye Porter, Ken Zen Ooi, and Kylee Schneeberger for helping me process mountains of data. I also want to thank Dr. Dina St. Clair, Bryce Kubond, and the rest of the St. Clair lab for conducting the breeding trial that made this project possible. I would also like to thank Dr. Paul Bosland for providing us with pepper samples Thank you to Tom Bell and Jed Roach for helping design and build the entire HTPP system. I also want to thank everybody in the Department of Biological and Agricultural Engineering. I want to thank all the students I had the honor of teaching and mentoring at UC Davis. Thank you to the USDA-NIFA for funding this project. I also want to thank PEGS21 and TOPS fellowships at UC Davis for giving me the opportunity to grow as a graduate student and funding my first year as a PhD student.

Thank you to my former lab-mate and one of my closest friends Clarice Roo for suffering in the field and in the computer lab alongside me. Big thanks to the coffee crew, Peter Russell and Lucy Knowles, for always being ready to get another cup of coffee with me.

I want to thank my partner Dr. Alexander Olenskyj; without you, I would have never been able to finish in one piece. I also want to thank my parents Kathie Hong Hoa Lee and Brian Vi Vuong; your sacrifices have allowed me to pursue my dream. Thank you to my sister Dr. Caresse Vuong for always listening to me, even though you don't know what I do. I would also like to thank my cat Mr. Milo for just being there. Finally, I want to acknowledge myself. We did it.

Abstract

Agricultural food crop production must increase 100-110% by 2050 in order to meet the predicted global population and production demands. In order to meet the increasing food demands from the growing population, as a society we are looking for ways to increase food yield without needing to further exploit land and water resources. Plant breeders look to solve this problem by breeding novel high-yielding crop varieties that can produce quality fruit in extreme weather and limited water conditions. This includes crossbreeding commercially available cultivars with wild types shown to react favorably in times of drought and heat stress in nature. The two key components in breeding commercial crop cultivars are quantifying genotypic and phenotypic data.

Prior to second generation sequencing, the bottleneck in producing commercial crop varieties was the inability to accurately and efficiently sequence a crop genome. The second generation of sequencing has simplified the process of genome mapping and allows for the identification of candidate genetic markers to utilize marker assisted selection (MAS). With these developments, the current bottleneck in producing new crop varieties is now phenotyping plant traits in in-field breeding trials. There is an increased need for higher throughput in relating genetic material to phenotypes.

Current in-field phenotyping methods rely on humans to go into the breeding fields to detect these phenotypes. These current methods are time consuming, labor intensive, and subjective. These phenotyping trials rely on repetition of genetic material in a study to maximize time and space and reduce the amount of human labor is needed. In order to meet current and future food demands, we need to look at new methods of high-throughput phenotyping to help plant breeders create new crops more efficiently.

In this study we look at three aspects of high-throughput phenotyping: developing and deploying a multi-camera and multi-sensor in-field phenotyping system for Solanaceae crops, developing algorithms to use with the phenotyping system to detect phenotypes in tomatoes, and exploring new sensor technology to develop low-cost methods of detecting green fruit.

A high-throughput phenotyping (HTTP) system was developed to be a high clearance tractor fitted with 9 color DSLR cameras, 9 pseudo-NDVI cameras, 2 Time of Flight cameras, 2 temperature sensors, 8 custom LED modules, with infrared and broad-spectrum white LEDs, 1 RTK-GPS, 1 National Instruments High Speed Controller, 1 Dell desktop computer, and 1 National Instruments USB controller. The system was used in 2018 and 2019 to collect multi-sensor data in a processing pepper and tomato breeding trial in Davis, CA.

Images from a single camera from the HTPP system was used to develop algorithms for object detection in tomatoes throughout the growing season. The algorithm utilized Mask R-CNN for object detection of flowers, green fruit, ripe fruit, and sunburnt fruit with an average mAP of 21.1% on a validation set. The number of ripe fruit and green fruit on the last date were used to predict the weight of ripe fruit and green fruit from manual phenotyping at harvest, the R values were 0.407 and 0.201 in 2018 and 0.202, and 0.142 in 2019 respectively.

A pseudo-NDVI camera was used to test if adding non-visible wavelengths to imaging would impact the detection of green fruit. DSLR cameras were modified to allow infrared and near-infrared wavelengths to be imaged, in hopes that this would be a low-cost method for incorporating multi-spectral imaging in the HTPP system. An infrared camera and color camera were compared for green fruit detection in 2019. 85% of the plant-plots imaged had more green fruit detected in the color images than the infrared camera, which could imply double counting in

the color images. More testing and ground truth data needs to be done to get conclusive answers about the green fruit detection in infrared.

In conclusion, this dissertation focuses on developing high-throughput phenotyping methods that rely on 2D imaging of in-field plants. The ability to quickly process quantitative phenotypic data is important for the development of new crops as the current bottleneck in plant breeding is phenotyping. This dissertation shows that there are new and old technologies and techniques that can be applied to high-throughput phenotyping for in-field phenotyping.

Table of Contents

1. Introduction 1
2. Literature Review 4
2.1. Food Insecurity 4
2.2. Population Growth 4
2.3. Climate Change and Crop Yield 5
2.4. Importance of Solanaceae Crops 6
2.5. Traditional Plant Breeding Methods 7
2.6. Traditional Plant Phenotyping Methods 8
2.7. High-Throughput Phenotyping Methods 9
2.7.1. Remote Sensing 10
2.7.2. Proximal Sensing 10
2.8. Phenotyping using Image Analysis 11
3. Objectives 12
3.1. General Objective 12
3.1.1. Objective 1 12
3.1.2. Objective 2 13
3.1.3. Objective 3 13
4. Chapter 1: High Throughput Phenotyping Platform Development 15
4.1. Introduction 15
4.2. Literature review 16
4.2.2. Population Growth 16
4.2.3. Climate Change and Crop Yield 17
4.2.4. Traditional Plant Breeding Methods 18
4.2.5. Traditional Plant Phenotyping Methods 19
4.2.6. High-Throughput Phenotyping Methods 19
4.2.6.1. Remote Sensing 20
4.2.6.2. Proximal Sensing 21
4.3. Background 21
4.4. Materials and Methods 24

4.4.1. Multi-Camera System 24
4.4.2. Multi-Sensor System 31
4.4.2.2.1. Height Width 33
4.4.2.2.2. Temperature 34
4.4.3. Geo-Referencing Hardware 36
4.4.5. Camera Wiring 39
4.4.6. Data Control Acquisition Software 41
4.4.7. Lighting Design 43
4.4.8. Solanaceae Crop Selection 44
4.4.9. UC Davis Research Field Implementation 45
4.5. Results 47
4.6. Experimental Field Design 52
4.6.1. Pepper 53
4.6.2. Tomato 54
4.7. Irrigation 56
4.8. Field Performance 57
4.9. Data Collection 58
4.10. Final Design 58
5. Chapter 2: Machine learning for plant component detection in high-throughput phenotyping of tomato. 60
5.1. Introduction 60
5.2. Literature Review 60
5.2.1. Traditional Plant Breeding Methods 60
5.2.2. Traditional Plant Phenotyping Methods 61
5.2.3. Importance of Solanaceae Crops 62
5.2.4. High-Throughput Phenotyping Methods 63
5.2.5. Phenotyping using Image Analysis 64
5.3. Materials and Methods 64
5.3.1. Experimental Design 64
5.3.2. Data Collection 65

5.3.3. Data Transfer 65
5.3.4. Data Processing 66
5.3.5. Object Detection 68
5.3.6. Data Labeling 69
5.3.7. Model Training 71
5.3.8. Model Performance 72
5.3.9. Manual Phenotyping 74
5.4. Results 76
5.4.1. Model Evaluation 76
5.4.1.1. 2018 Training, Testing, Validation Dataset 78
5.4.1.2. 2019 Season Dataset 81
5.4.2. Automated Time Series Data 90
5.4.3. Manual Phenotyping 92
5.4.4. Manual Phenotyping vs High Throughput Phenotyping 98
5.5. Discussion 102
5.5.1. Model Performance 102
5.5.2. 2018-2019 Data Collection 104
5.5.3. Automated Time Series Data 106
5.5.4. Manual Phenotyping vs High-Throughput Phenotyping 107
5.5.5. Manual Phenotyping 108
5.6. Conclusion 110
6. Chapter 3: Green Fruit Detection for High-Throughput Phenotyping 111
6.1. Introduction 111
6.2. Literature Review 111
6.2.1. Traditional Plant Phenotyping Methods 111
6.2.2. High-Throughput Phenotyping Methods 112
6.2.2.1. Remote Sensing 112
6.2.2.2. Proximal Sensing 113
6.2.3. Green Fruit Detection in Agriculture 113
6.2.4. Multispectral Data in Agriculture 114

6.2.5. Solanaceae in California 114
6.3. Materials and Methods 116
6.3.1. Experimental Design 116
6.3.2. Tomato 116
6.3.3. Pepper 119
6.3.4. Analysis Method 121
6.3.5. Sensor Testing 122
6.3.6. In-Field Testing 122
6.4. Results 123
6.4.1. Tomato Lab Testing 123
6.4.2. Camera Selection Test 129
6.4.3. In-Field Tomato Testing 130
6.4.4. Pepper 137
6.4.4.1. Pepper Lab Testing 137
6.4.5. In-Field Tomato Testing 145
6.5. Discussion 148
6.5.1. Tomato 149
6.5.2. Pepper 150
6.5.3. Sensor Selection 151
6.5.4. Pixel Segmentation 151
6.5.5. Neural Network Performance 152
6.6. Conclusion 152
7. Conclusions and Future Work 154

1. Introduction

Agricultural food production must increase by two-fold by the year 2050 in order to meet the predicted global population and production demands [1]. To meet the increasing food demand, researchers are looking for ways to increase food yield without needing to further exploit land and water resources. Plant breeders are looking to help solve this problem by breeding new crop cultivars that can produce high quality and high yielding food crops in the climate of the future and limited water conditions. In arid climates, such as the Western United States, the climate of the future is predicted to have increased periods of drought and higher incident of extreme weather events such as hail. Modern breeding methods includes expanding the gene pool by crossbreeding commercially available cultivars with wild types that naturally react favorably to changing climate conditions. The two major components in successful breeding of new commercial crop cultivars are quantifying genotypic and phenotypic data during the breeding process.

Prior to second generation sequencing, the bottleneck in producing new crop cultivars was the inability to sequence the crop genome accurately and efficiently. The second generation of sequencing has simplified the process of genome mapping and allows for identification of candidate genetic markers to utilize marker assisted selection (MAS) [2]. With these developments, the current bottleneck in producing new commercially viable crop cultivars is now quantifying the phenotypic data of the new plant breeds in in-field breeding trials [3]. With more efficient methods and decreased costs for genotyping, Genome-Wide Association Studies (GWAS) and genomic selection can be used to further understand crop genetics and accelerate the breeding process. GWAS is an approach used in genetics research to find new specific genetic variations that are associated with specific phenotypes. In agriculture, GWAS can look at

the DNA of different varieties and wild plants and compare phenotypes such as yield, acclimation to heat stress, and disease resistance [4], [5]. There is an increased need for higher throughput in relating genetic material to phenotypes.

In-field breeding trials are necessary for producing new crop cultivars that are commercially viable under varying growing locations and climates. In-field breeding trials allow researchers to observe how plants behave in a wide range of growing conditions. Current methods for in-field phenotyping depend upon human labor for subjective observation, ranking and manual measurements. Due to the cost and time associated with using a human to hand-phenotype a field trial, it is common to use a sampling approach to reduce the labor required for phenotyping. This means humans only look at a subsection of the plants in the entire breeding trial, possibly looking at only one plant per genotype even though there are multiple replicates of that genotype available in the trial to save labor and reduce costs. These human-based methods can also be subjective using indexes such as ranking a plant's height based on a 1-5 scale rather than measuring the actual height. High-throughput phenotyping technology is needed to create objective metrics and to expedite the development of new crop cultivars. Technology has evolved to develop high resolution and low cost 2D cameras, sensors capable of capturing high resolution 3D data, fast computers capable of parallel processing, robust controllers, and global position systems (GPS) with centimeter accuracy. This technological advancement creates the ability to take advantage of Big Data and machine learning to make in-field high-throughput phenotyping a reality. This also makes it possible to automate the collection of objective phenotypic data about plants such as: plant height, crop yield, etc. In addition to objectively detecting existing plant traits, this new age of big data, machine learning, and artificial

intelligence (AI) make it possible to create new phenotypes. These phenotypes would not be easy or possible for a human to identify but would be possible for a computer.

This dissertation explores the use of high-throughput phenotyping in horticulturally important food crops, specifically tomatoes and peppers. These plants growth habits often result in highly occluded fruit that grow under and within the plant canopy, making it a difficult crop to develop non-contact phenotyping methods. This study looks at using a multi-view and multi-sensor approach to maximize the likelihood of seeing a wide variety of phenotypes throughout the growing season. Additionally, this dissertation looks at exploring the use of novel sensors that image both visible and non-visible wavelengths to enhance the detection of green fruit in difficult in-field conditions. This dissertation explores various aspects of high-throughput phenotyping of in-field horticultural crops that have complex geometry and various physical factors that make them difficult to phenotype.

2. Literature Review

2.1. Food Insecurity

Food security is defined as “when all people, at all times, have physical, social and economic access to sufficient, safe and nutritious food that meets their dietary needs and food preferences for an active and healthy life” [6]. A combination of lack of access to nutritious food and increasing human population makes food insecurity a growing threat to the human population. It’s estimated that almost 2 billion people worldwide do not have regular access to nutritious and sufficient food supply [7]. It’s been identified that in 2023 there were 59 food-crisis countries/territories, where urgent action is required to protect and save lives at the local and national level [8]. In the 59 identified countries, 21.5% of the total population faces high levels of food insecurity [8]. This number increases in already vulnerable countries that experience sudden events such as political conflict and extreme weather occurrences [8]. Food insecurity is not about lack of food and calories, but also lack of nutritious food readily available to sustain human health and development [9].

2.2. Population Growth

The current world population is approximately 8.0 billion people. By the year 2050 the United Nations predicts the population will increase to approximately 9.7 billion [10]. This increasing population growth is attributed to increased wealth and higher purchasing power per capita, leading to an increase in demand for food, including fresh produce, processed food, meat, dairy and fish [1]. Currently, 1 in 7 people worldwide have an insufficient diet, lacking in protein and energy or having some form of micronutrient malnourishment [11]. Food insecurity is a complex subject with many socioeconomic factors including poverty, resource inequality, and a lack of

infrastructure for both on-farm and postharvest food production needs. Agriculture cannot solve all of these issues but can help in the solution and has a role to play in providing food security for all by ensuring that the food supply is adequate. Maize, rice, wheat, and soybean, which account for 2/3 of the global agricultural calories, needs to increase production by at least 2.4% to meet population predictions. However, these crops have only been increasing at 1.6%, 1.9%, 0.6%, and 1.3% annually, respectively [11]. Recent trends in agriculture show richer countries relying on intensive farming techniques, increasing capital and labor (e.g. fertilizers, pesticides, machinery) in relation to land. Meanwhile, poorer countries continue to exhibit extensive farming techniques, decreasing capital and labor with respect to land size [12]. If this agricultural trend continues, environmental repercussions including increased land clearing, CO_2 emissions, and nitrogen emissions will be inevitable.

2.3. Climate Change and Crop Yield

Adhering to sustainable agricultural practices is not the only concern in increasing agricultural production. Climate change is predicted to reduce crop yields and increase the frequency and severity of extreme weather events in food producing areas. In the United States cereal production during drought conditions has been reduced by 10%, and years with extreme heat led to a 9.1% production deficit [13]. For every 1℃ increase in seasonal temperature, major grains lose 2.5-16% of yield [14]. Our food production systems must overcome the effect of climate change on crop yield while sustainably increasing food production in order to meet the food security needs of the worlds' growing population.

2.4.Importance of Solanaceae Crops

Vegetable production in the US is a $13 billion industry, with California making up $7.3 of the industry in both fresh market and processed produce. California continues to be the leading state in vegetable crop land area harvested, utilized production, and value of production, with 39.1%, 57.3%, and 56.7%, of the total in the US respectively. The largest vegetable crops by acreage are potato, lettuce, sweet corn, and tomato. Major vegetable crops in the Solanaceae family include pepper, tomato, and potato. This family is the third most economically important food crop plant taxon, after Brassicaceae and Poaceae.

In the United States, approximately 90% of processing tomatoes are grown in California [15]. In California the most common practice for growing tomatoes is on raised beds (60 or 66 inches wide), which facilitates cultivation and drainage of the tomato. Almost all processing tomatoes are transplanted; tomatoes are commonly grown in single rows allowing easier cultivation and reducing weeding costs. Drip irrigation is the most commonly used irrigation method in California which allows for better drainage and reduces disease and weed emergence. Tomatoes require approximately 125-250 pounds of nitrogen, 40-120 pounds of phosphorus, and 0-200 pounds of potassium per acre in order to produce fruit [16]. All processing tomatoes in California are mechanically harvested. The destructive harvest occurs when at least 90% of fruit in a field is ripe.

In the United States, approximately 39% of chili peppers are grown in California and 54% are grown in New Mexico [17]. Chili peppers are direct seeded or transplanted into raised beds throughout California. Raised beds are commonly used for growing chili peppers with bed widths vary by location; the Central Valley grows peppers on 60-72 inch raised beds while Fresno County grows peppers on 36-40 inch raised beds [18]. Furrow and drip are the most

common method of irrigation; with more than 80% drip irrigation. Peppers are sprinkler irrigated after transplant or direct seeding to help establish roots or seedlings. Peppers require moderate to high rates of fertilizer, requiring 80-200 pounds of preplant phosphorus, 50-150 pounds of potassium, and 250+ pounds of nitrogen per acre. Chili peppers are usually harvested green before the development of the mature color; most harvested chili peppers in California are used for processing into salsa or are canned whole. All chili peppers in California are hand-harvested two to four times in 10- to 15-day intervals.

2.5.Traditional Plant Breeding Methods

Over the past century, several methodologies and technologies have been developed and adapted by plant breeders to expedite crop cultivar development. As methodologies, techniques, and technologies improve for cultivar development, the overall goal of sustaining a growing global population by increasing agricultural productivity (improving yields, increasing nutritional qualities, decreasing the levels of resources required for growth, etc.) with continual development of superior cultivars remains unchanged [19]. Plant breeding was revolutionized with the creation of transgenic plants with Agrobacterium and the invention of restriction fragment length polymorphism (RFLP). Coupling together Agrobacterium and RFLP, the total number of genetic markers available to plant breeders increased, creating the first marker-assisted selection (MAS) methodology and bringing first generation sequencing [20]. Plant breeders use the MAS systems to create high-resolution genetic maps and relate genetic markers to crop traits [2].

A new technology called CRISPR (clustered regularly interspaced short palindromic repeats) has a promising use in the future for plant breeding. CRISPR/Cas9 is a Type II prokaryotic adaptive immune system has been shown to facilitate in precise site-specific DNA cleavage [21]. This

new technology utilizes Cas9 nucleases, a protein that has a vital role in the immunological defense of bacteria against DNA viruses. CRISPR is not currently accepted as a method for genetic modification of agricultural crops and is not available in the market, but with the development of rules and regulations may lead the next genetic revolution [22]

2.6.Traditional Plant Phenotyping Methods

Cultivar breeding requires in-field phenotyping of thousands of plants grown in commercial field conditions across a range of environmental conditions like different elevations, sunlight levels, and soil composition. Multiple phenotypes must be assessed for each plant and potential cultivar, including: temporal cultivars (day of first green fruit, day of first ripe fruit), growth habit phenotypes (e.g. plant height, plant width, canopy density), and external phenotypes (e.g. fruit yield, fruit quality, abiotic stress tolerance). Current phenotyping methods for cultivar breeding trials are done manually by humans. During the growing season humans will go into the field a few times a week to observe these traits. This includes manually manipulating the plants to look at the internal structure or searching for flowers and fruit and destructive phenotyping at harvest. This method of human-based phenotyping is costly, labor- and time-intensive, subject to human error, and does not always allow (or is cost prohibitive) for repeated measures on the same plants over time. For processing tomatoes and peppers, important phenotypes are divided into exterior and interior traits, as shown on Table 1.

Table 1: Important phenotypes in processing tomato and pepper, as described by plant breeders.

Exterior Traits	Interior Traits
• Plant height and width • Plant shape (h/w) • Plant growth habit • Plant fruit carrying ability • Canopy light interception • Leaf temperature • Plant biomass	• Fruit yield • Proportion of ripe fruit in total yield • Fruit color • Fruit size • Fruit shape • Days to first: open flower, green fruit, mature fruit, sunburnt fruit

2.7.High-Throughput Phenotyping Methods

The development of in-field phenotyping technology lags behind that of genomics, creating a bottleneck in plant breeding [2], [3]. The key feature of high-throughput phenotyping is the ability to non-destructively, objectively, and quickly characterize plant traits [23]. Automated phenotyping utilizes various non-contact sensors to estimate traits such as biomass, yield, plant height, leaf segmentation, leaf area, and canopy temperature [24], [25], [26], [27]. Non-destructive phenotyping also permits a time-series approach that follows the growth of plants over time. Different systems have been developed for in-field phenotyping using permanent fixed-site platforms, unmanned aerial vehicles (UAV) including satellites, and terrestrial vehicles, all fitted with various sensors to collect a range of phenotypic data [28], [29], [30]. Regardless of platform type, the goal is to automate and expedite the acquisition of plant phenotypes and relate them to genotypic data to find superior breeding lines and cultivars more quickly [31].

2.7.1. Remote Sensing

Remote sensing in agriculture uses technology such as satellite imagery, manned and unmanned aerial vehicles fitted with sensors, and fixed-site platforms. UAVs look at spectral reflectance of the crops (visible, near infrared, infrared) using hyperspectral cameras, canopy temperature using thermal infrared sensors, and plant height and topography most commonly using Light Detection and ranging (LiDAR). In a broadacre grain crops, such as rice, the combination of high-density planting, narrow row spacing, consistent grain location at the top of the plant, and canopy closure makes it a perfect candidate for using UAVs as the phenotyping platform [24], [32], [33]. UAVs are not sufficient for all phenotyping situations, such as day of first bloom in vegetable crop breeding, because they can only provide vegetable crop breeders with a small number of phenotypes. Due to typical UAV altitudes and camera technology, the images and data are typically lower resolution than proximal methods, making it difficult to find small features like fruit phenotypes (day of first green fruit or first ripe fruit) and internal phenotypes in plants that have high canopy density and high visual occlusion.

2.7.2. Proximal Sensing

Proximal sensing in agriculture utilizes sensors mounted on terrestrial vehicles to traverse through a field and gather data. Recent technologies utilize terrestrial-based camera systems for creating realistic 3D models and phenotyping plants, leaves, fruits, and flowers [30]. The systems utilize a number of different technologies including: structured illumination, time-of-flight (ToF) sensors, high-resolution cameras, multi-view camera system techniques (structure-from-motion and stereovision), and software algorithms [34], [35], [36]. In a study at UC Davis using a high-throughput phenotyping system in Solanaceae crops and sunflowers demonstrated

the ability to recreate a 3D structure using multiple 2D images, though this method was time consuming and restricted to the height of the platform [37].

2.8.Phenotyping using Image Analysis

Currently non-destructive high-throughput phenotyping methods focus on traits that are easily quantifiable and compared to manual phenotyping. This includes traits such as total harvest yield in wine grapes, maize, rice, and citrus [38], [39], [40], [41], [42], [43]. These methods include using neural networks and traditional image analysis methods to compare yield and object or pixel count. These studies rely on comparing detected crop to crop yield at harvest. These crops are mechanically harvested with either an onboard yield monitor or postharvest yield monitor.

3. Objectives

3.1.General Objective

The objective of this dissertation is to develop a high-throughput phenotyping pipeline for Solanaceae crops. The pipeline starts with the development of a ground-based phenotyping system for in-field phenotyping of Solanaceae plants, including developing the software needed for georeferenced multi-sensor synchronization. This step includes finding affordable (typically consumer-grade) sensors that can be used for detecting the phenotypes outlined in Table 1 (page 9), which includes the detection of small objects like tomato flower petals located in the interior of the plant architecture. The final step is using the sensor data obtained from the high-throughput phenotyping system to develop neural networks and machine learning algorithms capable of automated detection of phenotypic traits from 2D images. The main objective is broken down into sub-objectives that are organized into three papers in this dissertation.

3.1.1. Objective 1: Design and develop a ground-based phenotyping machine for in-field use for economically important Solanaceae vegetable plants that can gather phenomic data on a non-contact basis from a continuously moving vehicle.

The objective of this paper is to develop and design a ground-based high-throughput phenotyping system for in-field phenotyping of Solanaceae plants. The phenotyping system must be able to continuously collect data using a multi-camera and multi-sensor approach to detect phenotypes outlined in Table 1. The system must be able to accommodate multiple types of Solanaceae plants and their growing habits. For this study, the research scope specifically focused on the economically important crops: Solanum Lycopersicon (tomato) and capsicum annum (pepper). The system must be able to traverse the field without interfering with plant

growth or jeopardizing plant health, including only taking non-destructive and non-contact measurements of phenotypes throughout the growing season without disrupting regular agricultural operations. To optimize the amount of useful data collected, the sensors will be triggered using geolocation signals from an RTK-GPS, which will ensure that data will only be collected in breeding plant plots.

3.1.2. Objective 2: Use computer vision, pattern recognition and machine learning to develop automated methods of producing meaningful phenotypes comparable to those used by plant breeders to allow them to evaluate in-field genotype performance in tomatoes

The objective of this paper is to explore the ability to utilize select images from the high-throughput phenotyping system to train and create neural networks and algorithms that can be used for phenotyping for tomatoes. The research scope of this study was restricted to the study of images captured from a single camera from the multi-camera set. The main neural network focuses on detection of flowers, green fruit, ripe fruit, and sunburnt fruit and the implications on how these values can be applied to interior phenotypes outlined in Table 1. Relationships between traits in Table 1and detected flowers, green fruit, ripe fruit, and sunburnt fruit are explored.

3.1.3. Objective 3: Explore the inclusion of non-visible wavelengths for distinguishing green fruit from green leaves and find viable affordable sensors that can detect these wavelengths.

This study focuses on using a benchtop spectrophotometer to quantify the spectral reflectance of green tomato fruit, tomato leaves, green pepper fruit, and pepper leaves at wavelengths 400 – 2498nm. Based on the data found from the benchtop experiment, non-visible wavelengths will

be identified for use in enhancing green fruit detection. From the data analysis, affordable sensors capable of detecting appropriate non-visible wavelengths will be proposed for use in the high-throughput phenotyping system. The performance of these modifications to the HTTP system, will be evaluated using in-field collected image data.

4. Chapter 1: High Throughput Phenotyping Platform Development

4.1. Introduction

High-throughput phenotyping requires a multi-sensor approach to account for the different types of traits. High-throughput phenotyping can be achieved using either a ground-based or aerial based approach. The most common aerial based approach is using a drone, which can collect exterior traits like plant height and width using an onboard LiDAR system and plant temperature using a thermal camera [44]. To gain plant level or plant-plot level resolution the LiDAR sensor and thermal camera must be very high-resolution. A drone can collect some interior traits like fruit yield but requires a high-resolution camera. Since the ground-based system is closer to the ground, cameras and sensors with lower resolution can be used to get the same or more precise measurements. A ground-based approach is more suitable to find specific interior traits like Day to First Open Flower because of the resolution needed to detect a single flower [45]. A ground-based vehicle can also us lower resolution depth sensors and temperatures sensors to obtain exterior traits.

Table 1: Important phenotypes in processing tomato and pepper, as described by plant breeders.

Exterior Traits	Interior Traits
• Plant height and width • Plant shape (h/w) • Plant growth habit • Plant fruit carrying ability • Canopy light interception • Leaf temperature • Plant biomass	• Fruit yield • Proportion of ripe fruit in total yield • Fruit color • Fruit size • Fruit shape • Days to first: open flower, green fruit, mature fruit, sunburnt fruit

4.2. Literature review

4.2.1. Food Insecurity

Food security is defined as “when all people, at all times, have physical, social and economic access to sufficient, safe and nutritious food that meets their dietary needs and food preferences for an active and healthy life” [6]. A combination of lack of access to nutritious food and increasing human population makes food insecurity a growing threat to the human population. It’s estimated that almost 2 billion people worldwide do not have regular access to nutritious and sufficient food supply [7]. It’s been identified that in 2023 there were 59 food-crisis countries/territories, where urgent action is required to protect and save lives at the local and national level [8]. In the 59 identified countries, 21.5% of the total population faces high levels of food insecurity [8]. This number increases in already vulnerable countries that experience sudden events such as political conflict and extreme weather occurrences [8]. Food insecurity is not about lack of food and calories, but also lack of nutritious food readily available to sustain human health and development [9].

4.2.2. Population Growth

The current world population is approximately 8.2 billion people [46]. By the year 2050 the United Nations predicts the population will increase to approximately 9.7 billion [10]. This increasing population growth is attributed to increased wealth and higher purchasing power per capita, leading to an increase in demand for food, including fresh produce, processed food, meat, dairy and fish [1]. Currently, 1 in 7 people worldwide have an insufficient diet, lacking in protein and energy or having some form of micronutrient malnourishment [11]. Food insecurity is a

complex subject with many socioeconomic factors including poverty, resource inequality, and a lack of infrastructure for both on-farm and postharvest food production needs. Agriculture cannot solve all of these issues but can help in the solution and has a role to play in providing food security for all by ensuring that the food supply is adequate. Maize, rice, wheat, and soybean, which account for 2/3 of the global agricultural calories, needs to increase production by at least 2.4% to meet population predictions. However, these crops have only been increasing at 1.6%, 1.9%, 0.6%, and 1.3% annually, respectively [11]. Recent trends in agriculture show richer countries relying on intensive farming techniques, increasing capital and labor (e.g. fertilizers, pesticides, machinery) in relation to land. If this agricultural trend continues, environmental repercussions including increased land clearing, CO_2 emissions, and nitrogen emissions will be inevitable.

4.2.3. Climate Change and Crop Yield

Adhering to sustainable agricultural practices is not the only concern in increasing agricultural production. Climate change is predicted to reduce crop yields and increase the frequency and severity of extreme weather events in food producing areas. In the United States cereal production during drought conditions has been reduced by 10%, and years with extreme heat led to a 9.1% production deficit [13]. For every 1℃ increase in seasonal temperature, major grains lose 2.5-16% of yield [14]. Our food production systems must overcome the effect of climate change on crop yield while sustainably increasing food production in order to meet the food security needs of the worlds' growing population.

4.2.4. Traditional Plant Breeding Methods

Plant breeding has an important role in providing food security to the world. Plant breeding is the process of changing traits in plants to produce new desirable traits. Over the past century, several methodologies and technologies, including biotechnology, have been developed and adapted by plant breeders to expedite crop cultivar development. As methodologies, techniques, and technologies improve for cultivar development, the overall goal of sustaining a growing global population by increasing agricultural productivity (improving yields, increasing nutritional qualities, decreasing the levels of resources required for growth, etc.) with continual development of superior cultivars remains unchanged [19]. Plant breeding was revolutionized with the creation of transgenic plants with Agrobacterium and the invention of restriction fragment length polymorphism (RFLP). Coupling together Agrobacterium and RFLP, the total number of genetic markers available to plant breeders increased, creating the first marker-assisted selection (MAS) methodology and facilitating first generation sequencing [20]. Plant breeders use the MAS systems to create high-resolution genetic maps and relate genetic markers to crop traits [2].

A new technology called CRISPR (clustered regularly interspaced short palindromic repeats) has a promising use in the future for plant breeding. CRISPR/Cas9 is a Type II prokaryotic adaptive immune system has been shown to facilitate in precise site-specific DNA cleavage [21]. This new technology utilizes Cas9 nucleases, a protein that has a vital role in the immunological defense of bacteria against DNA viruses. CRISPR is not currently accepted as a method for genetic modification of food crops and is not available in the market, but with the future development of rules and regulations may lead the next genetic revolution [22].

4.2.5. Traditional Plant Phenotyping Methods

Cultivar breeding requires a feedback mechanism called phenotyping to allow breeders to understand how different genotypes perform under different environments or locations. In-field phenotyping requires thousands of plants to be grown in commercial field conditions across a range of environmental conditions like different elevations or latitudes, sunlight levels, and soil composition. Multiple phenotypes must be assessed for each plant and potential cultivar, including temporal phenotypes (day of first green fruit, day of first ripe fruit), growth habit phenotypes (e.g. plant height, plant width, canopy density), and external phenotypes (e.g. fruit yield, fruit quality, abiotic stress tolerance). Current phenotyping methods for cultivar breeding trials are done manually by humans. During the growing season humans will go into the field periodically to observe these traits. This often includes manually manipulating the plants to look at the internal structure or searching for flowers and fruit and destructive phenotyping at harvest. This method of human-based phenotyping is costly, labor- and time-intensive, subject to human error and fatigue, and does not always allow (or is cost prohibitive) for repeated measures on the same plants over time. For processing tomatoes and peppers, important phenotypes are divided into exterior and interior traits, as shown in Table 1.

4.2.6. High-Throughput Phenotyping Methods

The development of in-field phenotyping technology lags behind that of genomics, creating a bottleneck in plant breeding [2], [3]. The key objective of high-throughput phenotyping is the ability to non-destructively, objectively, and quickly characterize plant traits [23]. Automated phenotyping utilizes various non-contact sensors to estimate traits such as biomass, yield, plant height, leaf segmentation, leaf area, and canopy temperature [24], [25], [26], [27]. Non-destructive phenotyping also permits a time-series approach that follows the growth of plants

over time. Different systems have been developed for in-field phenotyping using permanent fixed-site platforms, unmanned aerial vehicles (UAV) including satellites, and terrestrial vehicles, all fitted with various sensors to collect a range of phenotypic data [28], [29], [30]. Regardless of platform type, the goal is to automate and expedite the acquisition of plant phenotypes and relate them to genotypic data to find superior breeding lines and cultivars more quickly [31].

4.2.6.1. Remote Sensing

Remote sensing in agriculture uses technology such as satellite imagery, manned and unmanned aerial vehicles fitted with sensors, and fixed-site platforms. UAVs look at spectral reflectance of the crops (visible, near infrared, infrared) using multispectral (typically less than 10 wavebands) or hyperspectral (typically more than 100 wavebands) cameras, canopy temperature using thermal infrared sensors, and plant height and topography most commonly using Light Detection and ranging (LiDAR). In broadacre grain crops, such as rice, the combination of high-density planting, narrow row spacing, consistent grain location at the top of the plant, and canopy closure makes it a perfect candidate for using UAVs as the phenotyping platform [24], [32], [33]. UAVs are not sufficient for all phenotyping situations, such as day of first bloom in vegetable crop breeding, because they can only provide vegetable crop breeders with a small number of phenotypes. Due to typical UAV altitudes and camera technology, the images and data are typically lower resolution than proximal methods, making it difficult to find small features like fruit phenotypes (day of first green fruit or first ripe fruit) and internal phenotypes in plants that have high canopy density and high visual occlusion.

4.2.6.2. Proximal Sensing

Proximal sensing in agriculture utilizes sensors mounted on terrestrial vehicles to traverse through a field and gather data. Recent technologies utilize terrestrial-based camera systems for creating realistic 3D models and phenotyping plants, leaves, fruits, and flowers [30]. The systems utilize a number of different technologies including: structured illumination, time-of-flight (ToF) sensors, high-resolution cameras, multi-view camera system techniques (structure-from-motion and stereovision), and software algorithms [34], [35], [36]. In a study at UC Davis using a high-throughput phenotyping system in Solanaceae crops and sunflowers demonstrated the ability to recreate a 3D structure using multiple 2D images, though this method was time consuming and restricted to the height of the platform [37].

4.3. Background

Previous studies at UC Davis developed a 32-camera in-field phenotyping system capable of capturing a multi-view set of 256 images of each plant in the field in order to create a high-resolution, photo-realistic, 3D reconstruction of individual eggplants [37], [47], [48], [49]. This previous study was capable of individual leaf segmentation to determine the phenotypes: plant height, leaf count, and leaf area. For this previous study, it was crucial to create a high-resolution 3D reconstruction of each plant.



Figure 1: UC Davis 2016 high-throughput phenotyping system.

The original design was conceived to be a 3-row machine where the modules were placed side-by-side. Therefore, an X configuration, with the cameras at a 45-degree angle to the plant row as shown in Figure 1, was used to optimize space constraints and allow for three 32-camera modules side-by-side. A single module of this system, shown in Figure 1, was successfully operated in the field but was stationary when acquiring each multi-view set of 256 images, as it had to stop at each plant to reposition the cameras. The system fully enclosed the plant in a lighting chamber for illumination control, which allowed the illumination to be uniform, as the 32 cameras moved to take multiple sets of images of the same plant, in order to successfully to create a 3D reconstruction of the plant. This system was towed by a standard row-crop tractor, which limited the ground clearance. Because of the limited ground clearance, the system was operated in the beginning of the season before the plants became tall and was unable to operate when the plants were mature, as the clearance of the standard tractor was too low. The original system was designed for open-structured plants where leaf to leaf occlusion is minimal, and for early-stage plant growth where the maximum plant height was approximately 33 centimeters. This system would not be suitable for high-throughput phenotyping through the growing season because of the low ground clearance, limiting the imaging to only early season crops.

In 2017, the camera system described above was retrofitted onto a high-clearance tractor (Classic Spider, LeeAgra, Lubbock, TX 79404), allowing the system to collect data all season from planting to harvest without harming the crop, as shown in Figure 2. This system was configured to fit all the cameras within the furrow-to-furrow distance while keeping the camera to object (plant) distance at the same distance,

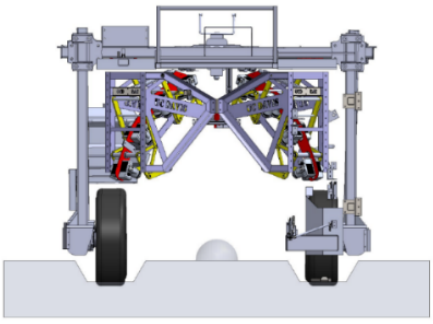


Figure 2: 3D CAD model of the interior structure of the high-throughput phenotyping platform in 2017.

this resulted in an object distance of 1-meter from the camera. Early in the season, this distance was ideal because the distance from the plant to the cameras and the system configuration created even illumination and enough overlap between cameras for image reconstruction. However, as the plants grew, they got closer to the cameras. Resulting in inconsistent lighting, drastic view changes between cameras and poor image quality, making reconstruction or object detection almost impossible.

From this discovery, the high-throughput phenotyping system was redesigned for the 2018 growing season, as shown Figure 3, to meet the needs of the plant growing habit and change in the desired phenotypes specified by the plant breeders, as explained in Table 1.

The final design for the 2018 high-throughput phenotyping system consisted of a high clearance tractor fitted with 9 color DSLR cameras, 9 pseudo-NDVI cameras, 2 Time of Flight cameras, 2 temperature sensors, 8 custom LED modules, with infrared and broad-spectrum white LEDs, 1 RTK-GPS, 1 National Instruments High Speed Controller, 1 Dell desktop computer, and 1 National Instruments USB controller. The system was custom created to fit in a standard breeding trial for processing tomatoes in Davis, CA and look for interior and exterior traits related for processing pepper and tomato phenotypes.



Figure 3: Comparison of the 2017 and 2018 high-throughput phenotyping system. The translucent white covering is where the sensors and LEDs are housed. The 2017 system was mounted entirely under the high clearance tractor. When the 2018 was redesigned the Multiview camera locations were changed, making the system wider.

4.4. Materials and Methods

4.4.1. Multi-Camera System

For this study, the phenotyping system needed to be redesigned to improve image quality across different plant growth stages and to increase the throughput of the system without sacrificing the multi-view aspect. The new high-throughput phenotyping system needed to accommodate a multi-view system; the multi-view aspect of the system was crucial for being able to observe all the desired phenotypes in Table 1, given the typical degree of visual occlusion in a plant architecture. To improve image quality and increase image consistency between cameras the 60-inch-wide maximum footprint constraint of the previous design was abandoned, allowing the cameras to be farther away from the soil and plant. The overall structure of the camera system was designed to use a semi-circular camera pattern, spanning the plant row perpendicularly, with

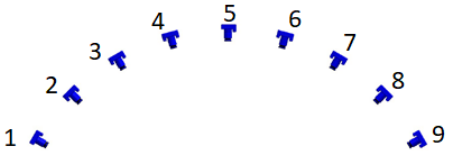


Figure 4: Representation of the desired camera arch on the phenotyping system.

multiple cameras that were evenly spaced on the perimeter and radially the same distance from the top of the plant bed. The camera semi-circle will be referred to as the camera arch, as shown Figure 4. By abandoning the 60-inch footprint and only spanning the plant-row perpendicularly it was possible to increase the camera to plant distance of the system. The goal of increasing the camera distance while maintaining the multi-view design was driven by three main factors: reducing occlusion, increasing the overlap between cameras, and eliminating the need for changing the lens depth of field throughout the season.

Imaging systems for agricultural scenes must address occlusion to fully analyze an agricultural scene. Occlusion occurs when there are overlapping objects in an image, resulting in the "front" object blocking the view of the "back" object. However, many agricultural systems are not able to manipulate the scene (i.e. move the plant around) to observe all parts of the object, so occlusion cannot be eliminated but rather minimized. In the previous phenotyping system, as the plants grew larger the object distance decreased, resulting in images with only a single leaf in the entire frame, blocking the view of the rest of the plant. The variation in the occlusion in the scene can be reduced by increasing the object distance to distance between object ratio, as shown in Figure 5. Since we were not able to change the distance between objects (i.e. change the distance between leaves and fruit), we increased the object distance so that the ratio of the object distance to the distance between objects was high. While this design does not eliminate occlusion, it does create views of the scene where the occlusion is more similar between adjacent cameras than the previous design which helps with 3D reconstruction, particularly as the crop matures.

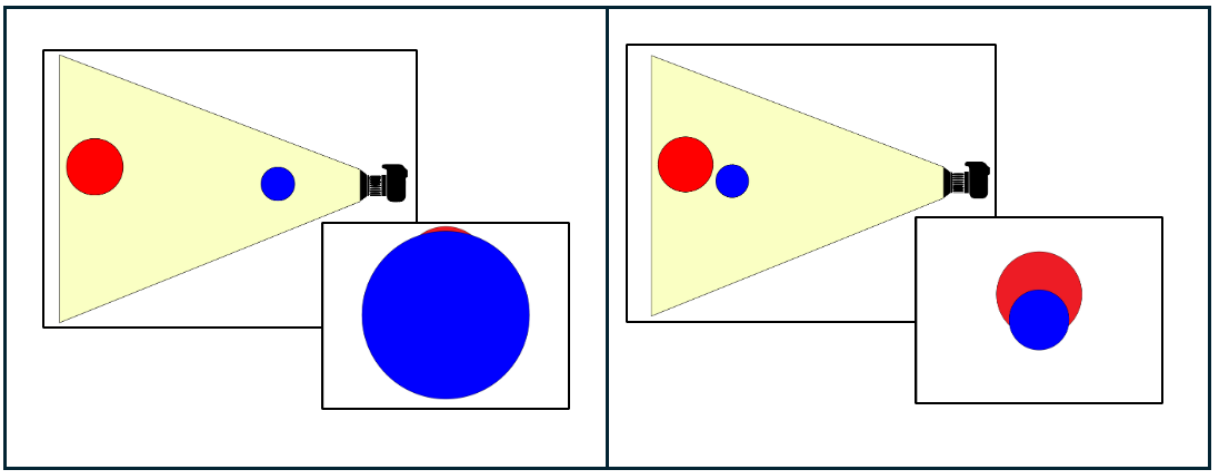


Figure 5: Graphical depiction of how camera to front object ratio affects the amount of occlusion visible in an image between two objects

Similarly, increasing object distance also increases the minimum distance between adjacent cameras needed to have adequate image overlap between cameras. This aspect is important because of the non-homogenous growth pattern of plants. The system needed to view the plant at multiple angles because one camera view would not be enough to see all aspects of the plant needed to estimate all the desired phenotypes. This design maximizes the likelihood that the system will be able to see most of the phenotypes at some angle of viewing the plant. In the previous phenotyping system, the views between adjacent cameras were drastically different for larger plants, due to the cameras being too close to the objects. The different views between cameras made it difficult to relate the information from different cameras to one another for 3D reconstruction. To get adequate overlap between two cameras it is important to consider the distance between the two cameras as well as the camera distance from the object. As shown in

Figure 6, when the camera object distance increases and the distance between cameras stays the same, the views between the two cameras have more overlap between images.

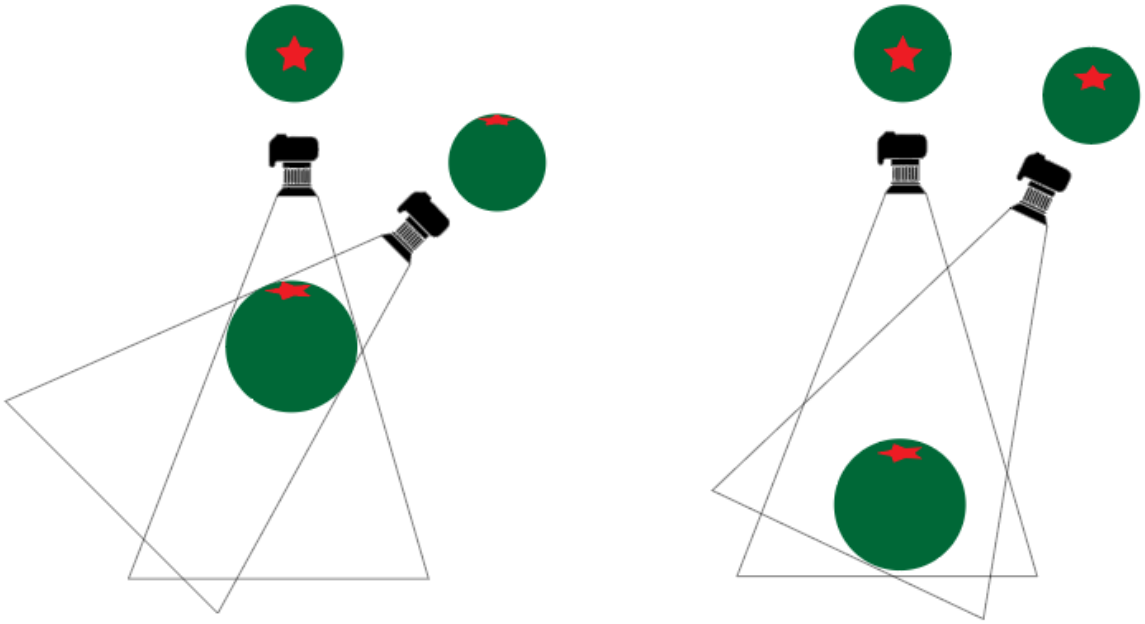


Figure 6: Depiction of how increasing camera distance to object creates more image similarity overlap, necessary for 3D reconstruction and 2D stitching.

Maintaining consistent depth of field between cameras and adequate distance from the plants was crucial in continuously acquiring good quality images throughout the growing season. Depth of field in image capture is the depth in a scene where the image is in focus, i.e., it is the distance between the nearest and farthest objects of a scene that are in focus in an image. A narrow depth of field means only a small part of the scene is in focus in the image and a wide depth of field means a large portion of the scene is in focus in the image. Depth of field is a relationship between lens focal length, distance to object, and aperture, as illustrated by Eq. 1. Focal length is the distance between the camera sensor and the center (or virtual center for compound lenses) of the camera lens. Distance to object is the distance from the lens to the object. Aperture is the size of the opening in the lens diaphragm, which dictates how much light passes through the lens to

the sensor. To image plants throughout the season a large depth of field was needed because that means more of the plant could be in focus. If the depth of field was narrow and calibrated at the beginning of the growing season, as the plants grow taller and wider the entire plant would no longer be fully in focus. By fixing the focal distance of the camera, the depth of field relies on distance to subject and aperture. Aperture and depth of focus have an inverse relationship, as the aperture gets smaller the depth of focus is wider. However, a smaller aperture comes at the high cost of needing large amounts of light. By increasing the distance to the subject, we were able to increase the aperture and keep a large depth of field.

$$\mathrm{DOF} = \frac{2u^2 Nc}{f^2}$$

Eq. 1

$\mathrm{DOF} = \text{depth of field}$

$u = \text{distance to subject}$

$N = \text{aperature}$

$c = \text{circle of confusion}$

$f = \text{focal length}$

Eliminating the 60-inch footprint constraint and proving that moving the cameras further away from the plant bed would be beneficial in many aspects meant that we had to identify what the ideal camera distance was for the system. From the previous high-throughput phenotyping system, it was identified that for tomatoes the most important camera view was the nadir view, with the camera looking directly down on the plant bed from above. Therefore, the camera arch geometry would be dictated by the camera pointing down at the plant bed. For the top camera, the field-of-view was selected to image the entire width of the plant bed while minimizing the

amount of tractor and system infrastructure in an image. The optimal field-of-view was dictated by the tractor infrastructure. The top camera needed to be able to image a 60-inch-wide bed with a sensor height-to-width-ratio, in the horizontal orientation, of approximately 2:3. Using the sensor geometry and plant-bed width, the optimal field-of-view for the camera would be a 60-inch by 40-inch area on the plant-bed. The same field-of-view can be realized with different combinations of camera distance and focal length, so the next step was to find the ideal camera distance and focal length combination that could achieve the desired field-of-view. This was done by mounting a camera with an adjustable focal length lens on an adjustable tripod at the proposed location of the top camera. The proposed location was determined to be at the center of the sensor enclosure where no beams were blocking the view. The height of the tripod base to the ground was approximately 165 centimeters, the tripod was adjusted to make the total height of the camera 165 centimeters to 225 centimeters from the ground. The tripod was adjusted every 10 centimeters, and the focal length was also adjusted accordingly to achieve the previously described field-of-view. Although each tested height had a corresponding focal length that could reproduce the desired field-of-view, 220-centimeters from the ground with a 35-millimeter lens was chosen because of the limited availability of affordable fixed-focal length lenses.

The next step after finding a suitable focal distance and camera distance for the ideal field-of-view was to identify how many cameras should be mounted on the camera arch system. The new camera system design allowed for cameras to exceed the 60-inch plant bed width, which means cameras could be placed above adjacent plant beds. From the previous years' data, the tallest plant was about 68-centimeters, meaning any infrastructure or cameras that are placed above the center of the plant-bed in adjacent rows must be at least 68 centimeters from the ground. The naïve decision would be to try to fit as many cameras as possible in the system to allow for

maximum number of angles and views of the canopy. The methodical decision would be to minimize the number of cameras on the system to reduce cost and power consumption. The latter decision also creates more physical space between each camera, this empty space could be used to mount lights on the camera arch in between each camera. The camera semi-circle was designed to accommodate external lighting sources (both visible and near infrared). Uniform lighting conditions are important in multi-angle imaging systems because uneven lighting creates inconsistent shadows and illumination between camera angles. To create uniform lighting using multiple lighting sources in an enclosed system it was important to consider uniform distance of the light sources to the object. The Inverse Square Law dictates that light intensity at a given distance from a light source is inversely proportional to the squared distance. $\left(I \propto \frac{1}{d^2}\right)$. To make sure there are no dark spots or saturated spots in an image, it was important for each lighting unit to be mounted the same distance from the center of the plant bed along the camera arch. With the lighting and camera system together, the final design for the camera arch was a nine-camera system, with lighting modules between every two cameras, on a semi-circle with a radius of 226-centimeters from the center of the plant-bed. The lowest camera on the arch was above the adjacent plant-bed and was 76-centimeters from the top of the adjacent plant bed as shown in Figure 7.

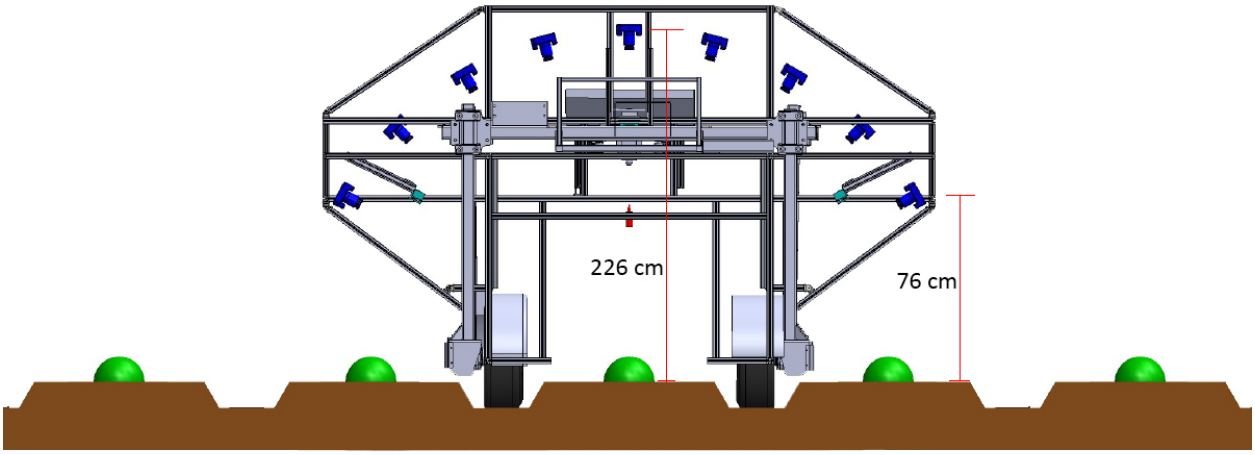


Figure 7: CAD model of interior structure of high-throughput phenotyping platform. Red lines depict the different heights of the tallest and lowest camera with respect to the top of the dirt.

4.4.2. Multi-Sensor System

4.4.2.1.Interior Traits

To capture the Interior Traits outlined in Table 1, a high-resolution camera capable of acquiring color accurate images while also detecting various sized objects was needed. An industrial camera was not considered for this system because many industrial cameras require a separate computer with special or proprietary software to capture images from a single camera. Industrial cameras, although rugged, are typically lower resolution at a higher cost compared to many consumer-grade digital cameras. For a system that requires a single camera using a single viewpoint an industrial camera may be adequate, but for a multi-sensor system that requires images from multiple angles it is not ideal. For the high-throughput phenotyping system high-resolution, digital-single-reflex-lens (DSLR) cameras (Canon EOS T6, Canon USA Inc., Melville, NY, USA) were chosen because of their very high-quality images, high-resolution making them suitable to detect small objects, and hardware triggering capabilities. One crucial aspect of image quality for image processing is a sensor capable of capturing high-resolution

images with low noise. The DSLR camera was favored because of the cost-to-resolution value of the camera, the low cost of the DSLR camera made it possible to develop an 18-camera imaging system within the project's budget.

The proposed 18-cameras were twice as many cameras as described in the nine-camera system; this was because each DSLR color camera on the camera-arch had a modified pseudo NDVI (Normalized Difference Vegetation Index) DSLR camera paired with it [50]. While the color DSLR cameras could capture high-resolution images, it was still difficult to distinguish green fruit from green foliage using a color-camera. In the visible spectra green fruit and green foliage can look similar, however preliminary research suggested that parts of the green fruit and green foliage were more distinguishable using a combination of visible and infrared wavelengths. This theory was tested on green tomato fruit and foliage and green pepper fruit and foliage using a benchtop spectrometer, which will be described in Chapter 2. The spectrometer study indicated that in the visible part of the spectrum the optical absorbances of pepper fruit and foliage and tomato fruit and foliage were very close to one another. The pepper fruit and leaves had more similarity in the visible spectrum than the tomato fruit and leaves. Parts of the near-infrared spectra showed differences between fruit and foliage. Electronic cameras with silicon-based sensors intended as color cameras, including DSLR cameras, will come with an infrared blocking filter installed that blocks infrared wavelengths from reaching the camera's sensor. Often the infrared blocking filter can be removed and possibly replaced with another filter that allows infrared wavelengths to pass through to the camera sensor. By proper choice of the replacement filter, both visible and infrared light can reach the sensor allowing a DSLR camera to be converted into a pseudo-NDVI camera. Based upon the spectral data collected in this study, it was hypothesized that using pseudo-NDVI cameras could enhance the detection of green fruit

among green foliage to increase the accuracy of automated green-fruit detection. With the pseudo-NDVI technology each color DSLR camera on the previously described camera arch was paired with a pseudo-NDVI-DSLR camera [51]. This created an 18-camera or 9-camera pair system capable of both color and pseudo-NDVI imagery of each plant.

4.4.2.2.Exterior Traits

4.4.2.2.1. Height Width

For some of the Exterior Traits outlined in Table 1, a sensor capable of acquiring both color and structural features of objects was needed. One sensor that was investigated was a high-speed industrial line profile sensor (GoCator Laser Line Profile Sensor, LMI Technologies Inc., Burnaby, BC, Canada) capable of capturing millimeter detail. The industrial sensor was not chosen because it did not have the ability to work outdoors and did not have the correct field-of-view to work with the geometry of the vehicle. Instead, a consumer grade time-of-flight sensor, the Microsoft Kinect (Microsoft Kinect V2, Microsoft Corp., Redmond, WA, USA) was chosen for identifying many of the Exterior Traits. The time-of-flight camera was an RGB-Depth camera, based upon a two-camera sensor with one RGB camera and one infrared time-of-flight sensor. The infrared time-of-flight sensor consists of two parts: an emitter and a receiver. The emitter projects an encoded pulsed infrared light beam onto a scene. When the light beam hits an object, the infrared light is reflected onto the infrared sensor. The infrared sensor has a known geometric relationship with the infrared light emitter and can calculate the amount of time it takes for the infrared light to reflect on to the sensor. Knowing the geometric relationship and the time it takes for the infrared light to reflect from an object, the distance between the sensor and object can be calculated. The output from this sensor is a depth map. This distance sensor also has an RGB camera that is synchronized with the time-of-flight camera. The output of this RGB

camera is a color image. There is a known registration between the RGB camera and time-of-flight camera, which can be used to reconstruct a 3-dimensional point cloud with color information from the depth image and RGB image. The 3D point clouds were calibrated to detect height and width of in-field objects by using known objects of different sizes and creating a calibration equation to match point cloud dimensions to real-world dimensions. The calibrated point clouds can be used to estimate exterior traits such as plant height, width, and shape [41].

4.4.2.2.2. Temperature

For the exterior trait leaf temperature, a sensor that could acquire temperature of the plant canopy without contacting the plant was needed. There are many sensors on the market capable of capturing temperature data using various technologies and techniques. One sensor that was considered was a high accuracy (1 ^{o}C) thermal camera (Xenics model ONCA, MWIR camera with a 640x512 InSb thermal imaging array and a Sterling sensor cooler, Leuven, Belgium). This thermal camera was able to capture temperature data of a scene and produced an image with a temperature map for each pixel. This sensor was capable of operating outdoors while having a wide temperature range. However, this camera was quite costly, had International Traffic in Arms Regulations (ITAR) use restrictions, and needed special software and a dedicated computer to operate. For this study, it was also decided that the use of this thermal camera was not justified. Instead, a high accuracy single point measurement or multiple single point measurements of canopy temperature was determined to be sufficient, and a temperature map within the plant was not considered to be necessary by the plant breeder. The sensor that was chosen for this application was a high accuracy, non-contact, surface temperature sensor (Apogee SIF-121, Apogee Instruments, Logan, UT, USA). This temperature sensor measured the average canopy temperature within a conical field-of-view of 18 degrees half angle, this narrow

view allowed the sensor to measure the plant foliage while minimizing the amount of soil that was in view. Two of these sensors were used in together, one pointing directly nadir and one at a 45-degree angle [45]. The temperature was calculated using equations and constants provided by the manufacturer (Eq. 2, Eq. 3). The angled sensor captured the temperature of soil and plants while the perpendicular sensor was used to capture plant temperature; both measurements were used to determine plant canopy temperature via a calibration process using multiple linear regression [45]. The temperature sensor was never fully integrated into the high-throughput phenotyping system to continuously collect data, but an in-field calibration was done to test the viability.

$$R_T = R_{bridge}\left(\frac{V_{EX}}{V_{OUT}} - 1\right)$$

Eq. 2

$R_T = \text{Thermistor resistance } (\Omega)$

$R_{bridge} = 24900\Omega$

$V_{EX} = \text{excitement voltage}$

$V_{OUT} = \text{output voltage}$

$$T_K = \frac{1}{A + B\ln(R_T) + C(\ln(R_T))^3}$$

Eq. 3

$T_K = \text{Temperature in Kelvin}$

$A = 1.129241 \times 10^{-3}$

$B = 2.341077 \times 10^{-4}$

$$C = 8.775468 \times 10^{-8}$$

$$R_T = \text{Thermistor Resistance } (\Omega)$$

$$A, B, \text{and } C \text{ are Steinhart} - \text{Hart constants}$$

4.4.3. Geo-Referencing Hardware

The HTPP system was equipped with an RTK-GPS unit (model 542 RTK-GPS, Trimble Inc., Sunnyvale, CA), enabling centimeter accuracy georeferencing in all phenotype data collected. Extraneous images are images that have no plants of interest in the view, such as the region between breeding-plots and in the field headlands. Geo-referencing has been explored for agricultural use, including applications in self-driving tractors, crop transplant mapping, and centimeter precision robotic weed control [53], [54], [55], [56].

High-resolution georeferencing has been made possible by the invention of Real-Time-Kinematic Global Positioning Systems (RTK-GPS). The RTK-GPS base station, at a fixed and known location, is continuously communicating with satellites and calculating it's estimated location based on satellite data. By knowing both the estimated satellite location and actual fixed location, the RTK-GPS base station can calculate a correction factor to account for environmental and GPS errors. The base station can communicate the correction factor to mobile or rover units that are in the vicinity and communicating via radio. The correction factor can be used if the rover and the base station see at least 5 common satellites and the rover is less than 20 kilometers away from the base station. This allows RTK-GPS to output 1-centimeter accurate geo-location data every second.

The RTK-GPS is continuously querying the satellites for location information while the vehicle is continuously driving over plant-plots. The RTK-GPS produces an 8-microsecond 5-volt pulse when it immediately measures its own location. About 80 milliseconds later the RTK-GPS outputs the string to be interpreted. Because of the continuous movement of the vehicle, the by the RTK-GPS listens to the satellites and the computer reads and interprets the data, the vehicle will be at a new location. To deal with this, we used linear regression to interpolate between GPS data points to get location of plants that will not have their location synchronized with the location at the GPS at the time that it takes the RTK-GPS to take its measurements. The linear regression model used the UTC, Northing (m), and Easting (m) values to interpolate and predict the rover location on a continuous basis while travelling across plant-plots. The modeled output was the next closest plant-plot in the rover's trajectory and estimated how long it would take to get to the plant-plot.

A ruggedized real-time-kinematic GPS (model 542 RTK-GPS, Trimble Inc., Sunnyvale, CA) was used in this study because of its RTK capability and robust design for use on agricultural vehicles. The RTK-GPS had two outputs that were utilized: NMEA-0183 GPS coordinates message and the synchronization pulse. To obtain Easting and Northing measurements the NMEA-0183 message from the receiver was configured to output the location using the PTNL-PJK string in the 10S UTM Zone. The RTK-GPS continuously received data from the satellites and corrections from the base station and output the PTNL-PJK string through an RS-232 serial port.

4.4.4. Data Acquisition Hardware

A ruggedized, real-time, embedded controller used to control the data acquisition process. The controller had both a real-time serial processer and a programmable Field Programmable Gate Array (FPGA, National Instruments Compact Real Time IO (cRIO) 9004, NI 9004, NI Co., Austin, TX). The FPGA could run multiple processes in parallel in real-time (e.g. reading voltages and switching relays) with a ~25 nanosecond response time. The controller performed higher level processes such as executing mathematical operations, reading strings, parsing strings, and image processing using the real-time serial processer. A serial interface module (model NI 9870, National Instruments, Austin, TX) equipped with four serial ports was added to the NI 9004, which was connected to the serial output of the RTK-GPS to read the GPS string. A digital input module (model NI 9411, National Instruments, Austin, TX) was added to the embedded controller. The GPS synchronization pulse (8-microsecond 5V) was connected to the digital input module. Two rugged relay output modules (National Instruments 9482, NI 9482), equipped with four single pole single throw solid state relays were used to trigger the synchronized data acquisition of the sensors in the sensor array. The time-of-flight sensors were triggered to acquire and save data directly from a computer through a universal serial bus (USB) 3.0 connection.

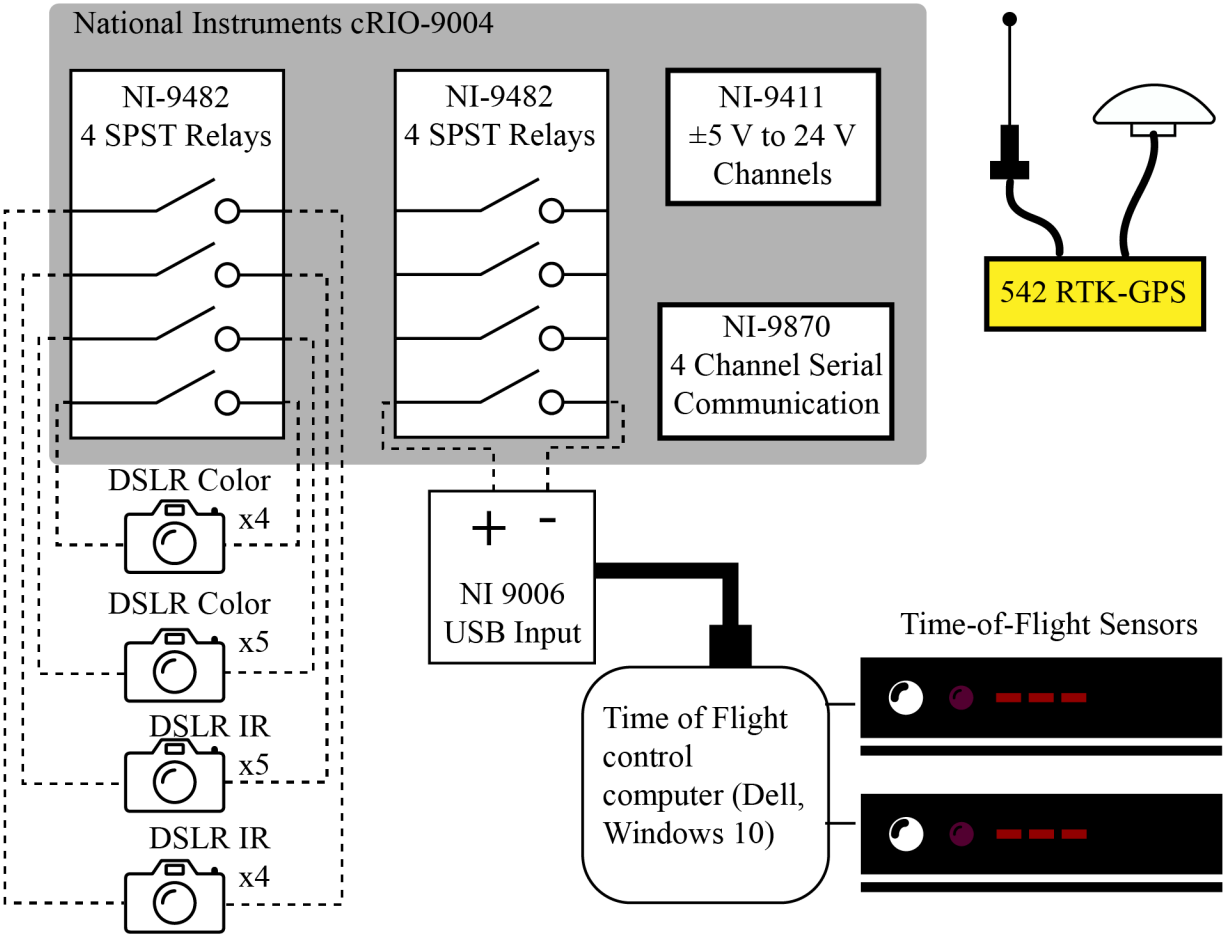


Figure 8: A graphical representation of the HTPP data control system and sensors. The grey box represents the NI-cRIO-9004 that contains the FPGA, CPU, and different modules. One NI-9482 controls the DSLR cameras and the other NI-9482 communicates with a Dell computer that controls the Kinects.

4.4.5.Camera Wiring

The Canon DSLR cameras had multiple methods of image capture triggering: the built-in shutter release button on the camera, timed-single image capture, timed-continuous data acquisition, and an external trigger. The external trigger was the method implemented because of the ability to electronically synchronize image capture of multiple cameras with external events. The external trigger interfaced with the camera using a 2.5 mm jack. The 2.5 mm jack had a metal plug that had 3 electrical connections: ground, focus, and shutter. The internal circuit contains two pull-up

resistor circuits, where each switch in the circuit is a physical switch. Looking at the shutter circuit, when the switch is open the shutter input is high, when the switch is closed it opens a path to ground and the shutter input is low. The 2.5 mm jack is intended to be connected to a wired Canon remote control for a person to use. The Canon remote control was replaced with a relay shown at the bottom of Figure 9.

The NI 9004 module was used as the relay control for the camera shutter to synchronize image capture with the GPS. For the high-throughput phenotyping system to work it was important for each camera to be triggered at the same time, to make sure the images were taken at the exact same time. Multiple cameras were wired in parallel together in 6 different groups. However, having multiple cameras in parallel causes multiple grounds to be wired together, resulting in multiple triggers from one switch actuation. To prevent this from happening, a diode was placed in-line with each trigger wire, as shown in Figure 9.

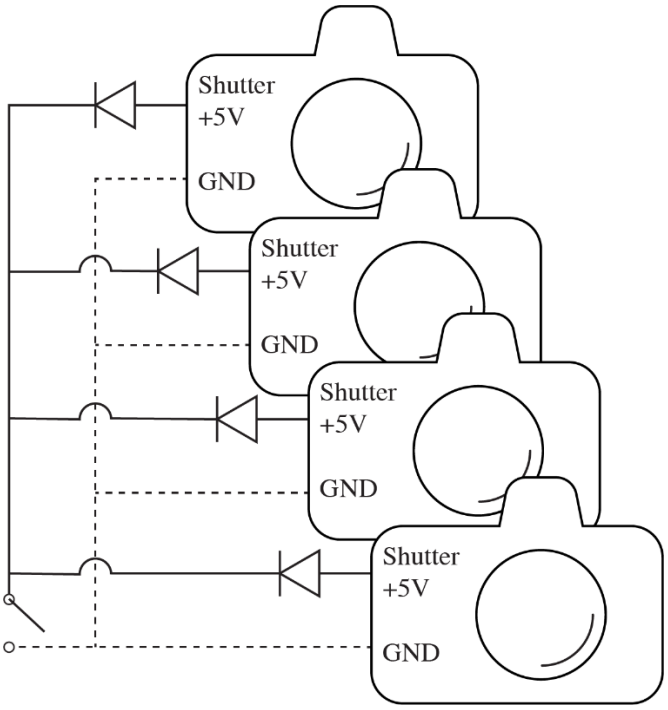


Figure 9: Wiring diagram of a set of 4 DSLR cameras with a common relay and individual

4.4.6. Data Control Acquisition Software

The in-field phenotyping data acquisition control program is divided into two components: continuous and time-sequence processes. The Field Programmable Gate Array (FPGA) handles the continuous processes because they are do not require complex computing algorithms but are able to handle multiple time-critical tasks in parallel. The on-board serial CPU handles time-sequence processes that require more difficult computing tasks but are not time-critical.

The FPGA continuously ran three processes in parallel: detecting for the 8-microsecond GPS pulse, triggering the camera relays, and triggering the Kinect relays. The serial CPU handled one main process reading, parsing, and interpreting the GPS string.

When the FPGA detected the 8-microsecond GPS pulse it sent a signal to the serial processor to wait 80 milliseconds for the full PTNL-PJK string to be received and then to read the string from

the serial port. The serial processor parsed the string and saved the UTC, Easting, and Northing values in a table. The program referenced an array of GPS data collected over time to create a linear regression model for the vehicle position vs time. Using this model equation, when it detected the vehicle was entering a plant-plot, the NI 9482 sent a 100-millisecond pulse to actuate the camera triggers. A flowchart of how the program worked is shown in Figure 10. The color DSLR and pseudo-NDVI cameras were triggered multiple times within a plant-plot, so the camera trigger signal looked like periodic square wave. In this situation it is known that the plant row was orientated in the North-South direction. If the plot ran in an arbitrary direction both the Easting and Northing values would be needed to calculate the distance along the row. The computer controlling the Kinect cameras continuously captured data while the input was true (i.e. when the HTTP was inside a genotype plot). Thus, the NI 9082 controlling the ToF computer did not need to pulse, rather it held the relay constantly closed while the vehicle was inside a genotype plot.

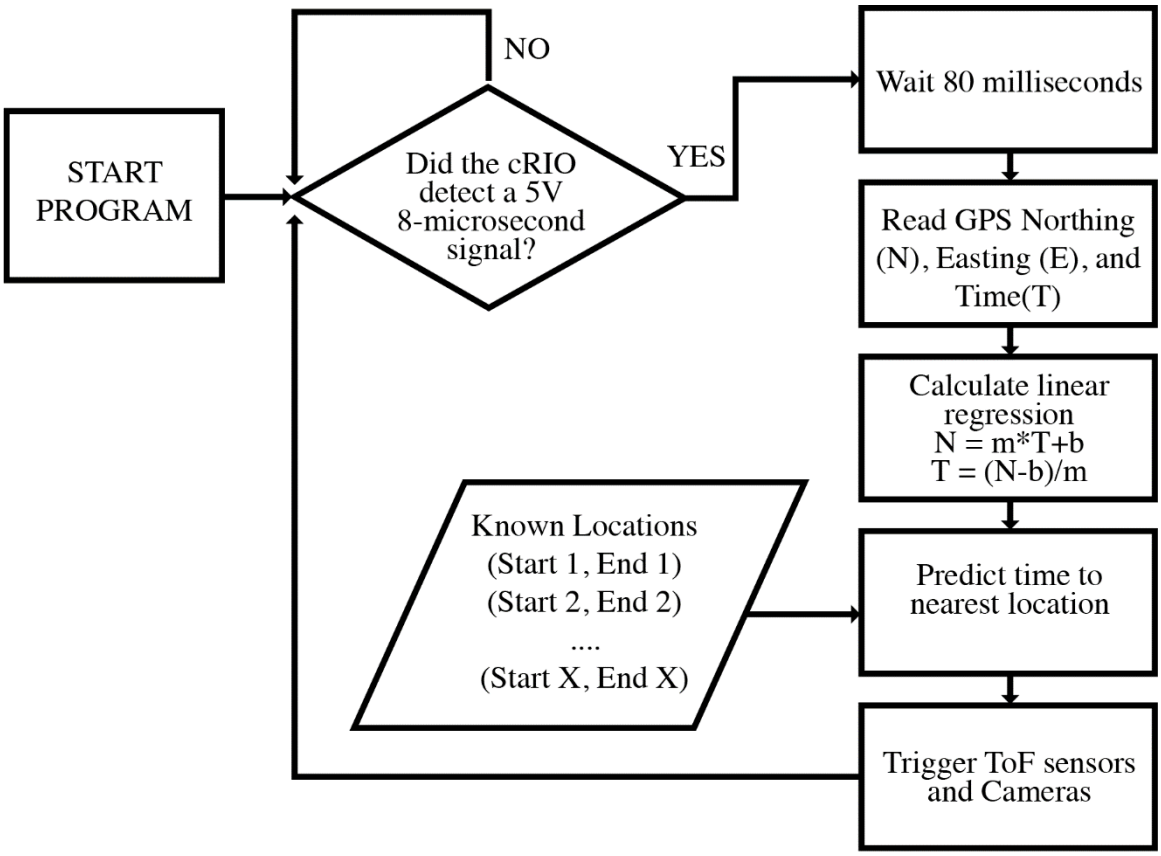


Figure 10: Flowchart describing the program used for georeferencing and data acquisition for the HTPP system.

4.4.7. Lighting Design

Custom lighting modules using both full spectrum white and specific 740 nanometer LEDs were designed to achieve uniform illumination in both spectra. Corrugated plastic was used to wrap the sensor chamber to maximize the use of natural sunlight while ensuring lighting uniformity. The chamber was not completely sealed off, there were holes at the entrance and exit of the chamber to allow plants to go through without getting damaged. At the entrance and exit of the chamber there was a custom shade cloth. The shade cloth was made of white polyester and made

rigid with fiberglass rods. The purpose of the shade cloth was to shield the interior of the sensor suite from direct sunlight, if there happened to be any direct sunlight leaking in.

The final design is a double arch, one for color cameras and one for color-infrared cameras, with cameras at 226 cm radially from the center, custom LED lighting modules in between cameras, two ToF cameras for an overhead view and side view, and room for other sensors to be added. As shown in Figure 11 there are two parallel rows of DSLR cameras, one row contains the color cameras and one row contains the color-infrared cameras. In between each camera pair is the custom lighting modules with half white LEDs and half infrared LEDs. The infrared LEDs and white LEDs are on different circuits in case only color cameras were used or only infrared-color cameras were used the LEDs could be turned on and off.



Figure 11: A view of the sensor chamber, from the ground looking directly up. The top row of cameras is the color cameras and the bottom row is the color-infrared cameras. The ToF cameras are on the top, right, and left, of the image.

4.4.8. Solanaceae Crop Selection

There are several important Solanaceae crops that are grown and consumed in the United States such as: eggplant, potato, tomato, sweet peppers, chili peppers, and tobacco. Two specific Solanaceae crops were chosen for phenotyping, processing tomato (Solanum L.) and processing peppers (Capsicum). These processing tomatoes and peppers were picked because of their economic importance in California and overall health benefits for humans in both market fresh and processed fruit [57], [58], [59], [60], [61], [62], [63]. Additionally, the growth habits and architecture of tomato and pepper plants are similar. Both plants have green leaves, flowers with

5-6 distinct petals, and fruit that grow on the stem. The edible tuber of potatoes grows underground, making it distinctly different than the other Solanaceae crops. Tobacco plants are harvested for foliage instead of fruit. Processing varieties were chosen for this project to limit the frequency of humans entering the field throughout the growing season and to allow the plants to develop fully before a single destructive harvest. Eggplants are generally grown for market harvest instead of processing, which means one plant can be harvested multiple times throughout a growing season rather than one time at the end. Finally, processing tomatoes and peppers were chosen because they have similar field requirements (i.e. transplant schedule, row width, irrigation methods) for planting and management [58], [62].

4.4.9. UC Davis Research Field Implementation

At UC Davis, in-field plant breeding experiments are designed so the research fields are typically only 200 feet long. Thus, having many rows with a limited number of plants in each row. This design was due to a historic farm management process that was designed to optimize land use for small, non-breeding, research experiments that predated GWAS concepts and the use of manual phenotyping by humans walking through the field without needing to follow furrows. For multiple reasons, this typical field design could not be utilized for a high-throughput phenotyping project that used an in-field ground vehicle that must follow furrows. First, the furrow irrigation method would not be compatible with an in-field ground vehicle that needed to enter the field multiple times per week. The furrow irrigation method wets the plant furrows to saturation according to the desired watering schedule. However, a ground-based high-throughput phenotyping vehicle would not be able to traverse the field several times per week without getting stuck, risking damage to the onboard sensors or causing soil compaction. For the vehicle to safely traverse the field, required the furrows to be relatively dry, to protect the sensors and

electronic components of the system, which meant both furrow irrigation and overhead sprinkler irrigation were not possible. With this field constraint, the only irrigation method that was compatible with the high-throughput phenotyping system was subsurface drip irrigation. Subsurface drip irrigation utilizes underground drip tape buried 8-12 inches beneath the surface of the soil, which meant the irrigation hardware was out of the camera views. The subsurface drip was also ideal because it used flexible irrigation pipes at the headlands instead of rigid polyvinyl chloride (PVC) pipes to connect irrigation lines to the main pipe. Flexible irrigation pipes are flat when there is no water running through them, which made it possible for the vehicle to drive over them at the beginning of each row. The subsurface drip irrigation method made it possible to keep the fields dry, which allowed the ground-based vehicle to enter the field independent of the irrigation schedule.

Another field modification that made high-throughput phenotyping feasible was creating a long and narrow field, having few rows with many plants in each row. The traditional short-row and wide field design at UC Davis was often used to accommodate large numbers of small research studies and furrow irrigation, having shorter rows allowed the furrows to have an even amount of flooding throughout each row. Since the irrigation method was not constrained to furrow irrigation, it was possible to create drip irrigated long and narrow fields. To increase field efficiency, it was important that as much time as possible spent driving was also spent imaging the field, which meant minimizing the amount of time driving in the headland areas that had no plants. For a ground-based vehicle this meant reducing the number of turns needed to traverse an entire field and minimizing the amount of time needed to travel between fields. The most ideal field layout for a ground-based imaging vehicle would be one long row, however this layout would not be feasible on a research field. The long narrow fields were ideal for this operation

because the vehicle could capture data for longer periods of time before needing to drive in the headlands to travel between fields or make a turn.

The long and narrow field layout used in this study was consistent with a standard in-field plant breeding layout. This layout is consistent with standard pepper and tomato growing practices done in California [58], [63].

4.5. Results

The final high-throughput phenotyping system was often called “The Driving Ice Cube”, because of the corrugated white plastic covering the sensor suite. It was also called “The Spider”, because of the manufacturers name, and the arches inside made it look like it had many arms. The HTPP system was able to image Solanaceae plants throughout the growing season without disturbing the plants.



Figure 12: HTPP system sitting in the pepper breeding trial, the white corrugated plastic is covering the sensor suite.

The HTPP system was able to collect 2D images throughout the growing season, including both color (Figure 14) and infrared (Figure 13) images. These high-quality images were used for neural network development and training for high-throughput phenotyping [64].



Figure 13: example of a pseudo-infrared image taken with the HTPP system of a tomato plant. The fruit that appear “yellow” are actually green fruit and the “red” foliage is actually green.



Figure 14: Example of an RGB image taken with a top view camera from the HTPP system.

Data collected from the time-of-flight cameras were used to estimate the height, width, and volume of plant-plots throughout the growing season [52]. This data was able to show plant growth habit and the strength of the plants to withstand fruit load.

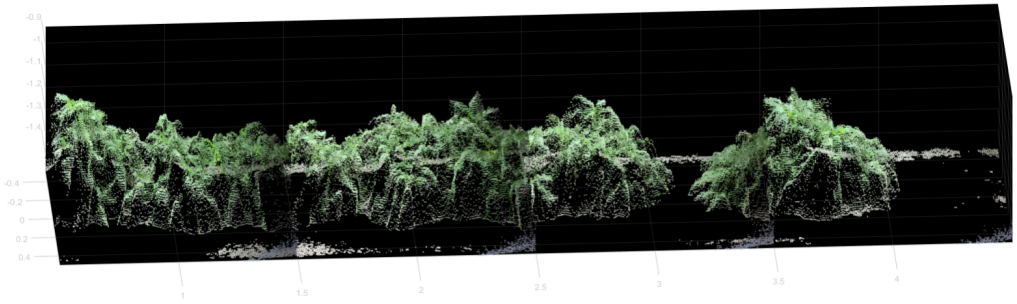


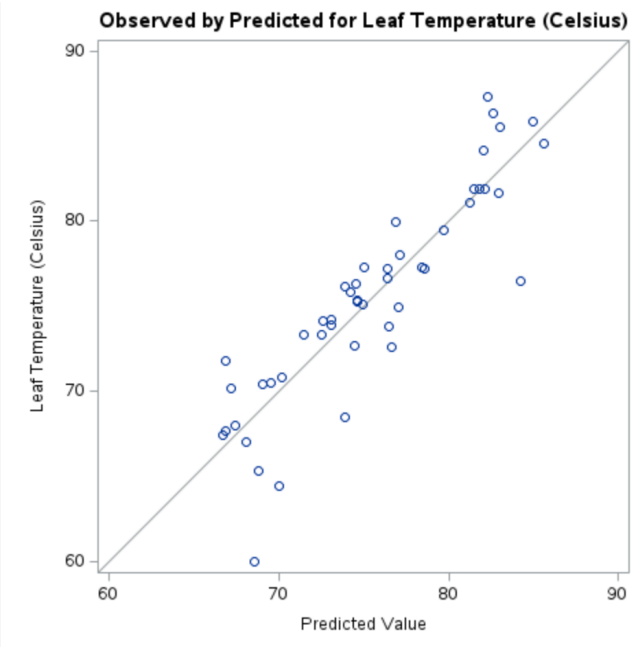
Figure 15: Example of a 3D point cloud representing pepper plants in the HTPP system, taken with the Kinect ToF sensor.

Interior phenotyping in horticultural crops, such as peppers need a multi-view camera system because how the plants tend to grow. In peppers, the pepper fruits hang toward the bottom and can often grow close to the ground and are covered by the canopy above it. The multi-view system is necessary in this case to see the fruit that are occluded by the canopy. In Figure 16, some of the fruit are completely invisible in the images that are looking from above, but as the camera moves down toward the ground more fruit become visible. If only a top camera or one side camera was used many fruits would not be seen.



Figure 16: Images of the same plant from the 9 different cameras of the multi-view camera system, certain objects can only be seen in certain images.

The temperature calibration was conducted using multiple linear regression, Figure 17. The two independent variables were the temperature values predicted from the two temperature sensors mounted on the HTPP system and the dependent variable was the actual leaf temperature measured manually. The actual leaf temperature was obtained by inserting a needle thermocouple in a leaf of a pepper plant in the field that was near the top and exposed to the sunlight. The HTPP system was stationary above each plant was not moving while the temperature was recorded. A statistically significant (p-value < 0.0001) linear association between the sensor data and the actual leaf temperature was obtained by calibrating the system. The coefficient of determination was high at $R^2 = 0.79$.



Analysis of Variance					
Source	DF	Sum of Squares	Mean Square	F Value	Pr > F
Model	3	1428.12944	476.04315	56.66	<.0001
Error	44	369.69662	8.40220		
Corrected Total	47	1797.82607			

Root MSE	2.89865
Dependent Mean	75.42167
R-Square	0.7944
Adj R-Sq	0.7803
AIC	155.99112
AICC	157.41969
SBC	113.47593

Parameter Estimates					
Parameter	DF	Estimate	Standard Error	t Value	Pr > |t|
Intercept	1	-21.195034	36.781345	-0.58	0.5674
Top Sensor	1	1.020326	0.534000	1.91	0.0626
Angled Sensor	1	1.193910	0.628279	1.90	0.0640
Top Senso*Angled Sen	1	-0.011025	0.008457	-1.30	0.1991

Figure 17: Calibration data and results for leaf temperature using two infrared temperature sensors mounted on the HTPP.

4.6.Experimental Field Design

In 2018 the pepper breeding trial had 16 genotypes, and the tomato breeding trial had 30 genotypes. In 2019 the pepper breeding trial had 16 genotypes, and the tomato breeding trial had 40 genotypes. There were two different treatments applied to the in-field growing conditions, full irrigation and an irrigation deficit. The overall field layout is shown in Figure 18.

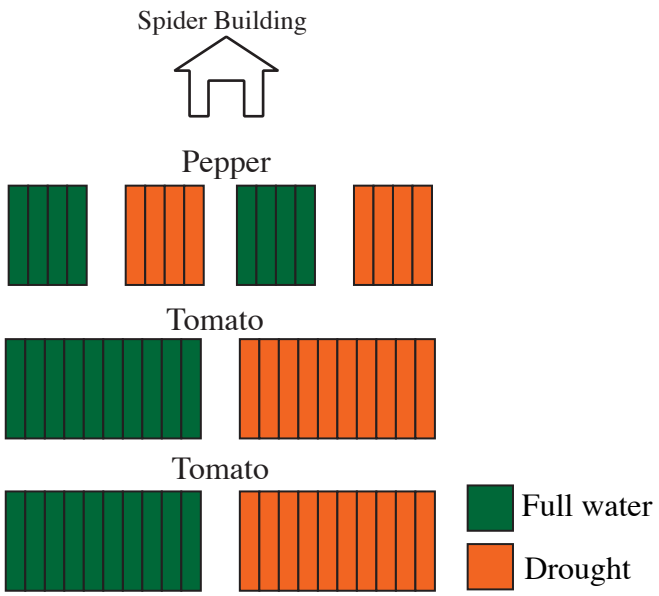


Figure 18: Overall HTPP field layout in 2018 and 2019 for both pepper and tomato breeding trials.

4.6.1. Pepper

In 2018 and 2019 the pepper breeding trial had 16 genotypes. There were two irrigation treatments in the experiment, full irrigation and irrigation deficit. The experimental design was an approximated agricultural split-plot design, created by the plant breeder. The pepper field had 4 main-fields, divided into two sets of whole-plots with full irrigation and two sets of whole-plots with deficit irrigation, shown in Figure 19 as green or orange, with 4 rows within each whole-plot. The physical separation and co-location of the whole-plot treatments was a hold-over from the historical use of furrow irrigation that affects adjacent planting beds. The 2018 and 2019 trials were placed in different locations on the UC Davis campus research farm. Within each whole-plot there were 4 blocks, shown in Figure 19 outlined in dark blue, each containing 16 genotype-plots, shown in Figure 19. Each genotype is randomly assigned to one of these plots within each block, allowing 8 replicates of each genotype for each treatment.

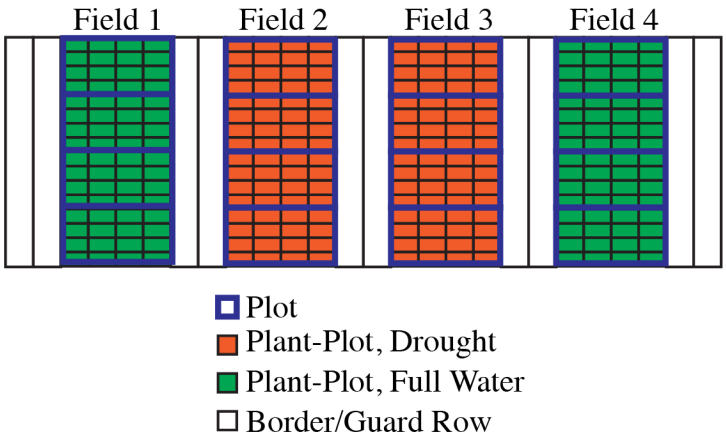


Figure 19: Graphical representation of the 2018 and 2019 pepper breeding trial.

4.6.2. Tomato

In 2018 the tomato breeding trial had 30 genotypes. Similar to the pepper trials, there were two applied irrigation treatments in the experiment, full irrigation and irrigation deficit. The experimental design was created by the plant breeder was an approximate agricultural split-plot for the same reasons as discussed in the pepper trials. The tomato field had 4 main-fields, two with full irrigation with deficit irrigation, shown in Figure 20 as green or orange, with 10 rows within each main-field. Within each main-field there were 4 blocks, shown in Figure 20 outlined in dark blue, with 30 plant-plots, shown in Figure 20with either green or orange outlined in black. Each genotype is randomly assigned to a plant-plot within each block, allowing 8 replicates of each genotype for each treatment.

In 2019 the tomato breeding trial had 40 genotypes. There were two irrigation treatments in the experiment, full irrigation and irrigation deficit. The experimental design was an agricultural split-plot. The tomato field had 4 main-fields, two main-fields with full irrigation and two main-fields with deficit irrigation, shown in Figure 21 as green or orange, with 10 rows within each main-field. Within each main-field there were 4 blocks, shown in Figure 21 outlined in dark

blue, with 40 plant-plots, shown in Figure 21 with either green or orange outlined in black. Each genotype is randomly assigned to a plant-plot within each block, allowing 6 replicates of each genotype for each treatment. The 2018 and 2019 trials were placed in different locations on the UC Davis campus research farm.

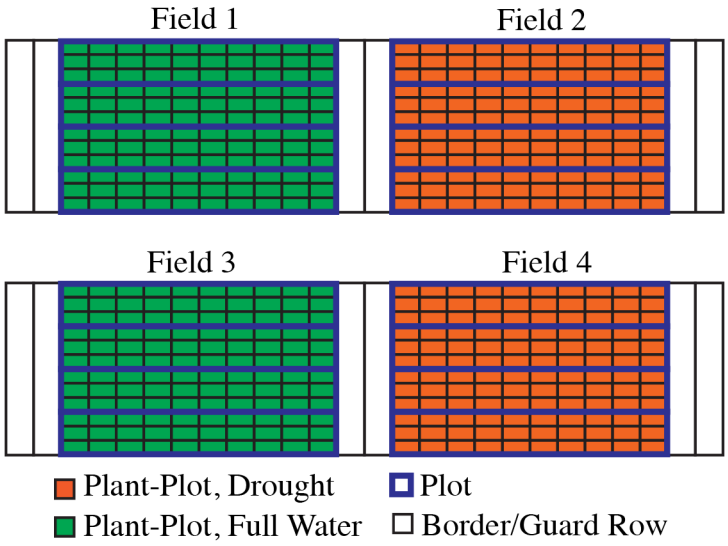


Figure 20: Graphical representation of the 2018 tomato breeding trial.

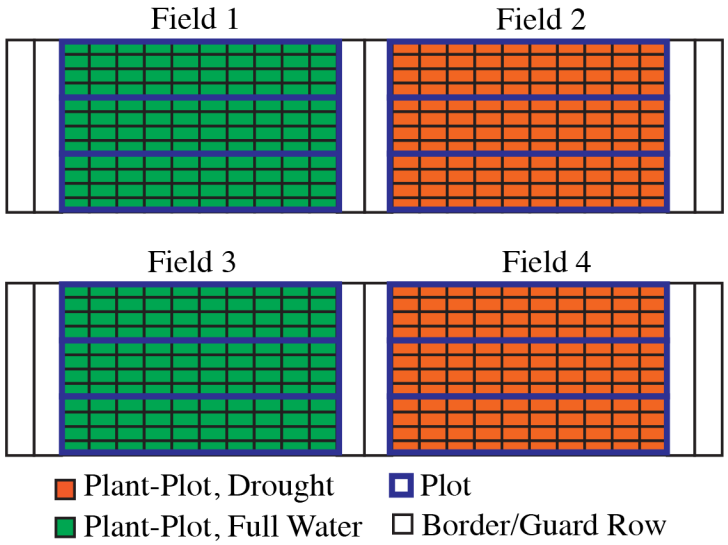


Figure 21: Graphical representation of the 2019 tomato breeding trial.

For both the pepper and tomato fields, the beginning and end of each row had guard plots to mitigate edge effects, genetically consistent with the guard rows dividing the drought and non-drought sections. The guard rows within the field were utilized to provide a physical space between the two irrigation treatments. If a pipe burst in the non-drought section of the field water might flood into the drought section of the field, compromising the treatment. The guard rows created a physical buffer space between the two treatments, allowing some time to shut off the water before the flooding affects the drought treatment.

4.7.Irrigation

The deficit irrigation reduced the amount of water applied to each row by 50% and started when all of the plants in a main-field expressed Day of First Ripe Fruit. The breeder planned irrigation deficit treatment in practice failed for this project. In both 2018 and 2019 there were extreme weather events that occurred during important points in the growing season. In 2018 there was a summer rainstorm that occurred 3 weeks after the plants were transplanted. Even with subsequent hot and arid weeks, this resulted in in saturated soil for most of the growing season, negating any effects of the simulated drought. In the 2019 growing season there was an extreme heatwave toward the end of the growing season. The heatwave resulted in two things, a reduction of severity of the drought simulation and an earlier harvest date. The reduction of severity of the drought simulation was a decision that was made to preserve plant health and insure most of the plants would survive through harvest. This reduction made it so that the drought plants only received deficit irrigation for a total of 2-3 weeks. Finally, moving up the harvest date meant the plants couldn’t experience drought conditions for very long.

4.8.Field Performance

As previously stated, the fields were oriented in a North-South configuration so the sunlight would not enter the sensor chamber throughout the day. The sunlight was also diffused using corrugated white plastic sheets to cover the chamber and sunshades at the entrance and exit of the chamber. The North-South field configuration coupled with the plastic sheet and sunshades was successful in preventing harsh sunlight from entering the chamber. However, the field configuration allowed for North winds, typical of Davis CA, to enter the chamber during imaging. The concern about this was wind creating plant movement during image capture, and potentially creating motion blur in the image. Analysis of the image data collected showed that the wind effect ended up being negligible because the shutter speed (1/2000 seconds) was fast enough to avoid any motion blur. Additionally, there was already movement made by the vehicle driving over the plant-plots which also required the high shutter speed and made the wind movement unnoticeable.

The original intention of the high-throughput phenotyping project was to allow a vehicle to enter the field and collect data 3 days a week for about 3 months, from transplanting to destructive harvest. In practice this was not feasible. The irrigation schedule for the field was every Monday, Wednesday, and Friday in the morning and Tuesday and Thursday in the afternoon. That meant on Monday, Wednesday, and Friday mornings the field was not available for the vehicle to enter, because it risked damaging the irrigation lines at the headlands and within the rows. So, the vehicle was scheduled to enter the field every Tuesday and Thursday 10AM-2PM, before the scheduled afternoon irrigation. Additionally, the combination of buried irrigation lines and unattended irrigation events sometimes produced water leaks in the field that accidentally flooded the field. When the field was too moist on the surface or below the surface it created

terrain that prevented the HTPP system from traversing the field. When there was standing water in the field it could damage the sensors during scanning as well. Thus, the field data collection plan was altered accordingly.

4.9.Data Collection

Each complete field scan using the HTPP system lasted about 4 hours and resulted in about 500 gigabytes of raw data collected. The total data collected was about 20 gigabytes per DSLR camera and 100 gigabytes per Kinect camera, totaling to about half a terabyte per day and 1 terabyte every week. Each DSLR camera had a 64 gigabyte SD-card installed in it. At the end of each field scan the SD cards were removed from the DSLR cameras to transfer files from the SD card to a computer. Due to the large amount of data, each SD card took about 20 minutes to transfer from SD card to the computer hard drive. Every scan date took about 6 hours to move files onto the computer hard drive. Each scan was also uploaded to an online server for redundancy. The Kinect data was saved directly onto a solid-state drive (SSD) in the computer on the HTPP system. The field location where the HTPP system was housed did not have internet access, so the data was transferred from the SSD to an external hard drive and uploaded to an online server after every field scan. Future research and development is needed to automate data transfer from camera to online server in order to achieve the high-throughput goal of the system.

4.10. Final Design

The final design for the high-throughput phenotyping system consisted of a high clearance tractor fitted with 9 color DSLR cameras, 9 pseudo-NDVI cameras, 2 Time of Flight cameras, 2 temperature sensors, 8 custom LED modules, 1 RTK-GPS, 1 National Instruments High Speed

Controller, 1 Dell desktop computer, and 1 National Instruments USB controller. The system was custom created to fit in a standard breeding trial for processing tomatoes in Davis, CA and look for interior and exterior traits related for processing tomato phenotypes. The system was able to successfully collect the desired multi-sensor data from a moving vehicle an in-field breeding trial designed by a plant breeder. The system was able to collect the data non-destructively without human interaction required in traditional manual phenotyping.

5. Chapter 2: Machine learning for plant component detection in high-throughput phenotyping of tomato.

5.1. Introduction

In-field breeding trials are important for plant breeding because it allows for the expression of phenotypes based on both biological and environmental factors. It is necessary to look at how plants would grow on a production level in real world conditions. Current in-field phenotyping methods ask humans to identify plant traits that are expressed in each plant variety. However, because of the time-consuming nature and physical rigor required for plant phenotyping for humans, plant traits are often simplified for humans to detect them quickly and efficiently. With the development of image processing techniques, decreasing costs of high-resolution cameras, and increasing efficiency of computer and graphics processing, using 2D images for plant phenotyping has become a viable option for plant breeding [65].

In this study we looked at the use of 2D images collected from a single camera from the high-throughput phenotyping system for phenotyping for processing tomatoes in an in-field breeding trial. The data analyzed was collected on a traditional crop breeding trial at the university research field at UC Davis during the summers of 2018 and 2019. Manual phenotyping that was performed concurrently during both growing seasons was compared to the results from the high-throughput phenotyping system.

5.2. Literature Review

5.2.1. Traditional Plant Breeding Methods

Plant breeding has an important role in providing food security to the world. Plant breeding is the process of changing traits in plants to produce new desirable traits. Over the past century, several

methodologies and technologies, including biotechnology, have been developed and adapted by plant breeders to expedite crop cultivar development [66]. As methodologies, techniques, and technologies improve for cultivar development, the overall goal of sustaining a growing global population by increasing agricultural productivity (improving yields, increasing nutritional qualities, decreasing the levels of resources required for growth, etc.) with continual development of superior cultivars remains unchanged [19]. Plant breeding was revolutionized with the creation of transgenic plants with Agrobacterium and the invention of restriction fragment length polymorphism (RFLP). Coupling together Agrobacterium and RFLP, the total number of genetic markers available to plant breeders increased, creating the first marker-assisted selection (MAS) methodology and facilitating first generation sequencing [20]. Plant breeders use the MAS systems to create high-resolution genetic maps and relate genetic markers to crop traits [2].

A new technology called CRISPR (clustered regularly interspaced short palindromic repeats) has a promising use in the future for plant breeding. CRISPR/Cas9 is a Type II prokaryotic adaptive immune system has been shown to facilitate in precise site-specific DNA cleavage [21]. This new technology utilizes Cas9 nucleases, a protein that has a vital role in the immunological defense of bacteria against DNA viruses. CRISPR is not currently accepted as a method for genetic modification of food crops and is not available in the market, but with the future development of rules and regulations may lead the next genetic revolution [22].

5.2.2. Traditional Plant Phenotyping Methods

Cultivar breeding requires a feedback mechanism called phenotyping to allow breeders to understand how different genotypes perform under different environments or locations. In-field phenotyping requires thousands of plants to be grown in commercial field conditions across a

range of environmental conditions like different elevations or latitudes, sunlight levels, and soil composition [67]. Multiple phenotypes must be assessed for each plant and potential cultivar, including: temporal phenotypes (day of first green fruit, day of first ripe fruit), growth habit phenotypes (e.g. plant height, plant width, canopy density), and external phenotypes (e.g. fruit yield, fruit quality, abiotic stress tolerance) [68], [69]. Current phenotyping methods for cultivar breeding trials are done manually by humans. During the growing season humans will go into the field periodically to observe these traits. This often includes manually manipulating the plants to look at the internal structure or searching for flowers and fruit and destructive phenotyping at harvest. This method of human-based phenotyping is costly, labor- and time-intensive, subject to human error and fatigue, and does not always allow (or is cost prohibitive) for repeated measures on the same plants over time.

5.2.3. Importance of Solanaceae Crops

Vegetable production in the US is a $13 billion industry, with California making up $7.3 of the industry in both fresh market and processed produce. California continues to be the leading state in vegetable crop land area harvested, utilized production, and value of production, with 39.1%, 57.3%, and 56.7%, of the total in the US respectively. The largest vegetable crops by acreage are potato, lettuce, sweet corn, and tomato. Major vegetable crops in the Solanaceae family include pepper, tomato, and potato. This family is the third most economically important food crop plant taxon, after Brassicaceae and Poaceae [70].

In the United States, approximately 90% of processing tomatoes are grown in California [15]. In Californian tomato production, approximately 125-250 pounds of nitrogen, 40-120 pounds of phosphorus, and 0-200 pounds of potassium per acre are required in order to produce a

commercially viable crop [16]. All processing tomatoes in California are mechanically harvested occurring when at least 90% of fruit in a field is ripe.

In the United States, approximately 39% of chili peppers are grown in California and 54% are grown in New Mexico [17]. Chili peppers are direct seeded or transplanted into raised beds throughout California. Peppers require moderate to high rates of fertilizer, requiring 80-200 pounds of preplant phosphorus, 50-150 pounds of potassium, and 250+ pounds of nitrogen per acre. Chili peppers are usually harvested green before the development of the mature color; most harvested chili peppers in California are used for processing into salsa or are canned whole [60]. All chili peppers in California are hand-harvested two to four times in 10- to 15-day intervals.

5.2.4. High-Throughput Phenotyping Methods

The development of in-field phenotyping technology lags behind that of genomics, creating a bottleneck in plant breeding [2], [3]. The key objective of high-throughput phenotyping is the ability to non-destructively, objectively, and quickly characterize plant traits [23]. Automated phenotyping utilizes various non-contact sensors to estimate traits such as biomass, yield, plant height, leaf segmentation, leaf area, and canopy temperature [24], [25], [26], [27]. Non-destructive phenotyping also permits a time-series approach that follows the growth of plants over time. Different systems have been developed for in-field phenotyping using permanent fixed-site platforms, unmanned aerial vehicles (UAV) including satellites, and terrestrial vehicles, all fitted with various sensors to collect a range of phenotypic data [28], [29], [30]. Regardless of platform type, the goal is to automate and expedite the acquisition of plant phenotypes and relate them to genotypic data to find superior breeding lines and cultivars more quickly [31].

5.2.5. Phenotyping using Image Analysis

Currently non-destructive high-throughput phenotyping methods focus on traits that are quantifiable and compared to manual phenotyping [71]. This includes traits such as total harvest yield in economically important or staple crops like wine grapes, beans, maize, citrus, and tomatoes[38], [41], [72], [73], [74] .These methods include using neural networks and traditional image analysis methods to compare yield and object or pixel count. These studies rely on comparing detected crop to crop yield at harvest. These crops are mechanically harvested with either an onboard yield monitor or postharvest yield monitor. Other phenotyping methods look at images to detect late-stage diseases present on leaves, where images are collected, and plant breeders are asked to classify the specific plants in images [75]. These phenotyping project take images at a single point in the growing season to determine different traits. Another style of high-throughput phenotyping development utilizes controlled environments such as greenhouses, synthetic images, and object specific analysis [76], [77], [78], [79]. Controlled studies are essential for the first stage of developing new crop cultivars, as they can eliminate environmental factors that may affect plant growth, allowing plant breeders to see genetic factors more easily. However, these crop cultivars need to be observed in in-field breeding trials to simulate real growth habits.

5.3.Materials and Methods

5.3.1. Experimental Design

The high-throughput phenotyping system was tested in a Solanaceae breeding trial in an experimental university research field in Davis, CA during June 2018 – August 2018 and June 2019 – August 2019, to replicate real world growing conditions. In this study we focused on the economically important Solanaceae crop processing tomatoes. In 2018 the tomato breeding trial

had 30 genotypes. In 2019 the tomato breeding trial had 40 genotypes. There were two different irrigation treatments applied to the plants, full irrigation and irrigation deficit. The experimental field was approximately 1.5 acres with approximately 256 pepper plant-plots with 8 plants and 480 tomato plant-plots with 8 plants.

5.3.2. Data Collection

The high-throughput phenotyping system collected data in the experimental research field twice a week for the entire growing seasons in both 2018 and 2019. The original intention was to drive from the North end of the pepper field to the south end of the tomato plots and back up, to reduce the amount of turning in the headlands. However, due to leaks in the buried irrigation lines the border rows were often flooded, and it wasn't possible to drive through the pepper border rows to the tomato fields. First the pepper field was imaged and then both tomato fields were imaged. This resulted in about 400 gigabytes of image data from 18 DSLR cameras (saved to a removable SD card) and 150 gigabytes of depth and depth-color images from 2 time-of-flight cameras (saved to a computer solid-state hard drive) every day. At the end of imaging the SD cards were removed for file transfer and the solid-state hard drive was copied to an external hard drive for data transfer and processing in an indoor facility. At the end of each growing season, we accumulated about 15 terabytes of data. In this study we will be focusing on the image data collected from the DSLR cameras.

5.3.3. Data Transfer

Each DSLR camera had its own labeled 64 gigabyte removable full-sized SD card (Sandisk Extreme 64 GB, SanDisk LLC, Milpitas, CA). The data transfer process started with removing the SD cards form the cameras and transporting them to a different facility. This facility housed two personal computers for file transfer, 1 computer for the time-of-flight data and 1 computer

for the DSLR camera images. The computer had two USB-A to SD card readers attached to it, because the computer had two USB 2.0 hubs, we were able to transfer the data from two SD cards at the same time. The limiting factors for transfer speed were the read speed for the SD Card (170 MB/second) and the write speed for the hard-drive (100 MB/second). It took 2.5 hours to transfer data from two SD cards to the computer hard-drive. From the computer hard-drive the data was moved into a .7z folder for lossless image compression and to upload onto an online server. The online server was a backup for the data and to allow multiple people to access the data remotely.

5.3.4. Data Processing

The data structure format followed Table 2. The first folder was NN_Month_Day, where here NN = Data collection number, month = month of data collection, day = day of data collection. Within each data collection date folder is a folder for each camera, CL = color camera and IR = infrared camera. The cameras are labeled 01-09 based on the position of the camera relative to facing the same direction as the drivers' seat. Cameras with the same number were placed in the same location perpendicular to the plant row, with the color camera in front of the IR camera. Within each camera folder were the images from data collection, they were named IMG_MMMM.jpg, where MMMM is a sequence number. The images were labeled sequentially as they were taken.

Table 2: The file-folder tree for how the images were transferred to the computer and uploaded onto the online server.

NN_Month_Day	↓	
NN_Month_Day	CL_01	↓
NN_Month_Day	CL_02	IMG_MMMM
NN_Month_Day	…	IMG_MMMM+1
NN_Month_Day	CL_08	IMG_MMMM+2
NN_Month_Day	CL_09	IMG_MMMM+3
NN_Month_Day	IR_01	IMG_MMMM+4
NN_Month_Day	IR_02	IMG_MMMM+5
NN_Month_Day	…	IMG_MMMM+6
…	IR_08	IMG_MMMM+7
	IR_09	…
		IMG_MMMM+X

Each of the images has inherent metadata associated with it including, date and time of image capture to the microsecond precision. Each DSLR camera has an internal calendar and clock that can be set either manually or synchronized with the internet. At the beginning of each season each cameras' clock was changed manually. The metadata for each image for image capture was relative to the camera clock. Knowing the time each image is captured and knowing the path the system drove we can georeference images to plant-plot locations. This was automatically done for each camera on each date and this folder structure (Table 3) was uploaded to the online server.

Table 3: Table describing the file-folder structure after the images were sorted into plant-plots.

NN_Month_Day	↓		
NN_Month_Day	19FD0001	↓	
NN_Month_Day	19FD0002	CL_01	↓
NN_Month_Day	19FD0003	CL_02	IMG_MMMM
NN_Month_Day	19FD0004	…	IMG_MMMM+1
NN_Month_Day	…	CL_08	IMG_MMMM+2
NN_Month_Day		CL_09	IMG_MMMM+3
NN_Month_Day		IR_01	IMG_MMMM+4
NN_Month_Day		IR_02	IMG_MMMM+5
…		…	IMG_MMMM+6
		IR_08	IMG_MMMM+7
		IR_09	

5.3.5. Object Detection

The classifier used in this study was an object detection neural network, which takes an image and locates, labels, and classifies specific objects in an image. Object detection neural networks consist of interconnected nodes that extract important information and pass the information to more nodes in new layers, to converge into detecting and classifying objects. An important part of neural network development is training. Most published neural networks are trained on large datasets like the Common Objects in Context (COCO) dataset, which consists of over 300,000 images including object boxes with 80 categories [80]. The COCO dataset has the objects of interest saved as a polygon with vertices (X, Y), a color in HTML HEX, and an object label. To use neural networks for more specific uses, like detecting objects not defined in the COCO dataset, it is necessary to train neural networks on images that have those specific objects labelled. This allows the neural network to retrain itself and tune the nodes and layers to be able to detect new objects.

In this study an open-source framework for object detection was used called detectron2 (detectron2, Facebook AI Research, Menlo Park, CA). Detectron2 is built on top of PyTorch, a Python library that has neural network training, testing, and development tools and models that were pretrained on COCO for image segmentation and object detection. The detectron2 framework was picked because it is open source and had accessible tools for retraining neural networks using new categories and images. From detectron2, the model Mask R-CNN-ResNet-101 (Mask R-CNN, Facebook AI Research, Menlo Park, CA) was chosen as the backbone for the neural network [81]. Mask R-CNN was trained on the COCO dataset, scoring an average 33.1% average precision on COCO test dataset for object detection and classification.

5.3.6. Data Labeling

To retrain Mask R-CNN it was important to have high-quality labeled images that represented the objects of interest, flowers, green fruit, ripe fruit, and sunburnt fruit. The datasets used to train and validate the model were hand-labeled by workers from Amazon MTurk. The workers were tasked with labeling the flowers, green fruit, ripe fruit, and sunburnt fruit in 213 images from the end of the 2018 growing season. Amazon MTurk workers manually labelled these objects in each image using a paint brush tool. The paint brush tool was used because it allowed the workers to label objects at the pixel level. Pixel level labelling is important for flower detection because an individual petal could be as little as 40 pixels wide, requiring highly accurate masking. Semantic masks were used so individual objects of the same class would have their own unique identifier. After the images were labeled, the images were split into 3 datasets, training, validation, and test. The 2018 dataset was randomly split by allocating 70% of images for training, 20% of images for validation, and 10% of images for testing, resulting in 149, 42, and 22 respectively.

Each image that was labeled from Amazon MTurk had 2 parts to it, a Base64 encoded image in the form of a string and a table with a color in HEX code and an associated object label. First, the image was decoded using a Base64 decoder and renamed according to what image it related to. Next each polygon was associated to an object label based on the HEX color code. These masks translated into a COCO dataset compatible file (TomatoCOCO) that could be used to train models that were pretrained on the COCO dataset. The COCO dataset file needed to contain 4 specific things the image names and file locations, the vertices of the polygons associated with each image, a key relating the polygons to objects, and which labels need to be detected. This was done for both the training, validation, and test datasets. An additional 19 images were labeled from the same date in 2018 to increase the amount of test images to 41. The test dataset in this case was not used during training, it was used for visual confirmation that the model was working. This was called the 2018 Training, Validation, and Test sets.



Figure 22: Example of a masked image processed from base64 encoding. Each polygon represents a masked object of interest.

5.3.7. Model Training

Mask R-CNN was retrained using the TomatoCOCO labeled dataset. The settings for training Mask R-CNN were 300 epochs, with a learning rate scheduler at 50 epochs, and a starting learning rate of 0.25 to 0.1. First, in the training step the neural network initializes weights and biases from previous training, which will be updated during training. Next the images from the training dataset are input into the neural network, where it tries to detect the objects of interest and categorize them. It then uses the known masks and labels to calculate error and adjusts the weights of the neural network accordingly. The new weights are then used to detect the images in the validation dataset, data that the neural network was not trained on. The validation dataset

score is used to decide if the new weights improved performance or not. If the validation dataset score is worse, it uses the old weights and if the validation score is better, it keeps the new weights. These steps are iterated 300 times and took 8 hours to finish training the model. At the end of training, the test set was held back and used to visually determine the performance of the model. One measure was taken to prevent overfitting during training, which was adding random dropout for 1% of the nodes in the first 50 epochs of training. Due to the small training dataset more steps should have been taken to prevent overfitting during training.

5.3.8. Model Performance

Model performance was calculated using two metrics, Average Precision (AP) (Eq. 6) and Average Recall (AR) (Eq. 5). AP and AR look at the Intersection of Union (IoU) (Eq. 4) of predicted boxes and ground truth boxes of an object and the classification label. Performance was quantified using average precision (AP) at intersection over ten union (IOU) values ranging from 0.5 to 0.95 in increments of 0.05 (mAP@0.5:0.95) over all classes as well as for each individual class. mAP at an IOU of 0.5 (mAP@0.5) was also calculated. AP is the metric used for Average Precision of one class and mAP is the metric used for Average Precision of multiple classes. These metrics were determined for each scan date individually, as well as averaged over all dates. These performance metrics were not used during training, the metrics used during training were the loss functions embedded in Mask R-CNN.

In this study, for each phenotype studied, the number and percentage of correctly and incorrectly classified objects were quantified using Average Precision (Eq. 6) and Average Recall (Eq. 5). If a predicted detection box has an overlap of at least 50% with the actual ground truth object, that means it is a true positive. Incorrectly classified objects were further labeled as false positive or false negative classifications. The metric used for characterizing the model performance was

Mean Average Precision (mAP) of mAP@0.5, which is the Mean Average Precision of detection of all object classes at 50% IoU. Another metric used for characterizing the model performance was Mean Average Recall (mAR), at 50 – 95% IoU, which is the Mean Average Recall of all object classes at 50 – 95% IoU. These model metrics were calculated on images with ground truth labels and predictions using Microsoft Common Objects in Context (COCO) evaluation metrics on a representative test set [80]. These metrics were reported on the 2018 training, validation, and test sets.

In addition to the 2018 data, an out of year test set was compiled from images collected in 2019 to simulate the case where a model trained on one year of data (2018) is applied to the following year (2019). The same IoU, AP, and AR metrics were used for this dataset. For each of the three scan dates, one image was selected at random from each of the 40 genotypes in the design, creating a test set of 120 images. These images were labeled by the author and then classification and analysis using the trained model was performed. This dataset is called the 2019 Test set.

$$\text{IOU} = \frac{\text{Area of Overlap}}{\text{Area of Union}}$$

Eq. 4

$$\text{Recall} = \frac{\text{TP}}{\text{TP} + \text{FN}} = \frac{\text{TP}}{\text{\# ground truths}}$$

Eq. 5

$$\text{Precision} = \frac{\text{TP}}{\text{TP} + \text{FP}} = \frac{\text{TP}}{\text{\#predictions}}$$

Eq. 6

$$\text{TP} = \text{True positives}$$

$$\text{FN} = \text{False negatives}$$

$$\text{FP} = \text{False positives}$$

5.3.9. Manual Phenotyping

During the growing season there were two main traits that are observed. Days to First Green Fruit (DTFG) is an important trait for plant breeders because it is the first phenotype of the season. DTFG is defined as the number of days after transplanting when 50% of a plant-plot has a 1-inch diameter green fruit. While looking for DTFG, plant breeders manipulate the plants by moving branches and leaves to look at the internal plant structure. Days to First Ripe Fruit (DTFR) is the number of days after transplanting when 50% of the plant-plot has a ripe fruit. A ripe fruit is defined as a fruit that is not green, which when squeezed has the proper texture of a ripe fruit. Like DTFG, ripe fruit must be found by manipulating the plant. Plant breeders begin to look for DTFR after 75% of the total plant-plots in the breeding field have expressed DTFG.

Prior to destructive harvest there are various traits that are observed by plant breeders. The first trait is canopy, scored on a scale of 1 – 5 based on the degree that the plants' canopy covers the furrow. The next trait is habit, scored on a scale of 1 – 5 based on the growth habit of the plant (flat and wide to tall and thin). Next is degree of sunburn, scored on a scale of 1 – 5 based on how much of the fruit canopy looks sunburnt before harvest.

During destructive harvest two of the eight (25%) plants in a plant-plot are chosen as the representative plants for a plant-plot. The two plants that were chosen by the plant breeder in this study were the second and third plants north of the southernmost plant in the plant-plot. If any of those plants are missing the next plant north is chosen. When a plant is destructively harvested, the plant is cut using plant shears at the base of the plant on the mainstem. The cut plant is turned upside-down and shaken on top of a plastic tarp to remove all the fruit, the fruit from both plants is combined into this tarp. The total mass in grams is weighed in the field on a hanging scale to find the Total Fruit Yield (TFY). Then, the tarp is removed from the scale, and the green fruit are

manually removed from the tarp and the remaining fruit reweighed for Ripe Fruit Yield (RFY), including both ripe and sunburnt fruit. Green Fruit Yield (GFY) is calculated by subtracting RFY from TFY. The remaining leaves and stems are stored and weighed for both fresh shoot weight (SFW) dry shoot weight (SDW). Destructive harvest is done for the whole field all at once, when at least 75% of the plant-plots are ready for harvest.

5.3.10. High-Throughput Phenotyping by Plant-Plot

Two full-field scan datasets were analyzed using the final trained model. The two datasets were split into the two years of scanning 2018 and 2019. For the 2018 dataset there were two dates that were analyzed and in 2019 there were 3 dates that were analyzed. To use the Mask R-CNN, the images needed to be translated into the COCO dataset format, with no labels or polygons. In total there were approximately 3,500 images per date. For each image it took about 10 seconds to detect, output, and save the number of objects detected and it took about 9 hours to complete each date. For further analysis a text file was created that saved how many of each object was detected in each image. Each text file was saved in the same folder structure as described in Table 3.

5.3.11. Comparing High-Throughput Phenotyping and Manual Phenotyping

Total fruit count from the high-throughput phenotyping system was compared to the manual phenotype total fruit yield in kilograms. For high-throughput plant-plot analysis, every other image within a plant-plot was analyzed using the Mask R-CNN model described previously and the count of each object was summed for each plant-plot. This was because two consecutive images had about 40% overlap between images, which is important for 2D and 3D image

reconstruction. But when looking at individual images within a plant-plot it would result in double or triple counting an object, overinflating the object count.

Total ripe fruit count was compared to the manual phenotype Total Ripe Fruit Yield (RFY) in kilograms and total green fruit count was compared to the manual phenotype Total Green Fruit Yield in kilograms (GFY). RFY and GFY were collected by plant breeders on a per plant-plot basis. Total ripe fruit count and RFY and total green fruit count and GFY were compared on a linear basis on count to kilograms. A linear regression model was created to see if there was any linear relationship between count and mass.

5.4. Results

5.4.1. Model Evaluation

The overall model evaluation was done twice, once using labeled training and validation data from 2018 and once using labeled data from 2019. The training and validation data were labeled using Amazon MTurk. Table 4 describes the number of flowers, green fruit, ripe fruit, and sunburnt fruit that were labeled in the 2018 training dataset. There a similar amount of green fruit (2716) and ripe fruit (2683) in the 2018 training dataset, making up 80% of the labels. Table 5 describes the number of flowers, green fruit, ripe fruit, and sunburnt fruit that were labeled in the 2018 validation dataset. About 50% of the labeled objects in the validation dataset are green fruit (846). Table 6 describes the number of flowers, green fruit, ripe fruit, and sunburnt fruit that were labeled in the 2018 testing dataset. There a similar amount of green fruit (676) and ripe fruit (696) in the 2018 testing dataset, making up 80% of the labels. Table 7 describes the number of

flowers, green fruit, ripe fruit, and sunburnt fruit that were labeled in the 2019 out of season test dataset. 68% of the 2019 out of season test set was green fruit.

Table 4: Total number of flower, green fruit, ripe fruit, and sunburnt fruit in the 2018 Training dataset.

	Flowers	Green Fruit	Ripe fruit	Sunburnt Fruit	Total Objects
Count	708	2716	2683	438	6590
					Image Count: 149

Table 5: Total number of flower, green fruit, ripe fruit, and sunburnt fruit in the 2018 Validation dataset.

	Flowers	Green Fruit	Ripe fruit	Sunburnt Fruit	Total Objects
Count	189	846	576	74	1685
					Image Count: 42

Table 6: Total number of flower, green fruit, ripe fruit, and sunburnt fruit in the 2018 Test dataset.

	Flowers	Green Fruit	Ripe fruit	Sunburnt Fruit	Total Objects
Count	187	676	696	119	1678
					Image Count: 41

Table 7: Total number of flower, green fruit, ripe fruit, and sunburnt fruit in the 2019 Test dataset.

	Flowers	Green Fruit	Ripe fruit	Sunburnt Fruit	Total Objects
Count	561	2447	358	191	3557
					Image Count: 120

5.4.1.1. 2018 Training, Testing, Validation Dataset

The overall mAP for the 2018 training data was 88.50% and the mAP@0.5 was 97.66% (Table 8). Within each class, the overall AP in 2018 was highest for the sunburnt fruit at 91.86% followed by ripe fruit at 90.46%, green fruit at 88.24%, and then flowers at 83.46%. The overall mAP for the 2018 validation data was 21.11% and mAP@0.5 was 39.76%. For the 2018 validation data, the overall AP was highest for green fruit at 32.41% followed by ripe fruit at 29.08%, flower at 19.30%, and finally sunburnt fruit at 3.65%. The overall mAP for the 2018 test data was 23.35% and mAP@0.5 was 44.01%. For the 2018 validation data, the overall AP was highest for green fruit at 38.58% followed by ripe fruit at 29.70%, flower at 20.22%, and finally sunburnt fruit at 4.90%. The overall mAP, mAP@0.5, and mAR@0.5:0.95 were calculated for each dataset. The AP@0.5:0.95 for flower, green fruit, ripe fruit, and sunburnt fruit detection for each dataset and in 2019 for each date was averaged together to get the mAP@0.5. In Figure 23, overall AP scores across all categories are higher in the training dataset than in validation and testing. Testing and validation tend to follow the same trends across all categories shown in Figure 23. Sunburnt fruit is the worst performing in AP for both testing and validation, while it's the best performing individual category in training.

The overall mAR for the 2018 training data was 91.1%, validation data was 32.3%, and testing data was 33.9% (Table 9). For the 2018 training data the AR for each object type was highest in sunburnt fruit at 94.9%, followed by ripe fruit at 93.8%, green fruit at 91.7%, and last flowers at 87.2%. For the 2018 validation dataset the highest AR for each object was ripe fruit at 46.2%, then green fruit at 43.5%, flowers at 26.9%, and finally sunburnt fruit with 12.4%. In the 2018 test dataset the AR was highest in green fruit at 48.8%, followed by ripe fruit at 48.1%, then flowers at 29.3%, and finally sunburnt fruit at 9.7%. Figure 24 shows the overall distribution for

AR across all categories, this follows a similar trend to Figure 23, where the training dataset has consistently higher values than validation and training. In testing the green fruit recall is the largest value while in validation the ripe fruit is the largest AR, though in both cases the numbers are close. Sunburnt fruit in validation and testing are the worst performing category but is the best performing category for testing in AR, similar to AP. In general, the recall scores across all categories and datasets were higher than the precision scores.

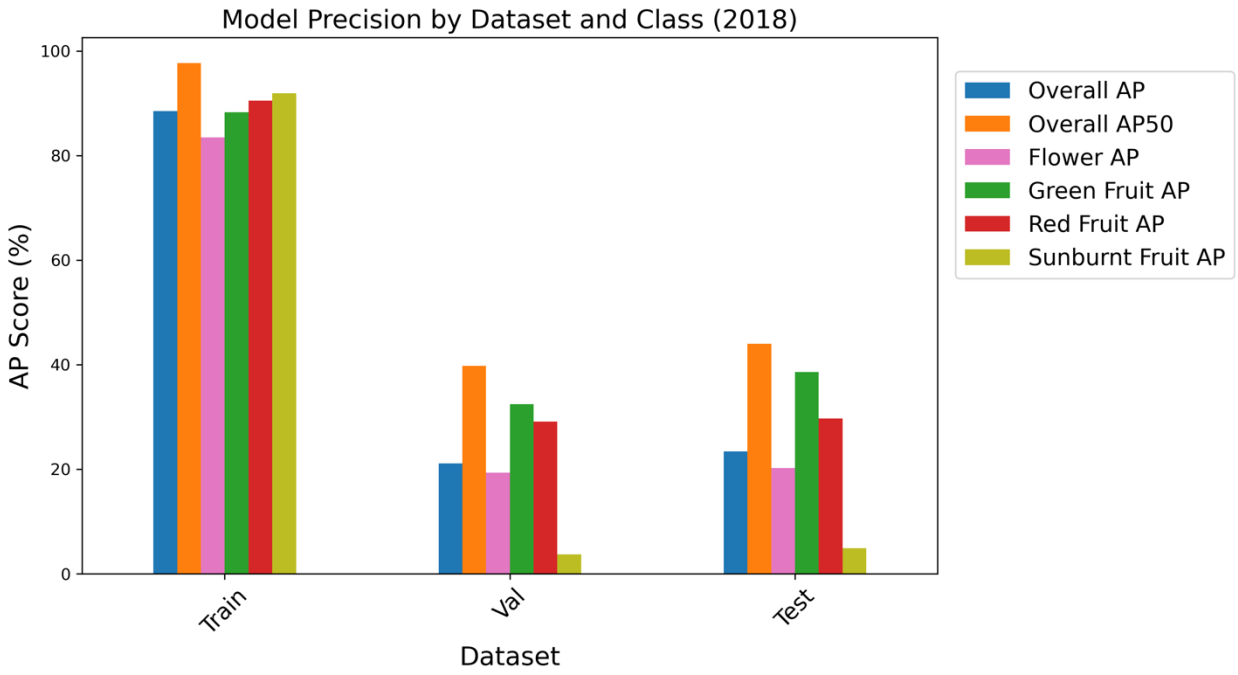


Figure 23: Performance of the model using average precision on training, validation, and testing data for 2018.

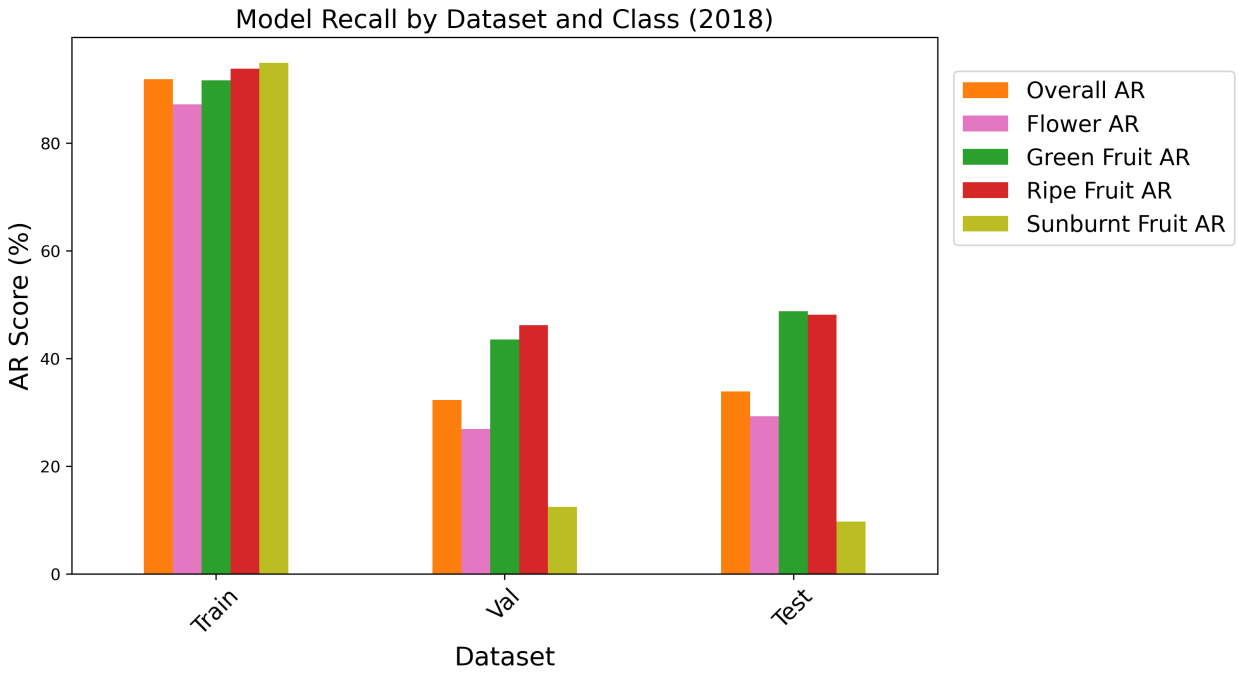


Figure 24: Performance of the model using average recall on training, validation, and testing data for 2018.

Table 8: Average precision for each training, validation, and testing data from 2018 for overall object detection and for each class.

Metric	Training	Validation	Testing
Overall mAP	88.50	21.11	23.35
mAP@0.5	97.66	39.76	44.01
Flower AP@0.5:0.95	83.46	19.30	20.22
Green Fruit AP@0.5:0.95	88.24	32.41	38.58
Ripe fruit AP@0.5:0.95	90.46	29.08	29.70
Sunburnt Fruit AP@0.5:0.95	91.86	3.65	4.90

Table 9: Average recall for each training, validation, and testing data from 2018 for overall object detection and for each class.

Metric	Training	Validation	Testing
mAR@0.5:0.95	91.9	32.3	33.9
Flower AR@0.5:0.95	87.2	26.9	29.3
Green Fruit AR@0.5:0.95	91.7	43.5	48.8
Ripe fruit AR@0.5:0.95	93.8	46.2	48.1
Sunburnt Fruit AR@0.5:0.95	94.9	12.4	9.7

5.4.1.2. 2019 Season Dataset

From Table 10, Overall mAP across all dates was 19.68%, and mAP@0.5 was 39.33%. Within each class, overall AP was highest for green fruit at 45.11%, followed by ripe fruit at 21.43%, flower at 11.16%, and sunburnt fruit at 1.0%. This pattern remained consistent over all dates. Examining performance across each date, both mAP and mAP@0.5 were highest at on June 25, 2019, with scores of 28.81% and 57.31%, respectively. On the last date, July 23, 2019, precision scores were 19.27% and 39.30%. The performance metrics of July 16 and July 23 are similar. This decline was also observed in green and ripe fruit mAP between dates, which dropped from 46.71% and 28.81% to 42.49% and 20.19% for green and ripe fruit, respectively. Flower detection AP was similar across dates, rising from 11.14% to 13.09%. Sunburnt fruit detection AP was similar across dates, rising from 0.53% to 1.31%. In Figure 25, AP scores across highest in June 25, except for flower. For individual dates and all dates, the green fruit had the highest AP.

The overall mAR for the 2019 training data across all three dates was 34.9%. (Table 11). For the 2019 testing data for all dates the AR for each object type was highest with green fruit at 61.3%, followed by ripe fruit at 52.8%, flowers at 21.7%, and finally sunburnt fruit with 3.5%. For June

25 the overall AR@0.5:0.95 for all objects is the highest among all dates with 31.8%. The object breakdown for AR@0.5:0.95 starts with green fruit at 59.8%, ripe fruit with 34.0%, and finally flowers at 20.7%. July 16 had an overall AR@0.5:0.95 of 36.4%. The individual object breakdown starts with green fruit at the highest with 62.3%, ripe fruit at 56.0%, flower at 24.8%, and sunburnt fruit at 2.6%. For July 23 the overall AR@0.5:0.95 was 35.3%. For the objects green fruit at the highest AR@0.5:0.95 with 61.6%, followed by ripe fruit at 51.8%, flower with 24%, and sunburnt fruit with 3.7%. Figure 26 shows the overall AR scores across individual dates and all dates. In this graph there is not a clear date that performs significantly better than other dates according to recall.

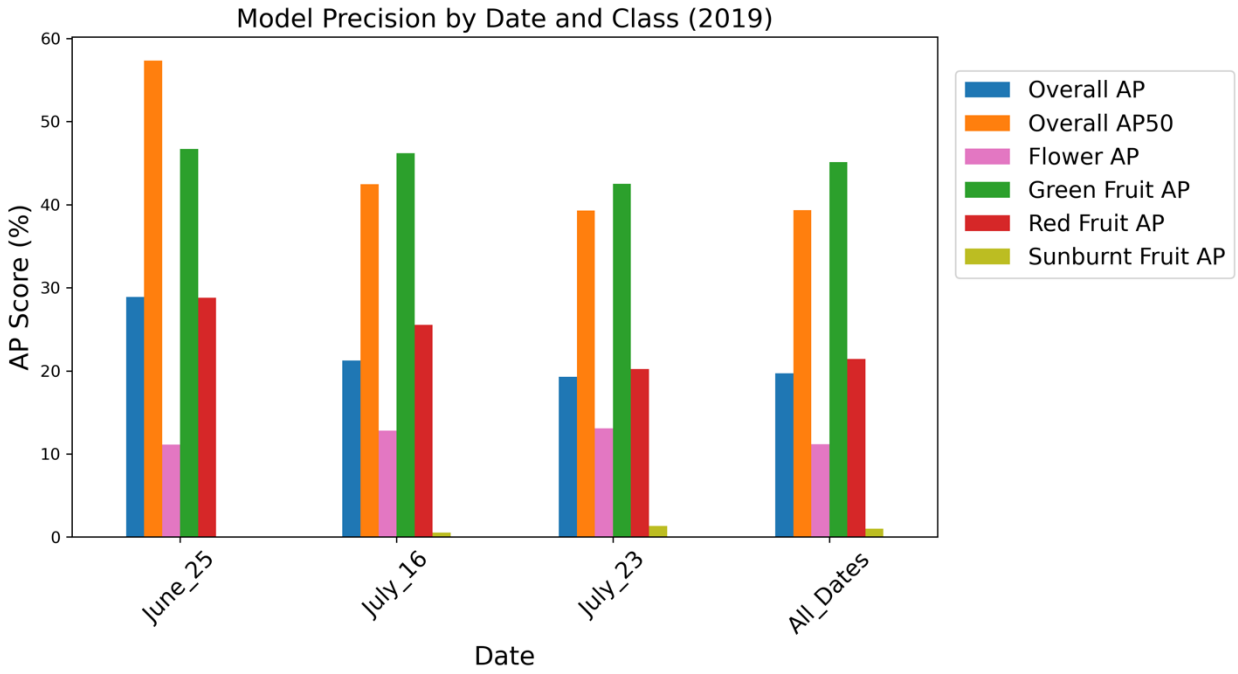


Figure 25: Performance of the model using average precision on 2019 Test data overall and per class for each scan date and for all dates together.

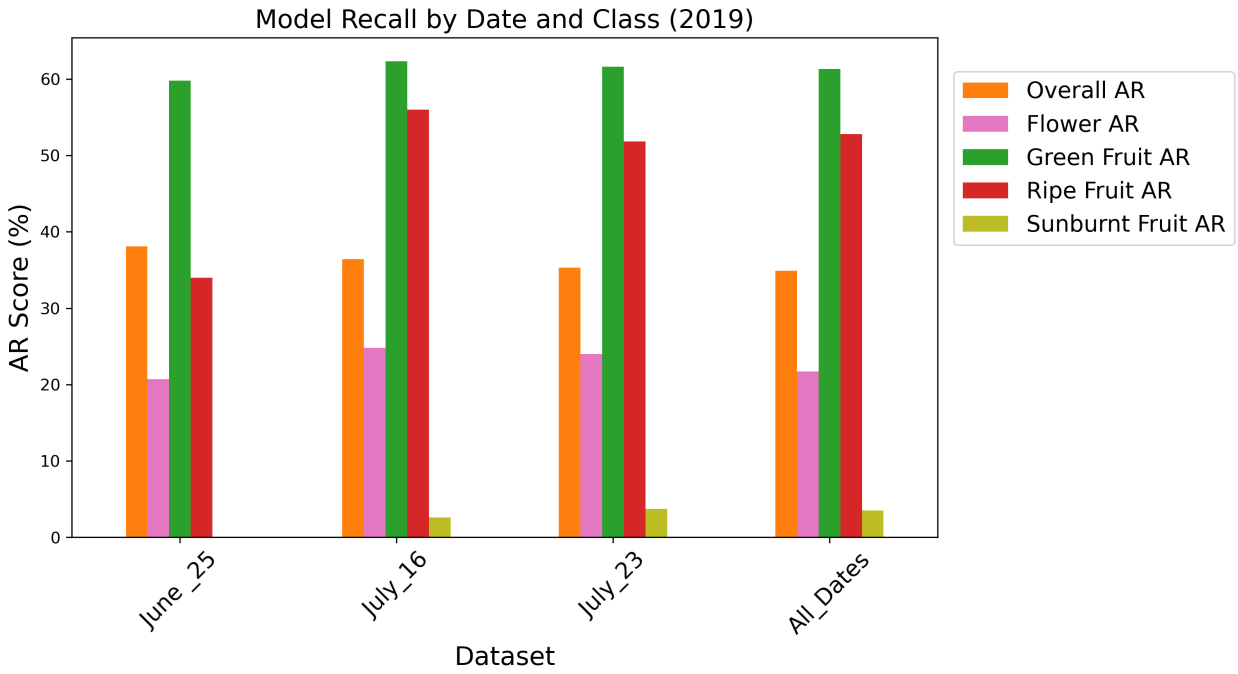


Figure 26: Performance of the model using average recall on 2019 Test data overall and per class for each scan date and for all dates together

Table 10: Average precision for the 2019 external test dataset for overall object detection and for each class

Metric	Test June 25 2019	Test July 16 2019	Test July 25 2019	All Test 2019 Dates
Overall mAP	28.89	21.25	19.27	19.68
mAP@0.5	57.31	42.44	39.30	39.33
Flower AP@0.5:0.95	11.14	12.79	13.09	11.16
Green Fruit AP@0.5:0.95	46.71	46.17	42.49	45.11
Ripe fruit AP@0.5:0.95	28.81	25.52	20.19	21.43
Sunburnt Fruit AP@0.5:0.95		0.53	1.31	1.00

Table 11: Average recall for the 2019 external test dataset for overall object detection and for each class.

Metric	Test June 25 2019	Test July 16 2019	Test July 25 2019	All Test 2019 Dates
mAR@0.5:0.95	38.1	36.4	35.3	34.9
Flower AR@0.5:0.95	20.7	24.8	24.0	21.7
Green Fruit AR@0.5:0.95	59.8	62.3	61.6	61.3
Ripe fruit AR@0.5:0.95	34.0	56.0	51.8	52.8
Sunburnt Fruit AR@0.5:0.95		2.6	3.7	3.5

The images shown in Figure 27 are example images with labeled objects from the 2018 Training Dataset. Figure 27a is the ground truth hand labeled image with the polygons as the objects labeled by humans. Figure 27b is the predicted labels on the same image using the neural network trained previously. Visually comparing the two images and labels can show what objects were correctly labeled using the neural network compared to the ground truth and which ones were incorrect. The top left corner of Figure 27a has a cluster of sunburnt fruit that was not detected in the predicted labels in Figure 27b The predicted labels also missed a big sunburnt fruit in the middle of the image in Figure 27b, labeling it as a ripe fruit instead. On the top left corner of Figure 27b there is a detected flower that was not labeled in the ground truth image of Figure 27a.


green_fruit
green_fruit
sunburnt_fruit
sunburnt_fruit
green_fruit
green_fruit
green_fruit
sunburnt_fruit
sunburnt_fruit
sunburnt_fruit
sunburnt_fruit
sunburnt_fruit
green_fruit
green_fruit
green_fruit
green_fruit
sunburnt_fruit
green_fruit
sunburnt_fruit
sunburnt_fruit
sunburnt_fruit
green_fruit
sunburnt_fruit
sunburnt_fruit
green_fruit
sunburnt_fruit

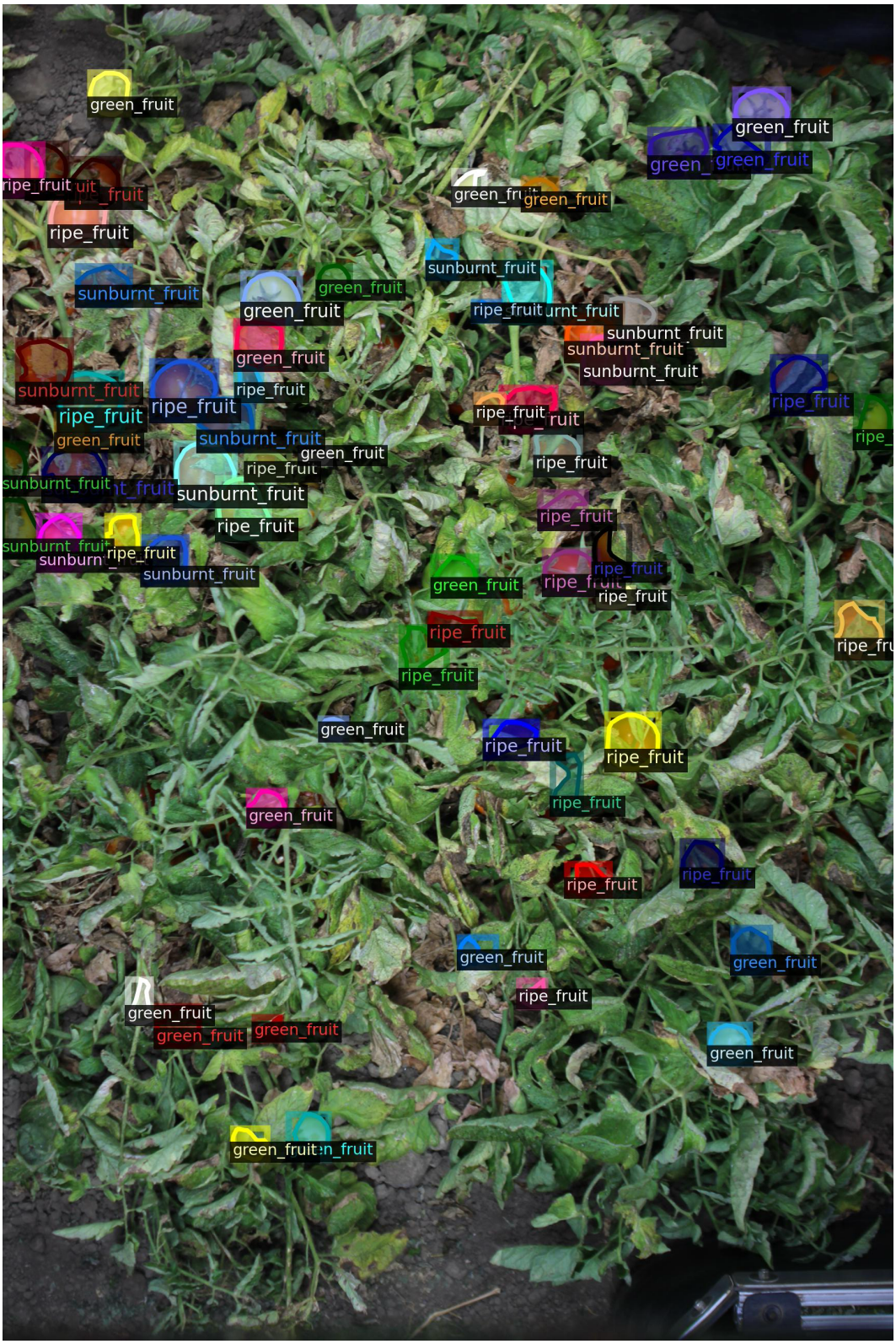
(a)



(b)

Figure 27: example images from the Training Dataset (a) shows the ground truth labeled image and (b) shows the predicted labels.

The images shown in Figure 28 are example images with labeled objects from the 2018 Validation Dataset. In the middle of Figure 28a there is a cluster of occluded ripe fruit that are labeled in the ground truth image but are not detected in the predicted image Figure 28b. On the top left corner of Figure 28b there are some misclassifications of ripe fruit as sunburnt fruit.


green_fruit
green_fruit
green_fruit
ripe_fruit
ripe_fruit
sunburnt_fruit
sunburnt_fruit
green_fruit
green_fruit
ripe_fruit
sunburnt_fruit
sunburnt_fruit
sunburnt_fruit
ripe_fruit
ripe_fruit
ripe_fruit
ripe_fruit
green_fruit
sunburnt_fruit
green_fruit
ripe_fruit
sunburnt_fruit
ripe_fruit
ripe_fruit
sunburnt_fruit
ripe_fruit
sunburnt_fruit
ripe_fruit
ripe_fruit
green_fruit
ripe_fruit
ripe_fruit
ripe_fruit
ripe_fruit
ripe_fruit
green_fruit
ripe_fruit
ripe_fruit
ripe_fruit
ripe_fruit
ripe_fruit
green_fruit
green_fruit
ripe_fruit
green_fruit
green_fruit
green_fruit
green_fruit
green_fruit
(a)



(b)

Figure 28: example images from the Validation Dataset (a) shows the ground truth labeled image and (b) shows the predicted labels.

5.4.2. Automated Time Series Data

One aspect of high-throughput phenotyping is the ability to collect data throughout the growing season, creating a time-series that demonstrates how the plant-plot grows and develops throughout the season. Figure 29 shows the total count of detected objects (flower, green fruit, ripe fruit, sunburnt fruit) from five example plant-plots that were imaged during the 2019 growing season. The total count is the number objects detected by the neural network within the same plant-plot. Each plant-plot had approximately 8 images in total, but because the images had 40% overlap between consecutive images, every other image was used in total count. Each image was input into the neural network, which output how many of each object (flower, green fruit, ripe fruit, sunburnt fruit) was detected in that image. The object count from every other image for each object type was summed to create the total count of each object.

The data from three dates are presented, June 25, 2019, July 16, 2019, and July 23, 2019. June 25th was chosen because it was the earliest date in the season, after the plants recovered from transplant shock and were established enough to not worry about root compaction, which allowed the high-throughput phenotyping vehicle to enter the field. July 16th was after 75% of the plant-plots showed the phenotype Day to First Ripe Fruit (DTFR). The three bar graphs show how many flowers, green fruit, ripe fruit, and sunburnt fruit were detected in plant-plot 19FD0007 on June 25th, July 16th, and July 23rd, respectively. The objects were detected using the Mask-RCNN neural network described previously.

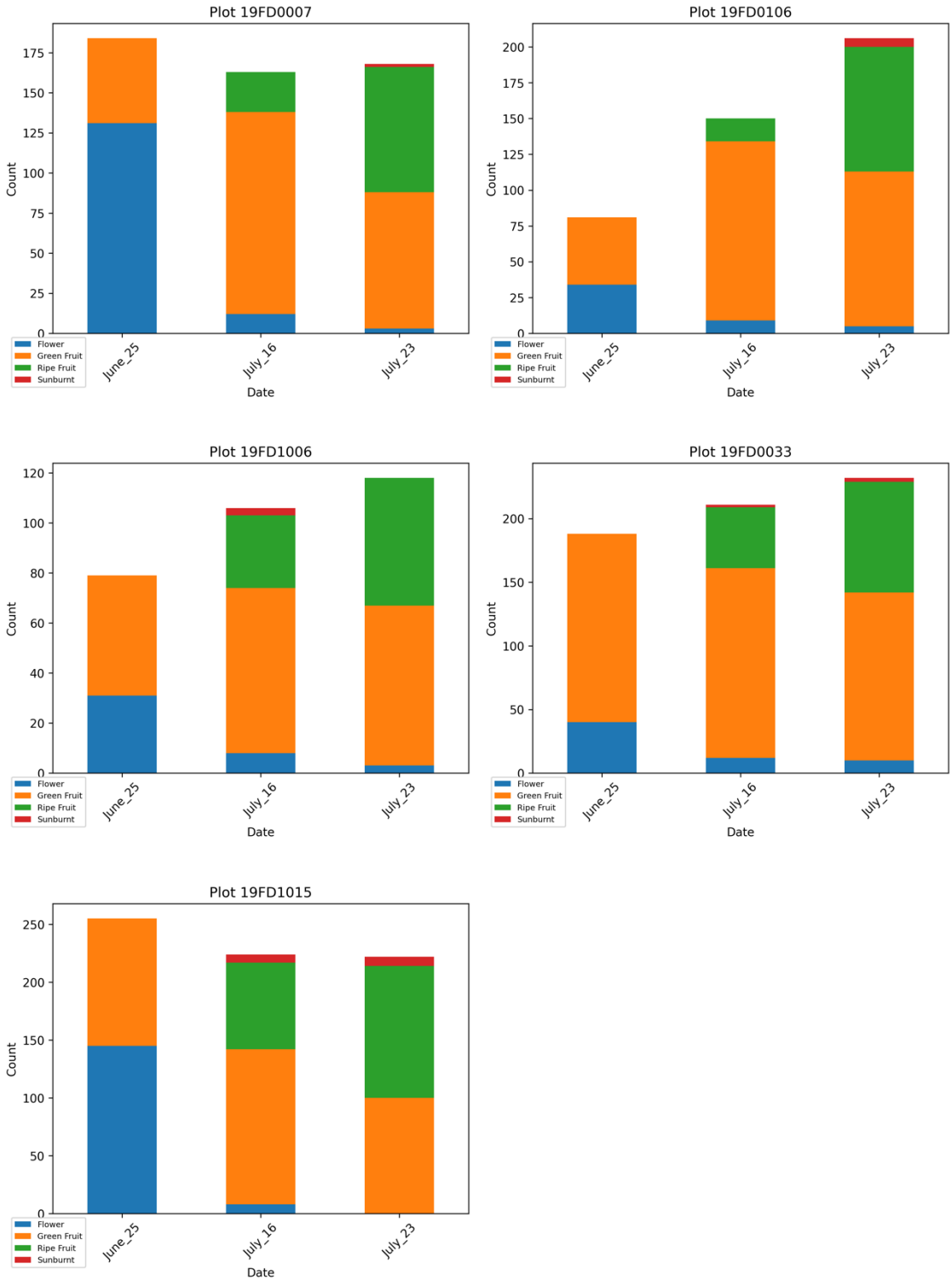


Figure 29: Example plant-plots of object detection results in 2019 across 3 dates.

5.4.3. Manual Phenotyping

Before comparing the high-throughput phenotyping method to the manual phenotyping method, it was necessary to establish the precision in manual phenotyping data. The two main phenotypes that were proposed to use with the high-throughput phenotyping system were Day to First Green Fruit and Day to First Ripe Fruit. Any effects from irrigation deficit were ignored because the irrigation treatment was a failure due to extreme weather and equipment failure. So, the manual phenotyping data was analyzed as a single factor completely randomized design with the genotype as the single factor.

The graph in Figure 30 shows a box plot of the results from manual phenotyping for Day to First Green Fruit (DTFG) in tomatoes in 2019. Each box represents a genotype, of which there are 40 in the manual phenotyping dataset. The diamond in each box represents on average how long each genotype took to express the DTFG phenotype. A Tukey multiple comparison test was performed on this data to find genotypes that can be differentiated at the 0.05 level of significance from the other genotypes based on DTFG. The F-value from the Tukey Test is <0.0001. Along with testing the means for similarity, the Tukey test performed grouping to find significant groups and to demonstrate which genotypes are similar. In Figure 31, the colored grouping bars overlap genotypes that have similar means and are not significantly different (alpha=0.05) from one another. There are eight groups identified by the Tukey test for Day to First Green Fruit, but none are distinct from any other (i.e. all have considerable overlap). The results show that the manual phenotyping method and the experimental design, had a lack of precision and power to establish a clear difference in DTFG for the genotypes studied.

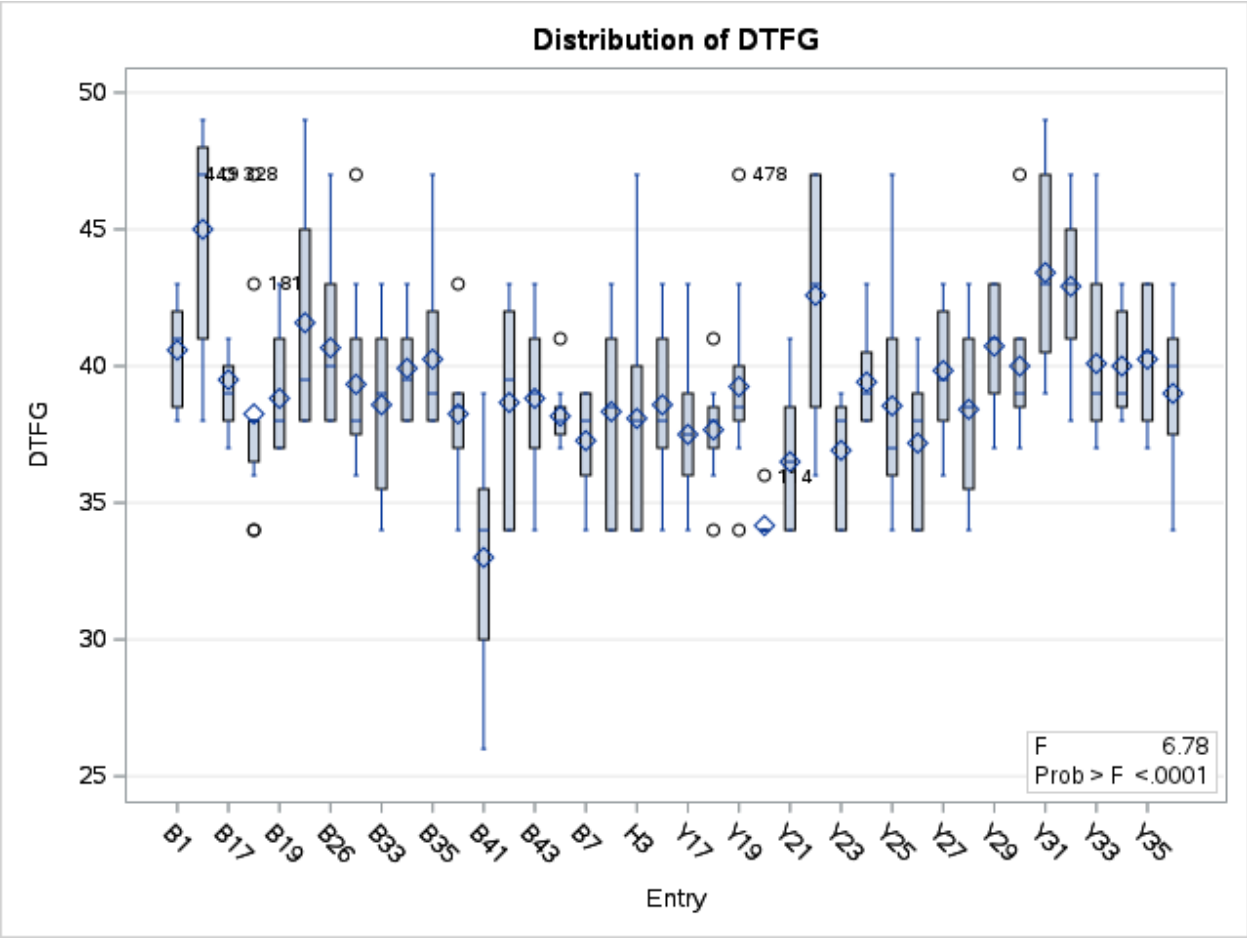


Figure 30: Distribution of average Day to First Green Fruit Grouped by Genotype Entry.

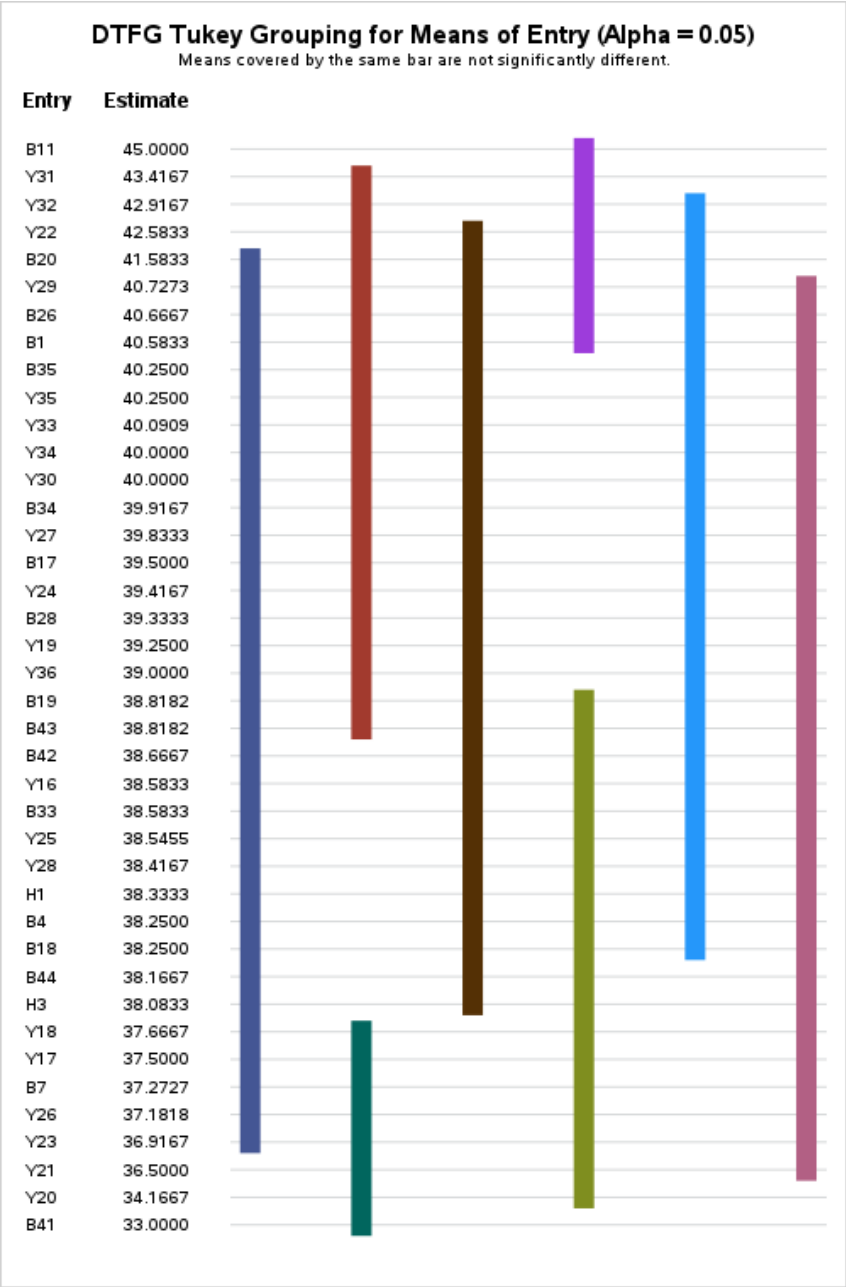


Figure 31: Tukey Test Grouping based on similarity of means across genotypes based on DTFG.

The graph in Figure 32 shows the results from manual phenotyping for Day to First Ripe Fruit (DTFR) in tomatoes in 2019. Each box represents one of forty genotypes, each represented 16 times in the field. The graph represents on average how long each genotype took to express the DTFR phenotype. A Tukey test was performed on this data to find significant and separable genotypes that can be differentiated from the other genotypes based on DTFR. The F-value from the Tukey Test is <0.0001. Additionally, the Tukey test performed grouping to find significant groups and to demonstrate which genotypes are similar. In Figure 33, the bars overlap genotypes that have similar means and are not significantly different from one another. There are 10 distinct groups identified by the Tukey test for Day to First Ripe Fruit that have genotypes that are not statistically different from one another.

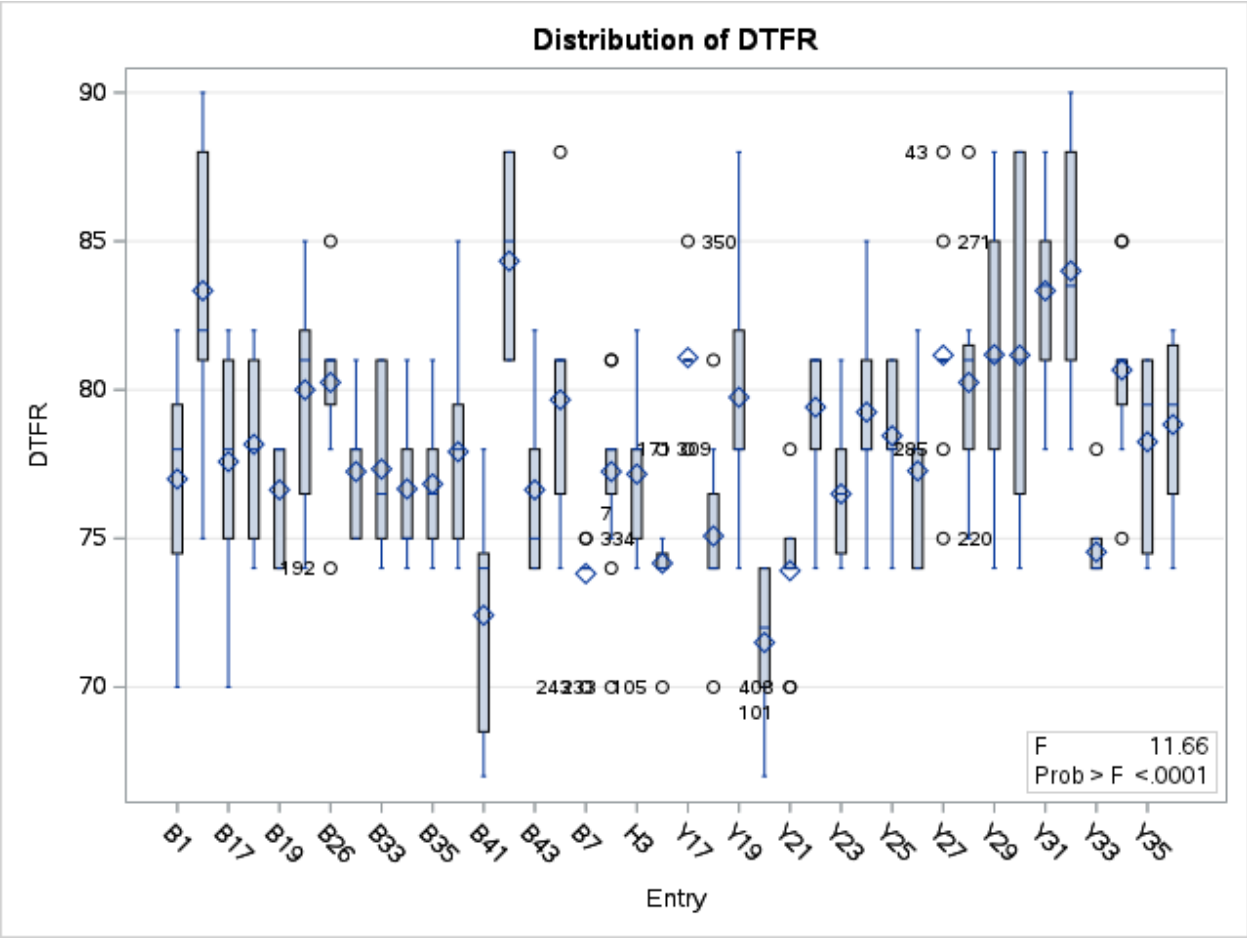


Figure 32: Distribution of average Day to First Ripe Fruit Grouped by Genotype Entry.

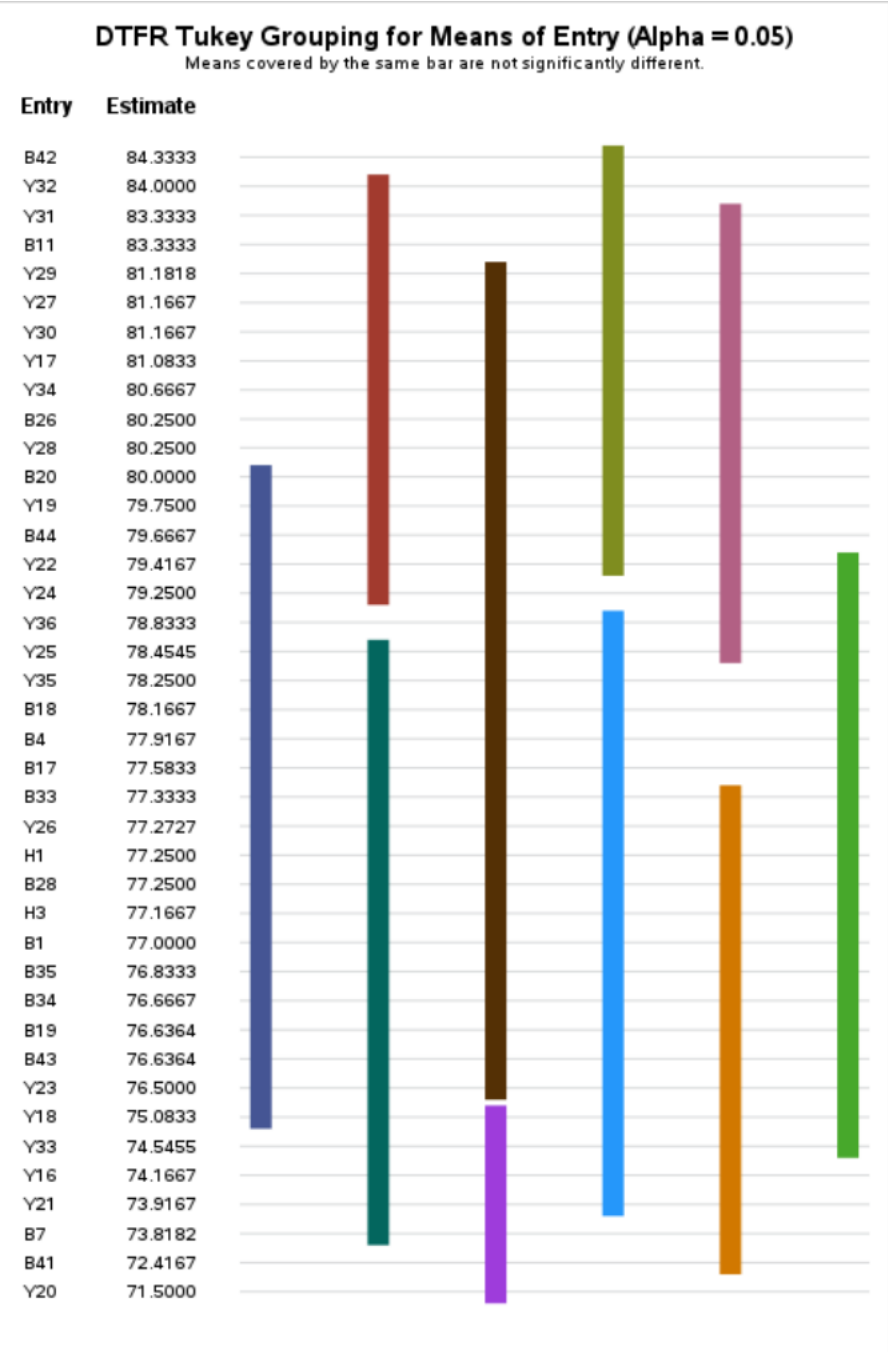


Figure 33: Tukey Test Grouping based on similarity of means across genotypes based on DTFR.

5.4.4. Manual Phenotyping vs High Throughput Phenotyping

Figure 34 shows the relationship between Ripe fruit Count determined by the HTPP system on August 23, 2018 (the same week as destructive plant harvesting) and the manual Ripe Fruit Yield (RFY) in kilograms. Destructive phenotyping occurs at the end of the growing season. The manual data for Ripe Fruit Yield was collected by harvesting 2 of 8 (25%) of plants within a plant plot and weighing the amount of ripe fruit are on those plants. The fruit weighed for RFY do not include green fruit but do include sunburnt fruit. Each point on the graph represents one plant-plot with a total of 354 datapoints. A statistically significant (give p-value) linear association between the number of HTPP detected ripe fruit and the manual RFY was found, with r = 0.407.

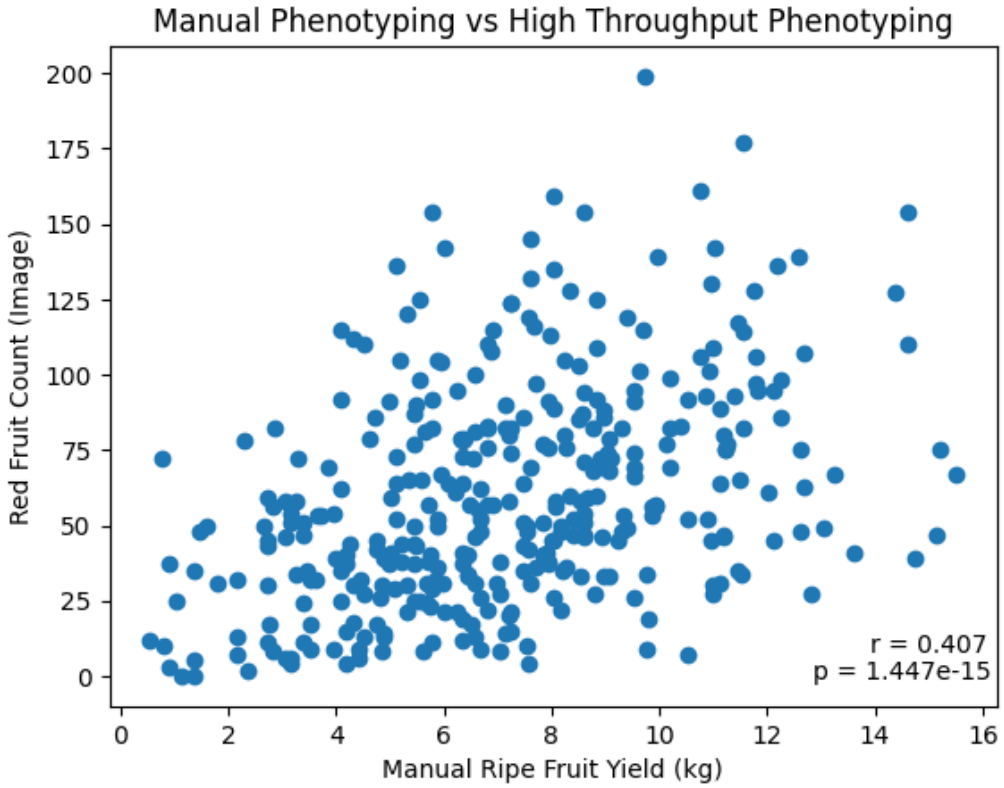


Figure 34: scatter plot of manually collected Ripe Fruit Yield and Automated Collection of Ripe fruit Count in 2018, n = 354. Red Fruit Count uses 8 plants for the count and Ripe Fruit Yield uses 2 plants for yield.

Figure 35 depicts the relationship between detected green fruit on August 23, 2018, the week of destructive plant harvesting, and manual Green Fruit Yield (GFY) in kilograms. Destructive phenotyping occurs at the end of the growing season. The data for Green Fruit Yield was collected by harvesting 2/8 plants within a plant plot and weighing the amount of green fruit on those plants. The data for Green Fruit Count (Image) was collected on July 23, 2019. Each point on the graph represents one plant-plot with a total of 354 data points. The correlation-coefficient of detected ripe fruit and RFY is 0.201.

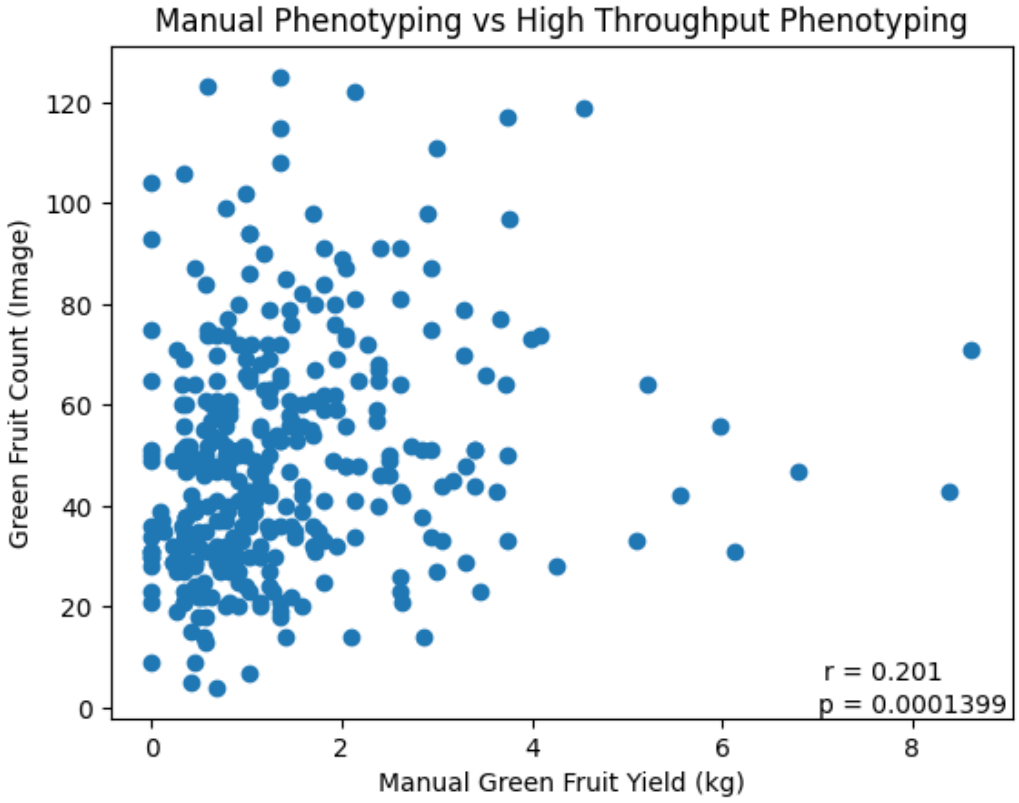


Figure 35: scatter plot of manually collected Green Fruit Yield and Automated Collection of Green Fruit Count in 2018, n = 354. Green Fruit Count uses 8 plants for the count and Manual Green Fruit Yield uses 2 plants for yield.

Figure 36 shows a scatter plot between detected ripe fruit on July 23, 2019, the last week before destructive plant harvesting, and manual Ripe Fruit Yield (RFY) in grams. Destructive phenotyping occurs at the end of the growing season. The data for Ripe Fruit Yield was collected by harvesting 2/8 plants within a plant plot and weighing the amount of ripe fruit are on those plants. The fruit weighed for RFY do not include green fruit but do include sunburnt fruit. The data for Image Ripe Fruit Count was collected on July 23, 2019. Each point on the graph represents one plant-plot with 439 points. The correlation-coefficient of detected ripe fruit and RFY is 0.202.

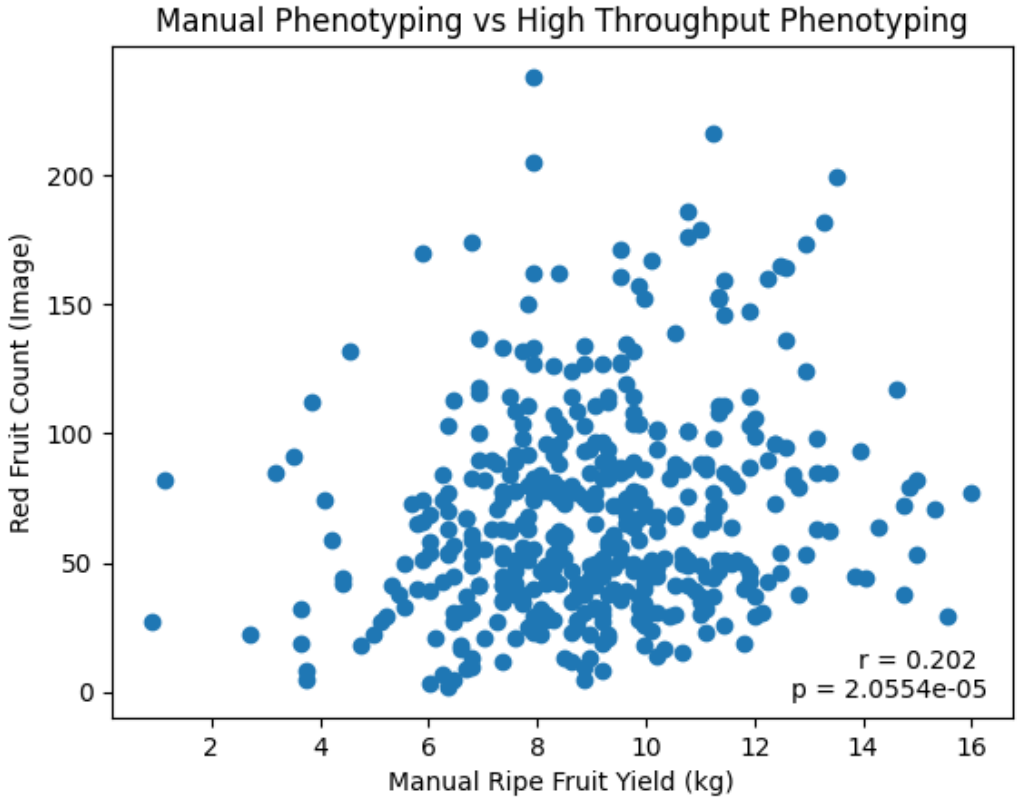


Figure 36: Scatter plot of manually collected Ripe Fruit Yield and Automated Collection of Ripe fruit Count in 2019, n = 439. Red Fruit Count uses 8 plants for the count and Ripe Fruit Yield uses 2 plants for yield.

Figure 37 shows the relationship between detected green fruit on July 23, 2019, the last week before destructive plant harvesting, and manual Green Fruit Yield (GFY) in grams. Destructive phenotyping occurs at the end of the growing season. The data for Green Fruit Yield was collected by harvesting 2/8 plants within a plant plot and weighing the amount of green fruit on those plants. The data for Green Fruit Count (Image) was collected on July 23, 2019. Each point on the graph represents one plant-plot with 439 total points. The correlation-coefficient of detected ripe fruit and RFY is 0.143.

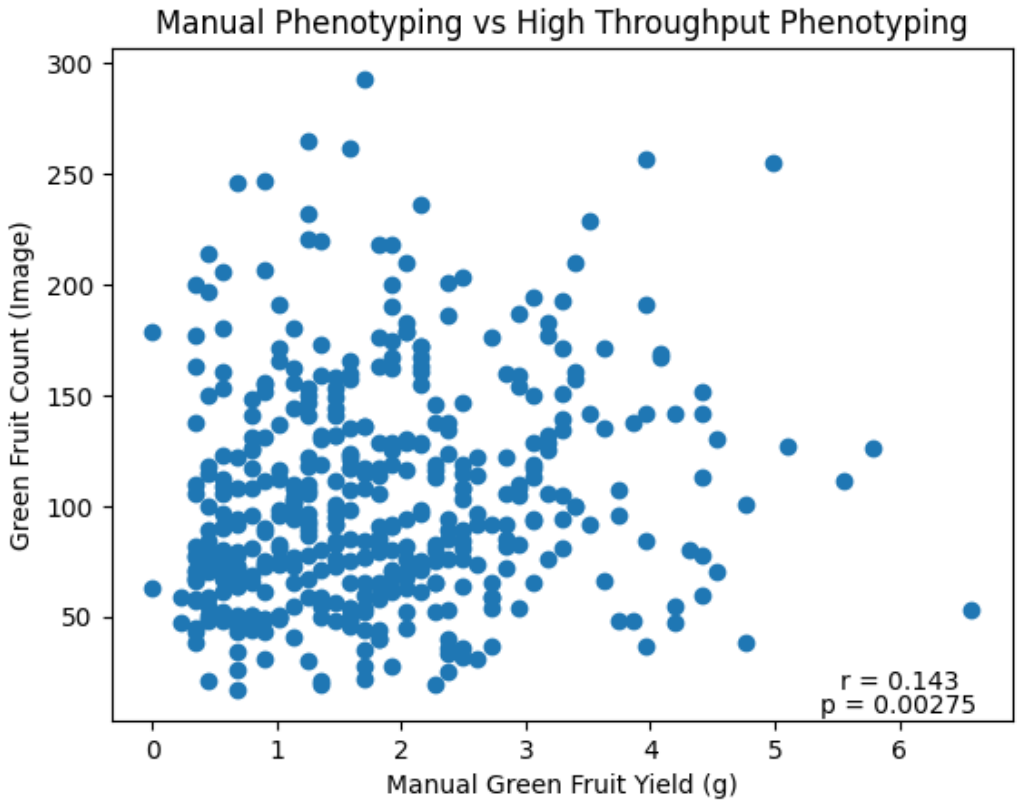


Figure 37: Scatter plot of manually collected Green Fruit Yield and Automated Collection of Green Fruit Count in 2019, n = 439. Green Fruit Count uses 8 plants for the count and Manual Green Fruit Yield uses 2 plants for yield.

5.5. Discussion

5.5.1. Model Performance

From the results in Table 8 the overall mAP in 2018 training is 88.50% but drops to 21.11% and 23.35% for 2018 validation and testing respectively. The 2018 training data shows that the system combined with the neural network have merit for detecting objects for phenotyping plants. However, the 2018 validation and testing data indicate that there was overfitting during training and better measures need to be put in place to create a more robust model. The 2018 validation and test data show performance to the 2019 test dataset (Table 10), with has an mAP of 19.68% across all dates. This indicates that all datasets outside of the 2018 training set perform similarly.

Other studies have tried to conduct phenotyping using imagery and neural networks previously. These studies generally look at single dates for both the training and validation and have low number of labeled images. Compared these studies, the mAP@0.5 across in the 2018 validation dataset, 2018 test dataset, and 2019 testing is low. A study in 2022 found the detection of grape clusters with ground-based imagery demonstrated an AP score of 76% [38]. However, the study had only 24 labelled images for training, testing, and validation. All of the labelled images were from the same date for data collection and the model was not used on new data. In our study we changed the dataset significantly between 2018 training and 2019 testing data. Future studies would train on a more robust dataset, that includes multi-season data, for tomato detection. Additionally, this grape study was only detecting one object “grape”, while our study was trying to detect many different objects at different stages of development. Comparing the AP score for grapes of 76% and the AP score of green fruit with 46.71%, the results are a little closer, but the grape detection still performed better. In another study in 2018, detection of tomato fruits using

deep learning models had a precision of 88% [82]. Although this study had good precision in detecting the fruit, this study was conducted in a greenhouse with manicured tomato plants. The plants had minimal fruit occlusion from leaves because of the wire trellis growing and training of the tomato plants. Like the first study, this study only used a small sample size of images and trained, validated, and tested on the same images. Both studies show the ability to use neural networks for object and fruit detection. Our study shows the novel ability of using a dataset from a different year to predict object detection on a new dataset, reducing the amount of data needed to overall training while resulting in accurate detections.

From Table 5, it's clear that the overwhelming majority of labeled objects was green fruit. This overwhelming majority may contribute to the mAP of the green fruit being higher than the mAP for flowers, ripe fruit, and sunburnt fruit. The other classes were not represented equally. This trend is seen across all dates together and on the individual dates, as shown in Figure 25. Flowers consistently had the lowest mAP score; this could be because of how small the objects are in relation to the picture, resulting in low confidence in object detection. This could also be due to how flowers change in appearance throughout the growing season, earlier in the season they are bright yellow and have 5-6 open petals while later in the season they are drier and have fewer petals. Training on more data throughout the growing season would help with this. Overall mAP is also highest in the first date, June 23. This could be attributed to increased occlusion as the season continues and the plant continues to grow new leaves and fruit. Future work would include testing making multiple object detection neural networks for each individual object or object detection neural networks for early, middle, and late season, since different phenotypes are present at different times during the season.

Comparing Table 8 and Table 9, it's clear that across the 2018 training, validation, and testing datasets the recall is consistently higher than the precision values. This indicates that there the model identifies true positives but is prone to false positives. When visually looking at the model detections and classifications for validation and testing the model often labeled the undersides of leaves as green fruit, labeled highly occluded objects that were not in the ground truth, and classified sunburnt fruit as ripe fruit or ripe fruit as sunburnt fruit. The same trends for recall were observed in Table 10 and Table 11 for the 2019 out of season data. A larger dataset with more examples of green fruit, ripe fruit, and sunburnt fruit could help with the misclassification and false positives. Additionally, obtaining higher quality ground truth labels that include more occluded objects could help. Adding more measures to prevent overfitting in the training would also help with this.

5.5.2. 2018-2019 Data Collection

In the 2018 growing season two extreme weather events occurred 1-week after transplanting the tomatoes, a heatwave followed by rainstorm. Due to this unforeseen weather event, the plant breeders believed it would affect the results of the breeding trial. The heatwave increased the amount of transplant shock the plants experienced. Due to this increased shock, the plants created flowers much earlier than normal rather than creating roots, presumably in the hopes of reproducing. If these flowers were able to get pollinated and grow into fruit it could create datapoints that are not representative of the genetic influence on traits such as DTFG and DTFR in a normal year. However, what would more likely happen is that the flowers would not get pollinated and die off. By the time the flowers die off, the plant would have expended most of its energy into creating the flowers and would suffer from the effects of transplant shock and a lack of root production. To prevent this, the plant breeders made the decision to go through the field

and remove any flowers during this time, to coax the plants into creating stronger roots instead. The second extreme weather event, summer rainstorms (which are not normal for Davis, CA), created an environment that helped the plants overcome transplant shock quickly by keeping the soil moist. However, the rain also created an environment that made it impossible for a vehicle to enter the field. Davis, CA received consistent rain for 5 consecutive days in the summer, right after a heatwave. The heatwave removed most of the moisture from the clay soil, creating soil with hard layers of soil. The hard and dry clay made it, so the water did not distribute through the soil, instead staying on the top of field and flooding the fields and furrows. This second weather event resulted in the inability to consistently collect early season data using the high-throughput phenotyping system. Although the high-throughput phenotyping system couldn't enter the field, the plant breeders were still able to enter and collect phenotypic data. By the time the fields were dry enough for the vehicle to enter, all the plant-plots expressed DTFG, and some had begun to express DTFR. It was decided that 2018 would focus on looking at end of season yield instead of any of the temporal phenotypes. The plant breeders harvested all the plant-plots at once during August 27-August 31, 2018.

In 2019 there were no extreme weather events early in the season, which allowed for data collection early in the season. Only three dates were analyzed for 2019 at this time. It was important to be able to look at the same plant-plots consistently throughout the growing season. In 2019 there were 25 days of data collection, due to the time constraint of the project only three dates were analyzed. These three dates were chosen because we were able to collect all the plant-plot data on those days with consistent GPS quality and they were spread apart enough to show temporal changes. Although there were no extreme weather events in the beginning of the 2019 season, there were extreme weather events at the end of the growing season. An extreme

heatwave that lasted over 2 weeks created an environment that forced the tomatoes to ripen quickly. Although some plots were ready to be harvested for yield, other plots did not express Day to First Ripe Fruit yet. If the plant breeders waited for all the plant-plots to be harvest ready it would cause many of the early DTFR plots' ripe fruit to get sunburnt and die off. This would make an inaccurate end of season yield estimation. This forced the plant breeders to continuously and selectively harvest plots starting in the end of July 2019 – the end of August 2019 instead of harvesting all the plant-plots at once. Overall, this suggests that a larger multi-season training dataset is necessary, particularly with more extreme weather due to climate change. This would create a dataset that includes how plant architecture and appearances are affected in response to stress.

5.5.3. Automated Time Series Data

Figure 29 show examples of the number of flowers, green fruit, ripe fruit, and sunburnt fruit detected throughout the growing season. Early in the growing season the most detected object was flowers and some green fruit, consistent with developmental expectations. As the season continues the number of flowers decreases while the number of green fruit and ripe fruit increases. On the last date the trend continues, where the number of flowers on the last date are very small, the green fruit population beings to decrease, the ripe fruit population begins to increase, and then the first sunburnt fruits are detected.

This type of temporal data can be useful for plant breeders in describing and quantifying the growth patterns of the plant-plots throughout the season. For example, between June 25 and July 16 in plots 19FD1015 and 19FD0007, there is a drop in total objects detected. This could be because some of the flowers that were detected in June 25 were not successfully pollinated, so they died off and were not detected in July 16. In plots 19FD 0106, 19FD1006, and 19FD0033

there is an increase in objects detected between June 25 and July 16. This type of data could be used by plant breeders to know the pollination rate per genotype or plot number. This could also show any relationship between rate of positive pollination and location in the field. In June 25 plots 19FD0007, 19FD0033, 19FD0106, 19FD1006, and 19FD1015 do not have any detected sunburnt fruit. This makes sense because there is no ripe fruit detected yet, which are more susceptible to sunburn than green fruit. However, on June 16 only plots 19FD0007 and 19FD0106 continue to have no detected sunburnt fruit. This difference could indicate genetic disposition for sunburnt fruit early in the season. Currently, sunburnt fruit data is not collected until the end of the season, and the data is ranked on a scale of 1-5 for how sunburnt the fruit on the canopy are. This temporal data and object detection could give plant breeders a better idea of when sunburn occurs and the rate at which it occurs. Additional collected data that was not mentioned is local weather data and environmental data, which could be fused with the detected phenotypes to identify sunburn and flower drop. These are examples of how object detection and classification from images can be used for creating new phenotypes that are more biologically relevant to the crop.

5.5.4. Manual Phenotyping vs High-Throughput Phenotyping

In Figure 34, the correlation coefficient is 0.407 for manual Ripe Fruit Yield (RFY) vs. HTPP Ripe fruit Count in Image (RFC) in 2018. Compared to the correlation coefficient for RFY vs RFC in 2019, which is 0.202, Figure 36. In 2018 we were able to collect data up until the week of destructive harvest for all plant-plots. This allowed us to analyze plant-plots that were close to harvest and more representative of RFY at the end of the season. In 2019, because the harvest was conducted continuously through August 2019, we were unable to analyze plants that were close to harvest. This is reflected in the lower R value (0.202) in 2019. The image dataset in

2018 was more in-line with when the destructive harvest occurred in 2018, resulting in a higher R value (0.407).

In Figure 35, the correlation coefficient for manual Green Fruit Yield vs HTPP Green Fruit Count in Images (GFC) in 2018 is 0.201. The correlation coefficient in 2019 for GFY vs GFC is 0.143. The difference in correlation coefficient for these two years may be affected by differences between the 2018 vs 2019 harvesting schedules, like the Ripe Fruit Yield. For both Figure 35 and Figure 37, the distribution is not as linear and the points have a wider spread than expected. This could be because of the 25% sampling rate for manual phenotyping, while the green fruit count uses the entire plant-plot. Another source of error in predicting GFY with GFC is that at the end of the season the green fruit are often various sizes. The GFC doesn't consider the size of the green fruit, so a detected small green fruit is the same as a large green fruit, but a small green fruit would weigh less than a large green fruit. This suggests that future research that incorporates area of detected fruit with total fruit count could make a better model for predicting fruit mass. The Ripe Fruit Yield could have a higher correlation because processing tomatoes are bred for once-over harvest, so there is less variation between detected Ripe fruit in the images. The 2018 and 2019 results show that it is promising to predict total yield for in-field breeding trials with images, but that future research to address the issues observed is needed to improve the prediction accuracy.

5.5.5. Manual Phenotyping

A Tukey Multiple Comparison Test was performed on the Day to First Green Fruit (DTFG) manual phenotyping data (Figure 31) and shows lack of power to distinguish between individual genotypes. The F-value of the ANOVA performed on the DTFG data is significant $p < 0.0001$, which implies that genotype is a significant factor in modelling DTFG. However, the Tukey Test

grouping shows seven large groups of similar genotypes. The smallest grouping has eight genotypes that were statistically similar, which makes up 20% of the total genotype population, and it overlaps with five of the eight groups. The largest group has 33 genotypes represented in it as not statistically different from one another, which makes up 82.5% of the represented population. We can conclude that the Day of First Green Fruit phenotype in the 2019 dataset was not a reliable phenotype for determining genotypic differences. Additionally, Figure 30 shows the distribution of the means and spread for DTFG for each genotype. Based on this post-hoc analysis, the Day to First Green Fruit metric was not used to compare the object detection in images to manual phenotyping.

An additional Tukey Multiple Comparison Test was performed on the Day to First Ripe Fruit (DTFR) manual phenotyping data (Figure 33). The F-value of the ANOVA performed on the DTFR data is significant $p < 0.0001$, which implies that genotype is a significant factor in modelling DTFR. However, when looking at the groups that are created from the Tukey test, it shows substantial similarity between the 40 genotypes. The 40 genotypes were split into 10 groups, where the genotypes in each group represents statistically similar DTFR. The smallest group contains of 7 genotypes Figure 33, representing 17.5% of the total genotypes. The largest group contains 29 genotypes Figure 33, representing 72.5% of the total genotypes in the population. We can conclude that the Day of First Ripe Fruit phenotype in the 2019 dataset was not a reliable phenotype for determining individual genotypic differences. Based on this post-hoc analysis, it was concluded that the Day to First Ripe Fruit would not be a useful ground truth phenotype to compare Total Ripe fruit Detected in images.

5.6. Conclusion

High-throughput phenotyping is projected to become the new norm in implementing in-field plant breeding trials [citation]. Many phenotyping projects for tomatoes utilize greenhouses, synthetic data, and very manicured plants for imaging [74], [75], [78], [79], [82], [83], [84], [85], [86], [87], [88]. This approach to phenotyping creates accurate data collection and reduces the amount of error due to environmental factors. In-field phenotyping is affected by external uncontrollable factors like weather, pollination rate, location effects, and field conditions. However, in-field phenotyping is important for plant breeders to see how a crop will grow in real-world conditions. This study shows the promise of using 2D imaging for high-throughput phenotyping in-field, however future research is required to address methods needed to improve the performance under the variable environmental factors which were observed in this study, and which are expected to become more common as the climate changes.

6. Chapter 3: Green Fruit Detection for High-Throughput Phenotyping

6.1. Introduction

In object detection, color differences between objects of interest and background is a fundamental feature. Detecting differences in colors can result in detecting edges, shapes, and eventually objects [89]. However, in agriculture the objects and backgrounds are often the same color because of changes in chlorophyll content throughout plant development and growth. These are usually green fruit with a background of green foliage [90], [91]. Neural networks and deep learning techniques have improved on detecting green fruit on green foliage, however there is still difficulty due to occlusion and environmental factors [92]. Current methods include using high-resolution 2D cameras and depth sensors to detect and classify green fruit, though these sensors together can be expensive.

6.2.Literature Review

6.2.1. Traditional Plant Phenotyping Methods

Cultivar breeding requires a feedback mechanism called phenotyping to allow breeders to understand how different genotypes perform under different environments or locations. In-field phenotyping requires thousands of plants to be grown in commercial field conditions across a range of environmental conditions like different elevations or latitudes, sunlight levels, and soil composition. Multiple phenotypes must be assessed for each plant and potential cultivar, including: temporal phenotypes (day of first green fruit, day of first ripe fruit), growth habit phenotypes (e.g. plant height, plant width, canopy density), and external phenotypes (e.g. fruit yield, fruit quality, abiotic stress tolerance). Current phenotyping methods for cultivar breeding trials are done manually by humans. During the growing season, humans will go into the field

periodically to observe these traits. This often includes manually manipulating the plants to look at the internal structure or searching for flowers and fruit and destructive phenotyping at harvest. This method of human-based phenotyping is costly, labor- and time-intensive, subject to human error and fatigue, and does not always allow (or is cost prohibitive) for repeated measures on the same plants over time.

6.2.2. High-Throughput Phenotyping Methods

The development of in-field phenotyping technology lags behind that of genomics, creating a bottleneck in plant breeding [2], [3]. The key objective of high-throughput phenotyping is the ability to non-destructively, objectively, and quickly characterize plant traits [23]. Automated phenotyping utilizes various non-contact sensors to estimate traits such as biomass, yield, plant height, leaf segmentation, leaf area, and canopy temperature [24], [25], [26], [27]. Non-destructive phenotyping also permits a time-series approach that follows the growth of plants over time. Different systems have been developed for in-field phenotyping using permanent fixed-site platforms, unmanned aerial vehicles (UAV) including satellites, and terrestrial vehicles, all fitted with various sensors to collect a range of phenotypic data [28], [29], [30]. Regardless of platform type, the goal is to automate and expedite the acquisition of plant phenotypes and relate them to genotypic data to find superior breeding lines and cultivars more quickly [31].

6.2.2.1. Remote Sensing

Remote sensing in agriculture uses technology such as satellite imagery, manned and unmanned aerial vehicles fitted with sensors, and fixed-site platforms. UAVs look at spectral reflectance of the crops (visible, near infrared, infrared) using multispectral (typically less than 10 wavebands) or hyperspectral (typically more than 100 wavebands) cameras, canopy temperature using

thermal infrared sensors, and plant height and topography most commonly using Light Detection and ranging (LiDAR). In broadacre grain crops, such as rice, the combination of high-density planting, narrow row spacing, consistent grain location at the top of the plant, and canopy closure makes it a perfect candidate for using UAVs as the phenotyping platform [24], [32], [33]. UAVs are not sufficient for all phenotyping situations, such as day of first bloom in vegetable crop breeding, because they can only provide vegetable crop breeders with a small number of phenotypes. Due to typical UAV altitudes and camera technology, the images and data are typically lower resolution than proximal methods, making it difficult to find small features like fruit phenotypes (day of first green fruit or first ripe fruit) and internal phenotypes in plants that have high canopy density and high visual occlusion.

6.2.2.2. Proximal Sensing

Proximal sensing in agriculture utilizes sensors mounted on terrestrial vehicles to traverse through a field and gather data. Recent technologies utilize terrestrial-based camera systems for creating realistic 3D models and phenotyping plants, leaves, fruits, and flowers [30]. The systems utilize a number of different technologies including: structured illumination, time-of-flight (ToF) sensors, high-resolution cameras, multi-view camera system techniques (structure-from-motion and stereovision), and software algorithms [34], [35], [36]. In a study at UC Davis using a high-throughput phenotyping system in Solanaceae crops and sunflowers demonstrated the ability to recreate a 3D structure using multiple 2D images, though this method was time consuming and restricted to the height of the platform [37].

6.2.3. Green Fruit Detection in Agriculture

Green fruit in agriculture is a complex trait because it changes by crop, location, variety, and harvesting method. In some crops, like peaches, detecting green fruit is important for automated

mechanical thinning to increase fruit quality for market fresh peaches [91]. In this case the green fruit are detected once early in the season before the fruit begin to ripen. In citrus fruit it's common for ripe and unripe fruit to have some degree of green on the exterior of the fruit because of this sensor fusion with temperature and color need to be utilized to detect fruit ripeness [93].

6.2.4. Multispectral Data in Agriculture

Multi-spectral sensors have a special use case in agriculture that is often limited by cost. Multi-spectral cameras can capture and detect wavelengths beyond the visible wavelengths. These non-visible wavelengths can be used to detect differences and changes in plants [94], [95]. Many vegetation indices have been developed using multi-spectral data obtained from satellite images to quantify things like soil brightness, water content, greenness above soil, and redness index [50]. Satellite images lack the resolution required to look at individual plants in a field. To increase image resolution while still using the vegetation indices, it's common in agriculture to capture multi-spectral data using a drone or aerial system [96], [97], [98], [99]. Drones are commonly used in cover crops or plants with large canopy cover, like trees in orchards [100], [101], [102]. Drone images do have an increase in resolution when compared to satellite images, but the resolution is still not enough for imaging individual plants that are not cover crops or have large canopy. Some methods have been created to use handheld sensors for detecting multi-spectral data in-field, but these handheld sensors are not scalable for a field level [86], [103], [104].

6.2.5. Solanaceae in California

In the United States, approximately 90% of processing tomatoes are grown in California [15]. In California the most common practice for growing tomatoes is on raised beds (60 or 66 inches

wide), which facilitates cultivation and drainage of the plant. Almost all processing tomatoes are transplanted; tomatoes are commonly grown in single rows per bed allowing easier cultivation and reducing weeding costs. Drip irrigation is the most commonly used irrigation method in California which allows for better water use efficiency, drainage and reduces disease and weed emergence. In Californian tomato production, approximately 125-250 pounds of nitrogen, 40-120 pounds of phosphorus, and 0-200 pounds of potassium per acre are required in order to produce a commercially viable crop [16]. All processing tomatoes in California are mechanically harvested. The destructive harvest occurs when at least 90% of fruit in a field is ripe.

In the United States, approximately 39% of chili peppers are grown in California and 54% are grown in New Mexico [17]. Chili peppers are direct seeded or transplanted into raised beds throughout California. Raised beds are commonly used for growing chili peppers with bed widths varying by location; Fresno County grows peppers on 36-40 inch raised beds, while other locations in the Central Valley grow peppers on 60-72 inch raised beds [18]. Furrow and drip are the most common method of irrigation in peppers; with more than 80% drip irrigation due to improved water use efficiency. Peppers are sprinkler irrigated after transplanting or direct seeding to help establish roots or seedlings. Peppers require moderate to high rates of fertilizer, requiring 80-200 pounds of preplant phosphorus, 50-150 pounds of potassium, and 250+ pounds of nitrogen per acre. Chili peppers are usually harvested green before the development of the mature color; most harvested chili peppers in California are used for processing into salsa or are canned whole. All chili peppers in California are hand-harvested two to four times in 10- to 15-day intervals.

The objective of this study is to use near infrared spectroscopy to explore the possibility of using NIR wavelengths to more accurately segment green fruit from green foliage in Solanaceae crops. The hypothesis of the study is that there are wavelengths in the near infrared region that can give a better level of discrimination between green fruit and green leaves than can be done in the visible portion of the spectrum. A secondary objective is to use this information to provide guidance for sensor selection in the design of an HTPP for Solanaceae crops. To test this hypothesis, in-field samples of tomato and pepper fruit and leaves were harvested, processed, and analyzed using a benchtop spectrometer in a controlled environment.

6.3. Materials and Methods

6.3.1. Experimental Design

To test the feasibility of using near infrared reflectance for distinguishing between green fruit and green leaves, a benchtop spectrometer (model 6500, FOSS NIRSystems Inc. Silver Spring, MD, USA) was used to measure the reflectance of different biological materials. To obtain the spectral absorption curves of in-field samples it was necessary to obtain green fruit and green leaves from an actual in-field trial for spectrometry. Samples were collected in 2017 from tomato and pepper breeding trials on the UC Davis research farm.

6.3.2. Tomato

An in-field tomato breeding trial was conducted in 2017 in Davis, CA. This breeding trial was the preliminary step for developing a high-throughput phenotyping system. Four biological materials were collected from the field to make sure the tomato leaves and fruit were exposed to the typical in-field environment and would be as close to in-field conditions as possible.

The selected tomato fruit and leaves were collected from four different plants of the same genotype, a market ready processing tomato cultivar. These tomatoes were used as guard rows for the breeding trial. Each plant had one tomato fruit and leaf harvested for testing. The leaves and fruit selected were not occluded by other vegetation, exposing them to full sunlight conditions. Additionally, the leaves and fruit that had no visible sun or insect damage.

Spectrometry results of biological materials are highly affected by the amount of water in a sample. Therefore, it was important to ensure that leaves and fruit lost a minimal amount of water between harvesting and scanning. Water loss occurs due to respiration from both the leaf and fruit. To reduce the respiration from the leaves and fruit, each sample was placed in a zip-tight bag with a damp paper towel and placed in an insulated bag with cold packs for transportation. This was done to increase the humidity inside the bag and decrease the ambient temperature, reducing the rate of respiration and water loss.

After harvest, the samples were transported to the laboratory and stored in a room temperature incubator for approximately 24 hours to make sure each sample was the same temperature at the time of measurement. Storing the samples in a refrigerator would prolong the duration the samples could last after harvesting and reduce the amount of respiration. However, the decreased sample temperature would affect the vibrational state of the molecules and result in invalid spectral data. Keeping the samples are room-temperature and measuring the samples at room temperature would reduce the effects of temperature on the scans.

After 24 hours of storage, it was assumed that all samples were at room temperature. The spectrometer that was used was the model 6500, FOSS NIRSystems Inc. Silver Spring, MD, USA. This is a vertical sample loading spectrometer, requiring each sample to fit in a sample

tray. The leaves were prepared to make sure the sample did not contain excess veins and midrib, had an undamaged section of leaf lamina, and was large enough for the sensor to scan, shown in Figure 38. The leaf samples were secured to the sample tray using metal prongs. The tomato fruit samples required preparation to fit inside the sample tray. Each fruit was cut in half longitudinally and a 0.25-inch slice was used as the sample, as shown in Figure 39. The sample included the exocarp and the mesocarp of the fruit. The locular cavity, seeds, and placenta were not included in the scans because the spectrometer would be difficult to clean. Additionally, only including the exocarp and mesocarp allowed for consistent thicknesses between samples. The tomato fruit slice was placed into the tomato tray and secured using prongs. The leaves were scanned twice, once on the top and once on the bottom. This was done because some tomato varieties have curly leaves where the underside of the leaf is exposed. The fruit was scanned once on the epidermis side, which is the part that would be exposed to any sensors and cameras. The spectrometer was programmed to measure the reflectance of each sample every two nanometers between 400-2498 nm. The samples were prepared immediately before scanning to reduce water loss and temperature fluctuations. Calibration was required between each sample. Calibration for each sample was done using a room temperature, ceramic calibration disk.



Figure 38: Illustration of preparation for tomato leaf spectroscopy scanning.



Figure 39: Illustration of tomato fruit preparation for spectroscopy

6.3.3. Pepper

An in-field pepper breeding trial was conducting in 2017 in Davis, CA. The pepper breeding trial included multiple breeds of processing peppers and one variety within each breed of processing peppers. All the processing peppers used for study were commercially available varieties. The processing pepper plants, and fruit had differing color, size, and growth habit. A total of 22 biological materials of different pepper breeds were collected from the field.

Unlike the tomato trial, it was not possible to collect both leaves and fruit from the same plants. Destructive harvest occurred prior to this data collection event. Which lead to the remaining pepper plants having few high quality, intact leaves. Pepper plants that had intact leaves were the guard rows, which consisted of commercially available bell pepper plants. The pepper leaves that were used for multispectral scanning were from bell pepper plants and banana pepper leaves. The pepper fruit that was collected for multispectral scanning were jalapeno, New Mexico Big Jim, banana, bell, and poblano peppers. Sample storage and transportation was like tomato. After harvest, the samples were transported to the laboratory and stored in a room temperature

incubator for approximately 24 hours to make sure each sample was the same temperature at the time of measurement.

The pepper samples required preparation to fit in the spectrophotometer sample tray. The fruit was cut longitudinally and included the endocarp, mesocarp, and exocarp of the pepper fruit. Unlike the tomatoes, the pepper locules are hollow and do not contain any material, making it easier to prepare, shown in Figure 40. The pepper leaf sample did not contain excess veins and midrib, had an undamaged section of leaf lamina, and was large enough for the sensor to scan. However, visually the pepper leaves had a more reflective surface than the tomato leaves, so each leaf was also inspected for an intact waxy coating. The pepper leaves were also scanned both on the top and bottom.

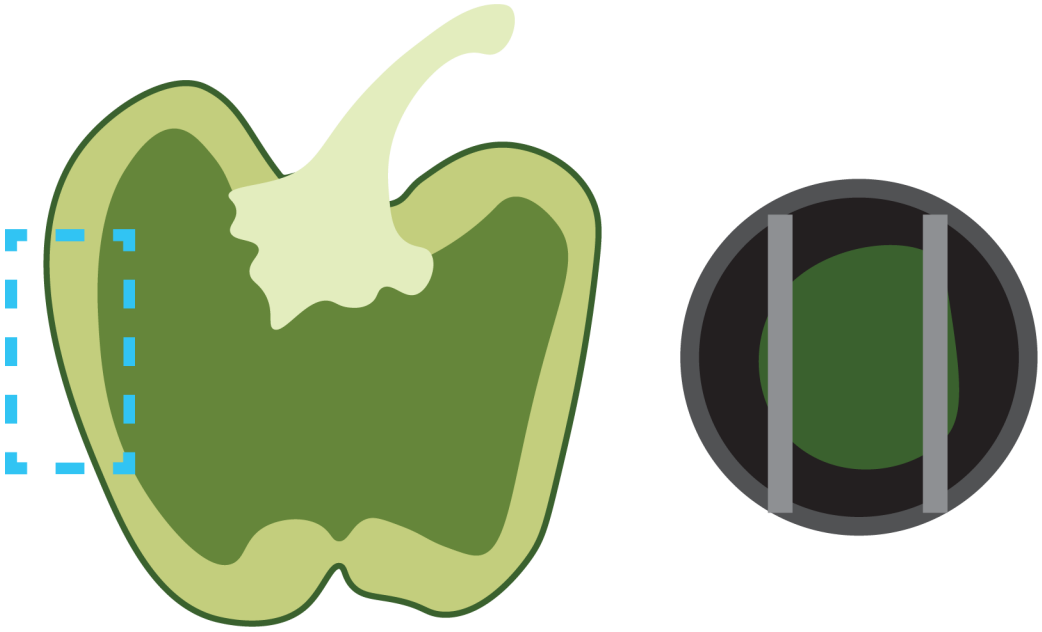


Figure 40: Illustration of bell pepper fruit preparation for spectroscopy.

6.3.4. Analysis Method

The first step of preprocessing is to fix an artifact from the two sensors in the NIR System. The NIR system has two different sensors to detect the reflectance data, one for 400-1098 nm and one for 1100-2498 nm wavelengths. The system calibration is supposed to automatically compensate for the different sensors. However, looking at the raw data, there was a reflectance discontinuity between 1098 and 1100 nm. To rectify this, the difference between the reflectance of 1098 and 1100 is calculated per sample and subtracted from each reflectance 1100-2498nm to normalize the samples and create a smooth reflectance curve for analysis, Eq. 7.

Before analysis, the data was converted into reflectance using Eq. 8, because in traditional 2D imaging, the more interpretable measurement is the reflectance of each wavelength with respect to the object being imaged. Imaging the plant measures the wavelengths that are not absorbed by the plant and are reflected. Eq. 8 converts absorbance into percent reflectance. 100% reflectance indicates the subject does not absorb any of that wavelength. The equation gives the percent of light the sample reflects. The mean and standard deviation of reflectance of each sample type was calculated for each wavelength in the visible and NIR regions. Due to the small sample size and limited statistical power of this preliminary exploration, no formal statistical test was used to analyze the results. The results were graphed to compare the reflectance of each sample per on each wavelength.

$$A_{1100-2498} = A_{1100-2498} - (A_{1100} - A_{1098})$$

Eq. 7

$$\text{reflectance} = 100 \times 10^{-\text{absorbance}}$$

Eq. 8

6.3.5. Sensor Testing

A DSLR camera conversion provided for turning DSLR color cameras into pseudo-NDVI cameras was tested as an option adding infrared reflectance as a component for multi-spectral imaging on the high-throughput phenotyping system (Canon DSLR NDVI Conversion, LifePixel, Mukilteo, WA 98275). To test the success of the cameras on green fruit and green foliage discrimination, a tomato plant that was grown in a greenhouse during December 2017 was used as the test subject. The imaging took place outside to simulate field lighting conditions, most indoor lights do not emit the correct wavelengths in the NDVI spectrum. An unmodified DSLR camera and a modified pseudo-NDVI DSLR camera (Canon EOS T6, Canon USA Inc., Melville, NY, USA), were tested using the same lighting conditions with the same plant.

6.3.6. In-Field Testing

As described in Paper 1, the high throughout phenotyping system was designed to have 2 sets of DSLR cameras, one modified for NDVI and one unmodified [64]. The cameras were paired together so they would see the same plant at the same time. The in-field testing occurred during both the 2018 and 2019 growing season, as described in the previous chapter. A neural network similar to the one described in Paper 2 was trained on infrared images, but only detected green fruit. One early date with a lot of green fruit, June 25, 2019, was chosen to test the performance of infrared vs color images [64]. The test was to see how many total green fruit were detected per plant-plot on the same day using infrared and color images.

6.4.Results

6.4.1. Tomato Lab Testing

The tomato fruit reflectance is shown in Figure 41a, displaying each individual sample reflectance curve and the mean reflectance curve for all samples from 400nm – 2498nm. The tomato leaf top reflectance spectra is shown in Figure 41b, displaying each individual sample reflectance curve and the mean reflectance curve for all samples from 400nm – 2498nm. The tomato leaf bottom reflectance spectra is shown in Figure 41c, displaying each individual sample reflectance curve and the mean reflectance curve for all samples from 400nm – 2498nm.

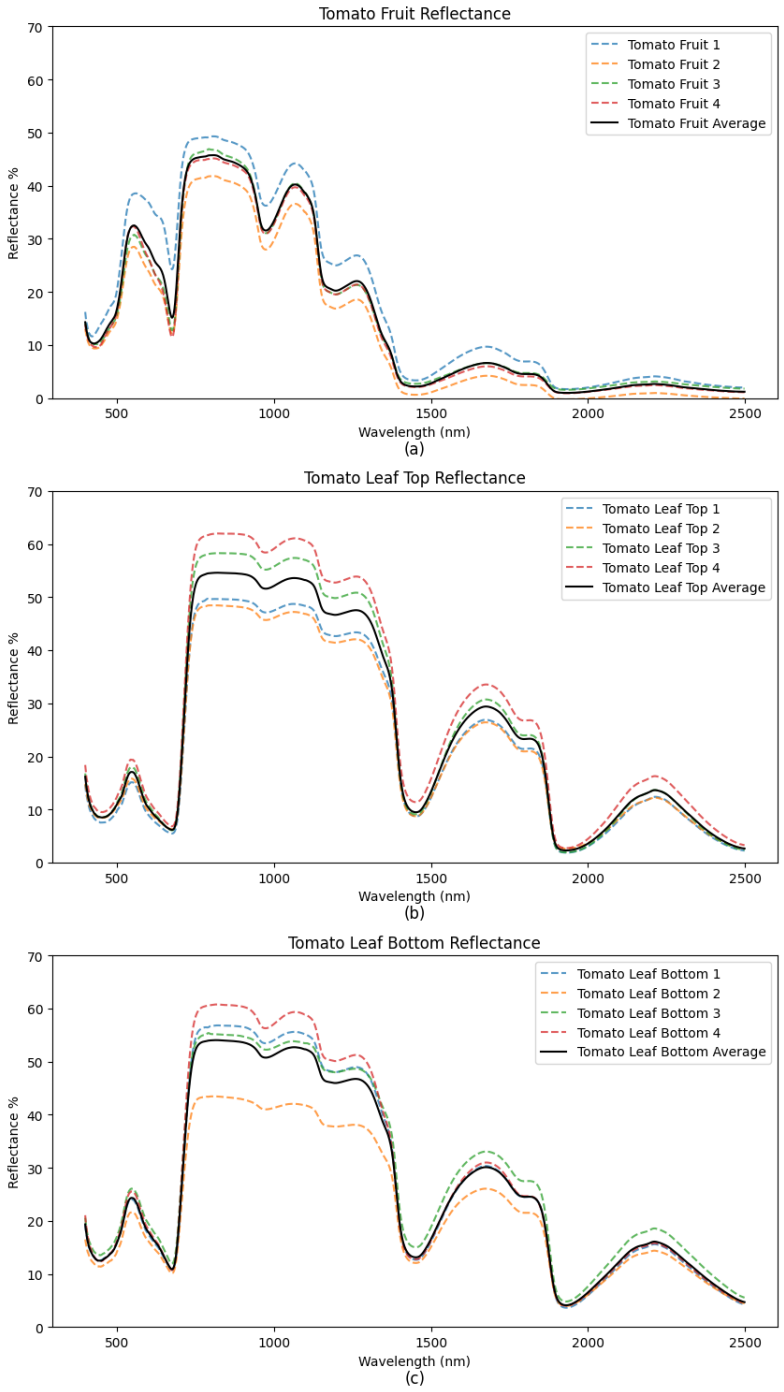


Figure 41: Reflectance data for tomato fruit (a) top of tomato leaf (b) and bottom of bottom leaf (c).

Figure 42 shows the average reflectance for tomato fruit, top of leaf, and bottom of leaf with 95% error bars shaded in grey. In the visible range, 380 – 700 nm, the tomato fruit has generally higher reflectance than both the leaf averages. For the infrared range 700 – 1000nm the tomato fruit has a lower reflectance average than both leaf averages but overlaps the in the 95% error bars. At around 1000 nm tomato fruit has a sharp decrease and deviates significantly from the leaf top and bottom averages.

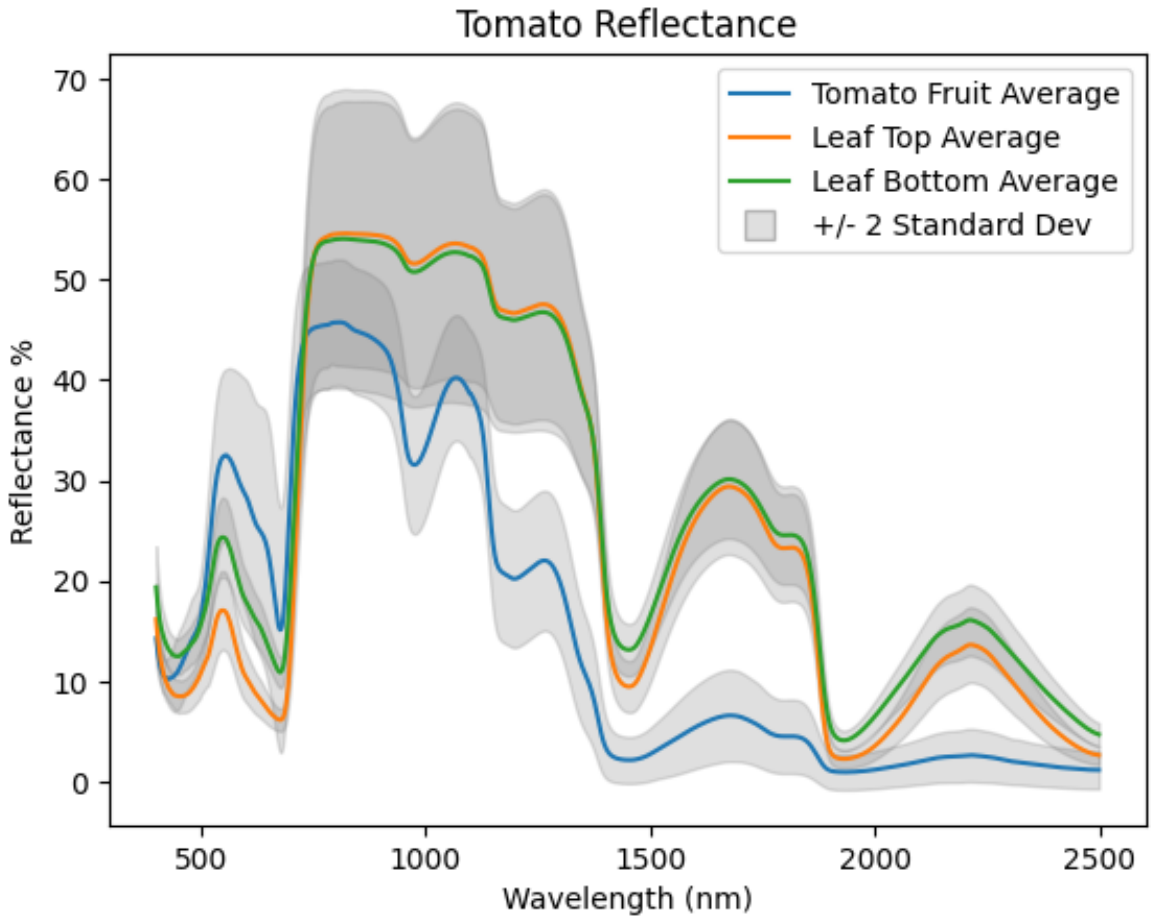


Figure 42: Reflectance data for average reflectance for tomato fruit, top of leaf, and bottom of leaf with 95% error bars.

Figure 43 shows the average reflectance curves from Figure 42 for leaf top and leaf bottom for clarity, with the shaded 95% error bars. The error bars of the top and bottom of the leaf completely overlap in the infrared and near infrared regions at 700 – 1000nm. Leaf top has generally lower reflectance compared to the leaf bottom in the visible range, though they follow the same curve, spiking at about 550 – 600 nm. The error bars in the visible range have minimal overlap.

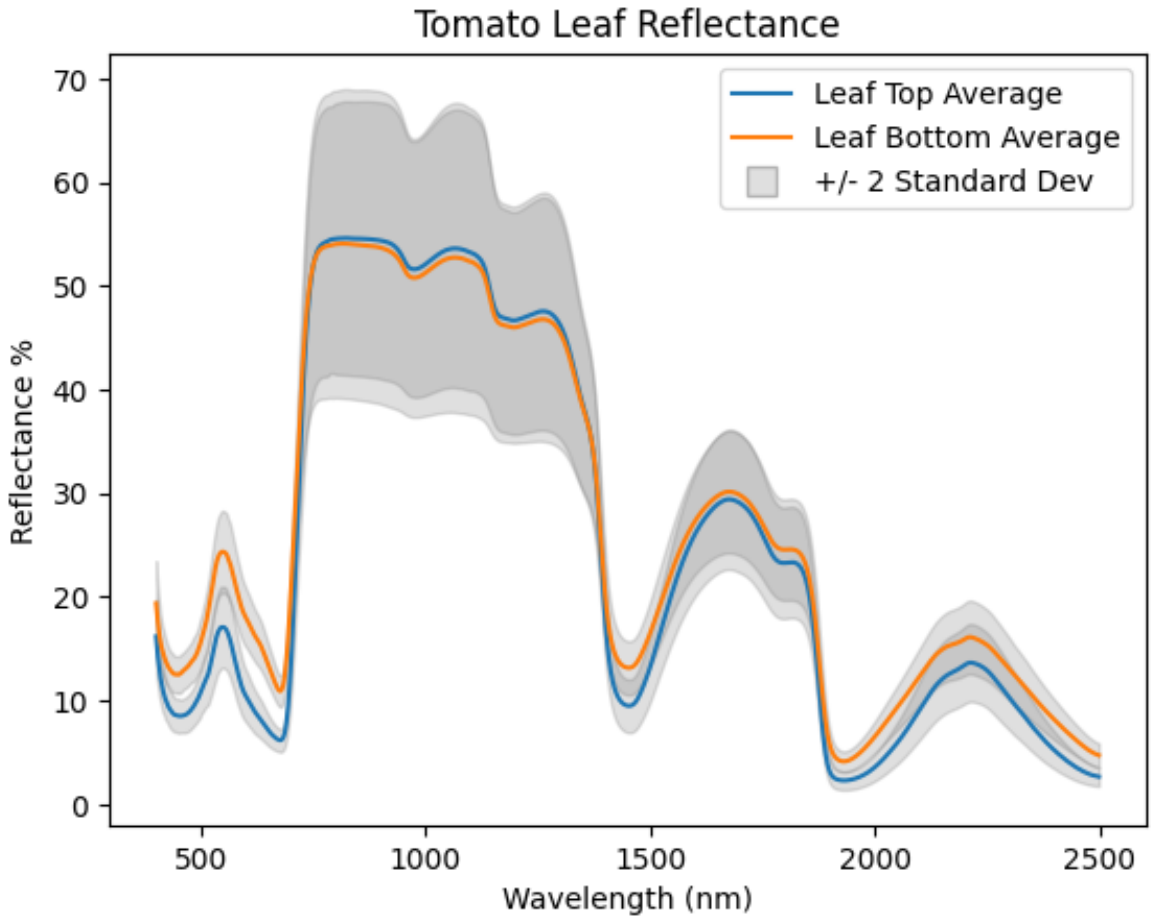


Figure 43: Reflectance data for average reflectance for tomato top of leaf and bottom of leaf with 95% error bars.

In the visible range the average difference between tomato fruit and tomato leaf is 10.0242%, the maximum difference is 18.071886% at 598 nm, and the minimum difference is 0.029539% at 418 nm. In the IR-A range the average difference between tomato fruit and tomato leaf is 12.6078%, the maximum difference is 20.034438% at 974 nm, and the minimum difference is 8.788509% at 794 nm. In the IR-B range the average difference between tomato fruit and tomato leaf is 13.5653%, the maximum difference is 27.659091% at 1332 nm, and the minimum difference is 1.314568 % at 1930 nm. Figure 44 shows the average reflectance values of tomato fruit and leaf at each of the 3 ranges with 95% error bars.

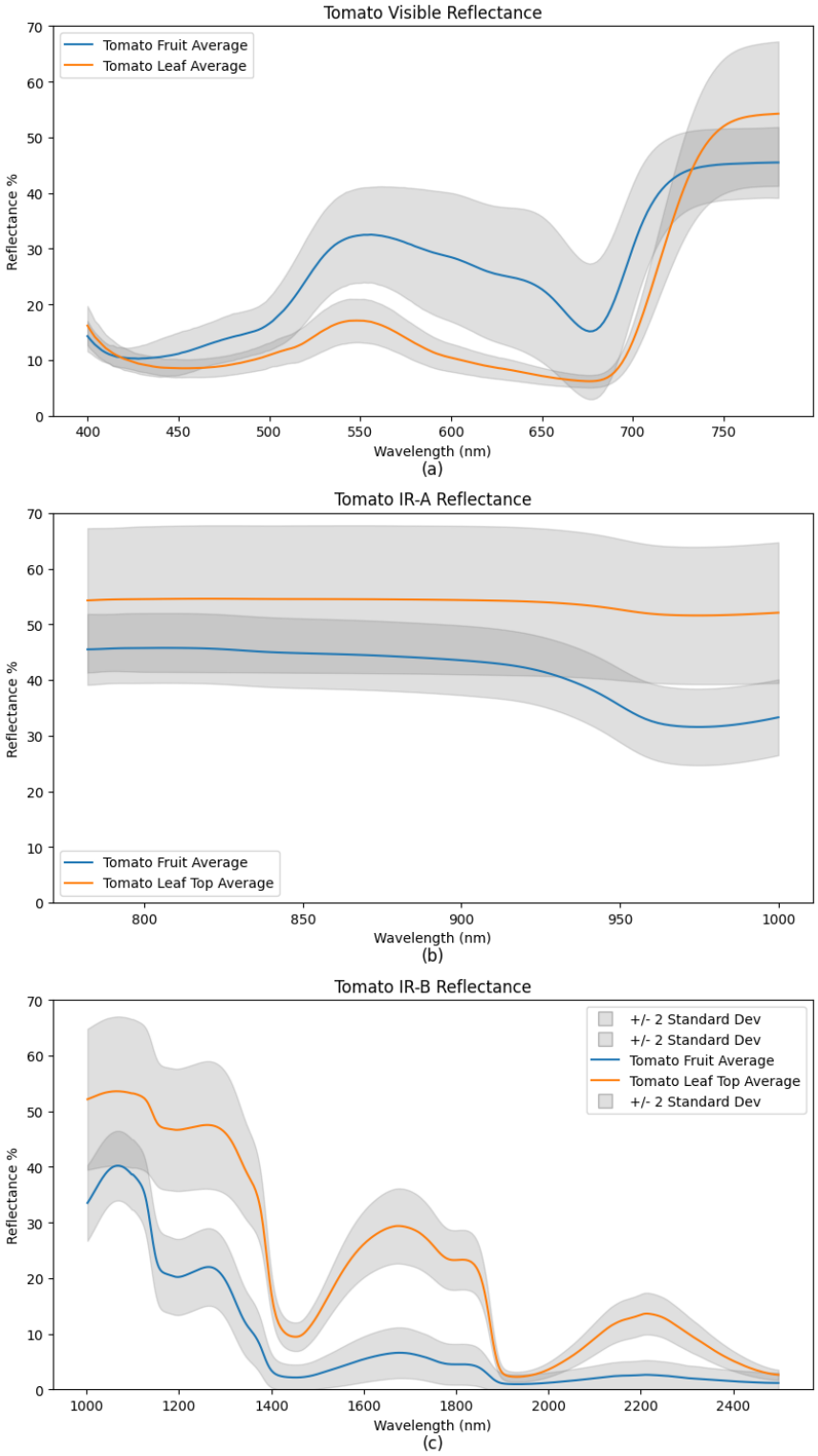


Figure 44: The average reflectance values of the tomato fruit and top of tomato leaf broken down into visible and near IR 380-780nm (a), Infrared-A 782-1000nm (b), and Infrared-B 1000-2498nm (c) ranges.

Table 12: the average, minimum, and maximum absolute difference between tomato fruit and tomato top of leaf reflectance is displayed in the table and split into the 3 wavelength ranges.

	Average diff (%)	Max Diff (%)	Wavelength nm Max	Min Diff (%)	Wavelength nm Min
Visible	10.0242	18.071668	598	0.029539	418
Infrared A	12.6078	20.034438	974	8.788509	794
Infrared B	13.5653	27.659091	1332	1.314568	1930

6.4.2. Camera Selection Test

A preliminary test was performed with a regular color camera and a pseudo-NDVI camera outdoors to see if there was any visual significant difference in green fruit. This test was performed before modifying multiple DSLR cameras for multi-view high-throughput phenotyping. Figure 45 and Figure 46 from the field simulation shows images from the color and pseudo-NDVI cameras. The regular color image of a tomato plant is as expected, dark-green foliage with a light-green fruit. The infrared image of the tomato plant has dark-orange foliage and a light-green fruit. Using the ImageJ software to look at the color histogram of a portion of the plant that has both the fruit and foliage shows that the color image has an even distribution of pixels in the green space. The infrared image has a condensed histogram with two spikes, one at dark-orange and one at yellow.



Figure 45: Example of color DSLR (left) and LifePixel pseudo-NDVI DSLR (right) taking a picture of the same tomato plant and fruit in ambient outdoor lighting

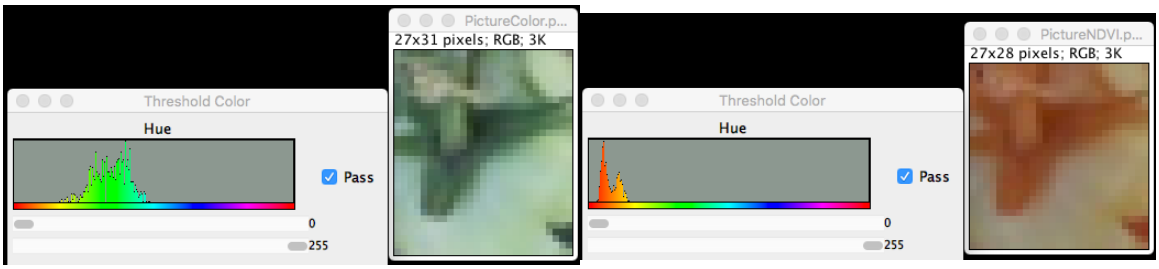


Figure 46: Hue histograms of zoomed in views of the color DSLR (left) and pseudo-NDVI camera (right) images. The zoomed in images have both the green fruit and green foliage.

6.4.3. In-Field Tomato Testing

The in-field images show the same plant imaged with a normal color DSLR and a modified infrared DSLR. The imaging was done using the high-throughput phenotyping system described in Paper 1, including using the custom lighting modules to enhance the infrared [64]. The in-field infrared images have dark-orange foliage and yellow-orange fruit, and the color images have dark-green foliage and medium-green fruit. ImageJ was used to segment the fruit from the foliage in the HSV color space. Both images segmented fruit from the foliage. The infrared image have a smaller threshold in the hue (17-28) than the color image (44-73). The infrared

image and color image both segmented yellow flowers. The color image segmented some dirt and light green foliage.



Figure 47: Example of the same tomato plant in the field captured with a color DSLR (left) and pseudo-infrared DSLR (right). The pseudo infrared camera makes the leaves turn orange and the green fruit turn yellow.

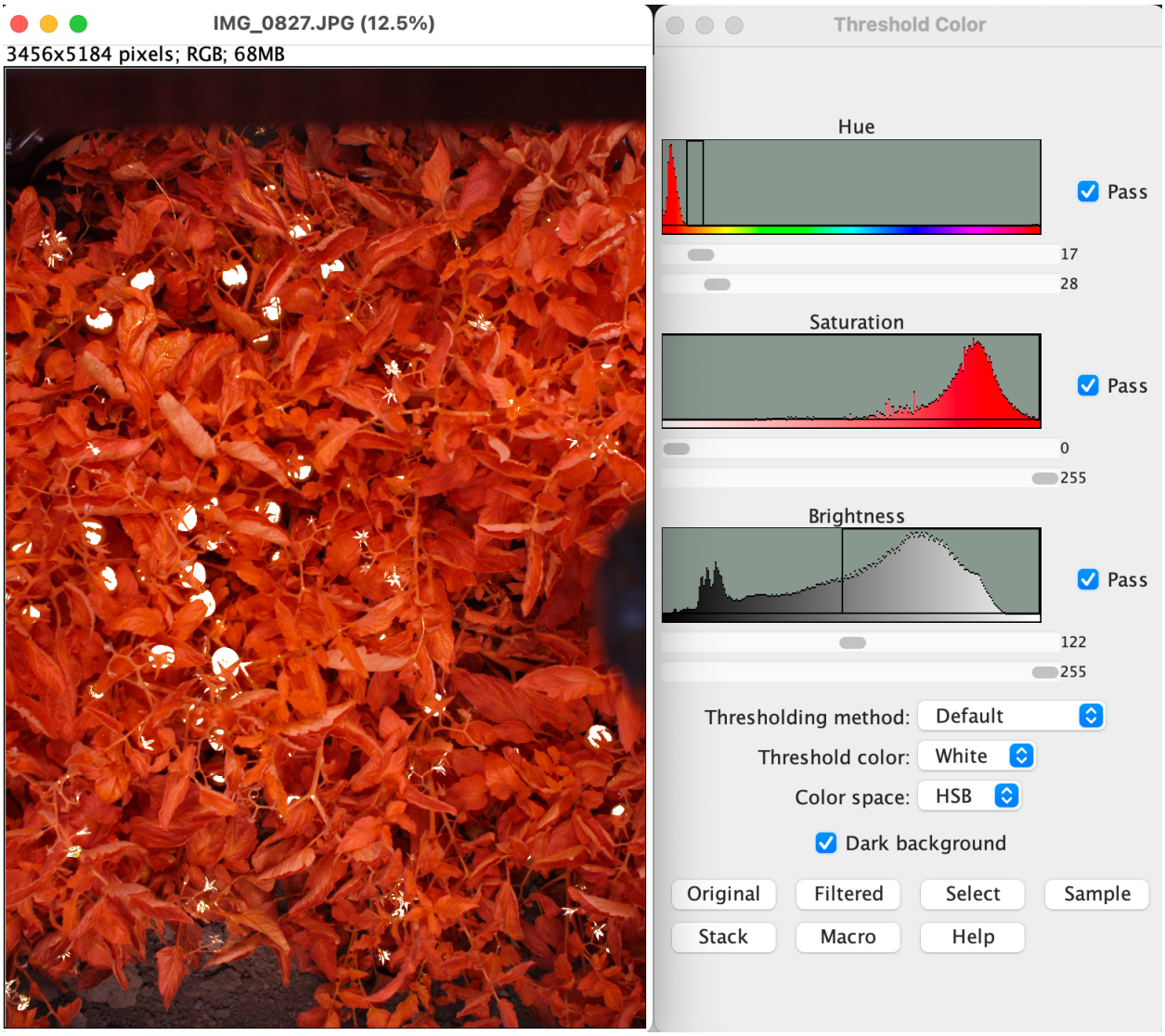


Figure 48: Pixel segmentation of a pseudo-infrared image using ImageJ for detecting green fruit. The segmentation was done in the Hue/Saturation/Brightness space and pixels that were in the hue range for green fruit in an NDVI image are highlighted in white.

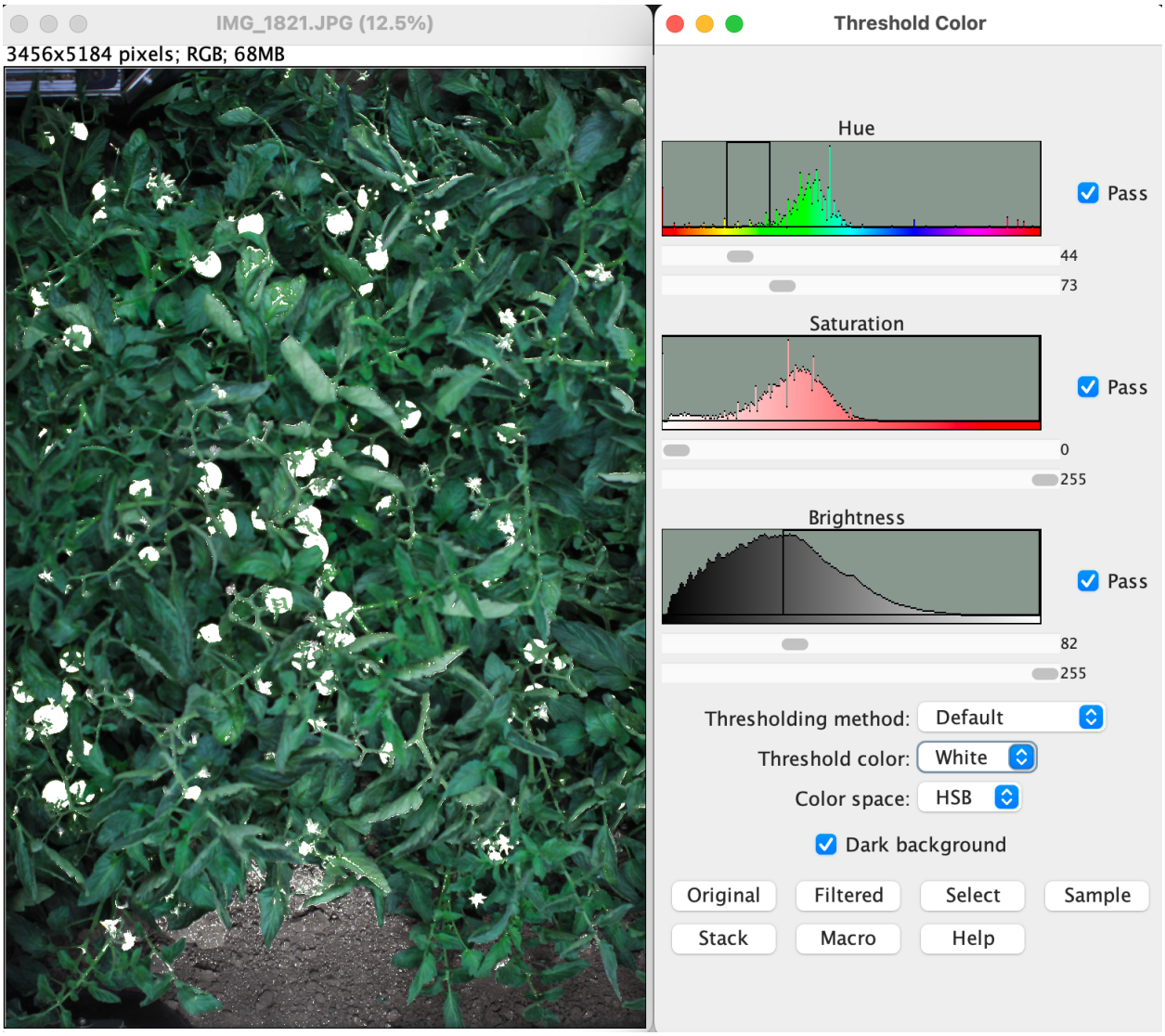


Figure 49: Pixel segmentation of a RGB image using ImageJ for detecting green fruit. The segmentation was done in the Hue/Saturation/Brightness space and pixels that were in the hue range for green fruit are highlighted in white.

In this sample of 20 tomato plots in the IR images, fewer green tomato fruit were detected than in the RGB images. Plot 19FD0001 shows a discrepancy of almost double. 19FD0003, 19FD0004, 19FD0007, and 19FD0021 detected about the same amount. 19FD0016 detected more green fruit in the IR image than in the RGB image. In Figure 51, 340/400 plant-plots had a higher green fruit count in the RGB images. As shown in Figure 52 the median number of green

fruit detected in each plant-plot is less in infrared images than in color images. In Figure 53 the median difference between Color Image Green Fruit Count and Infrared Image Green Fruit Count is about 25 fruit and the upper and lower quartile are both above 0.

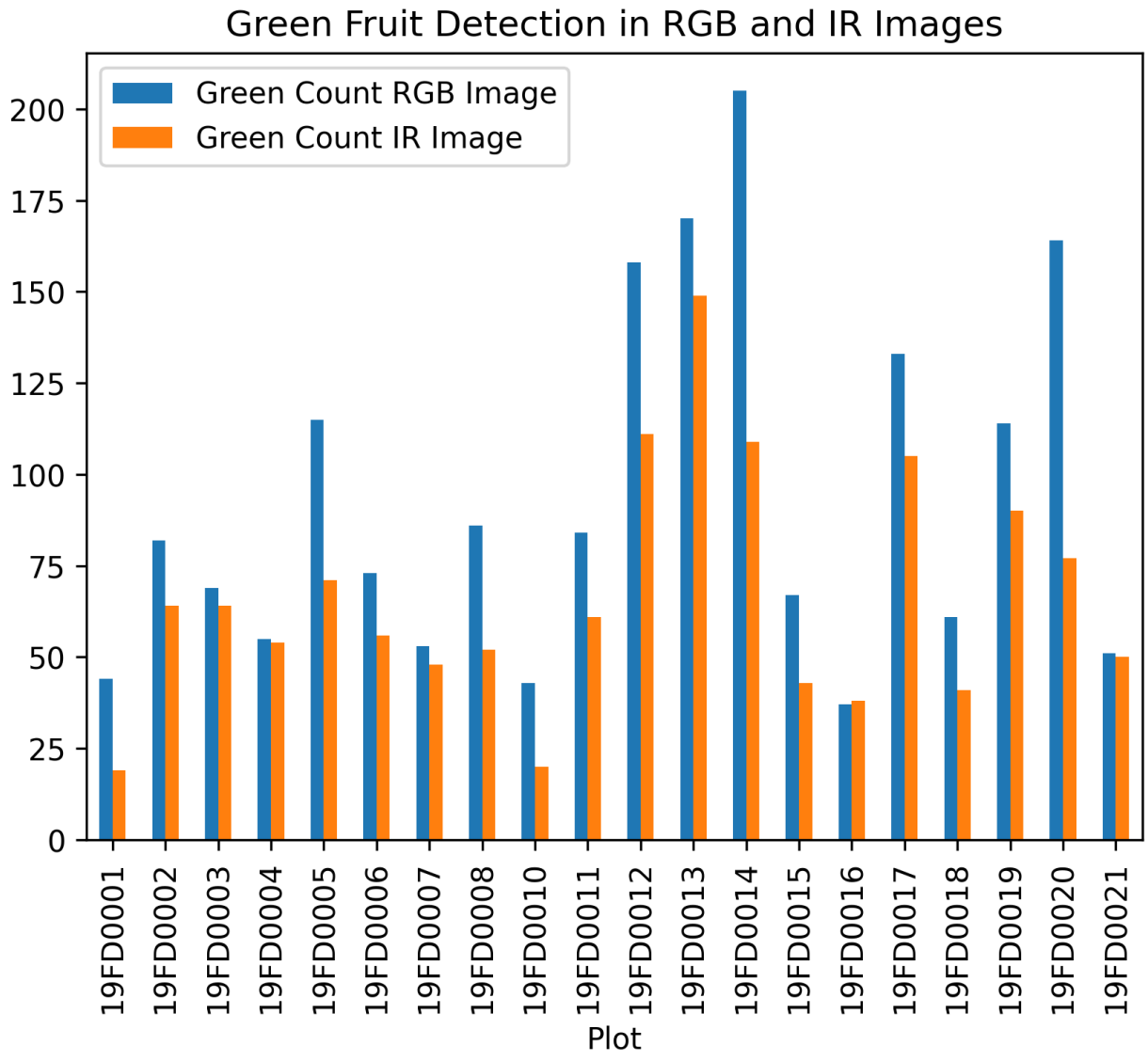


Figure 50: 20 tomato plant-plots showing detected green fruit from RGB images and IR images

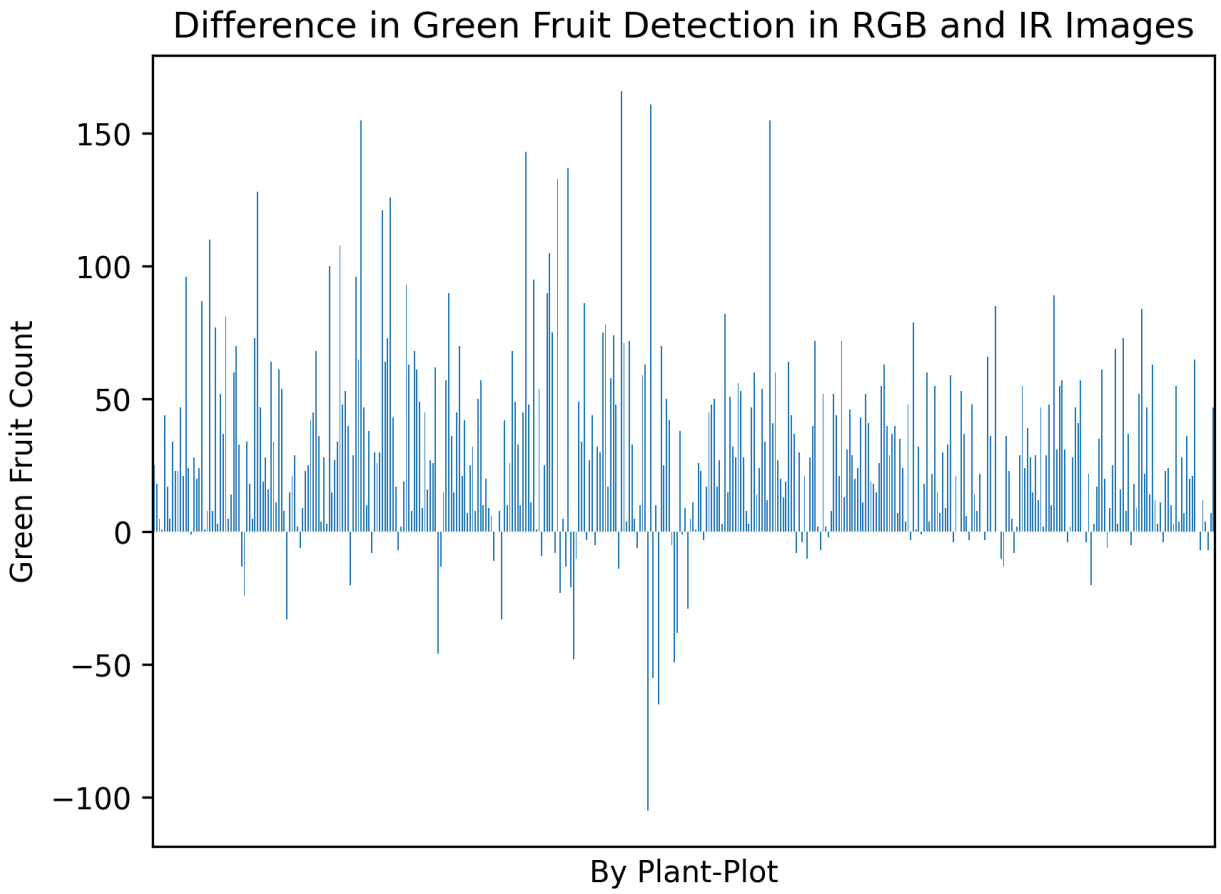


Figure 51: difference of green tomato fruit count by plant-plot on June 25, 2019. Positive means there were more green fruit detected in the color image. 340 of 400 plant-plots had more green fruit detected in the color images and 60 of 400 images had the same amount of more detected in the infrared images.

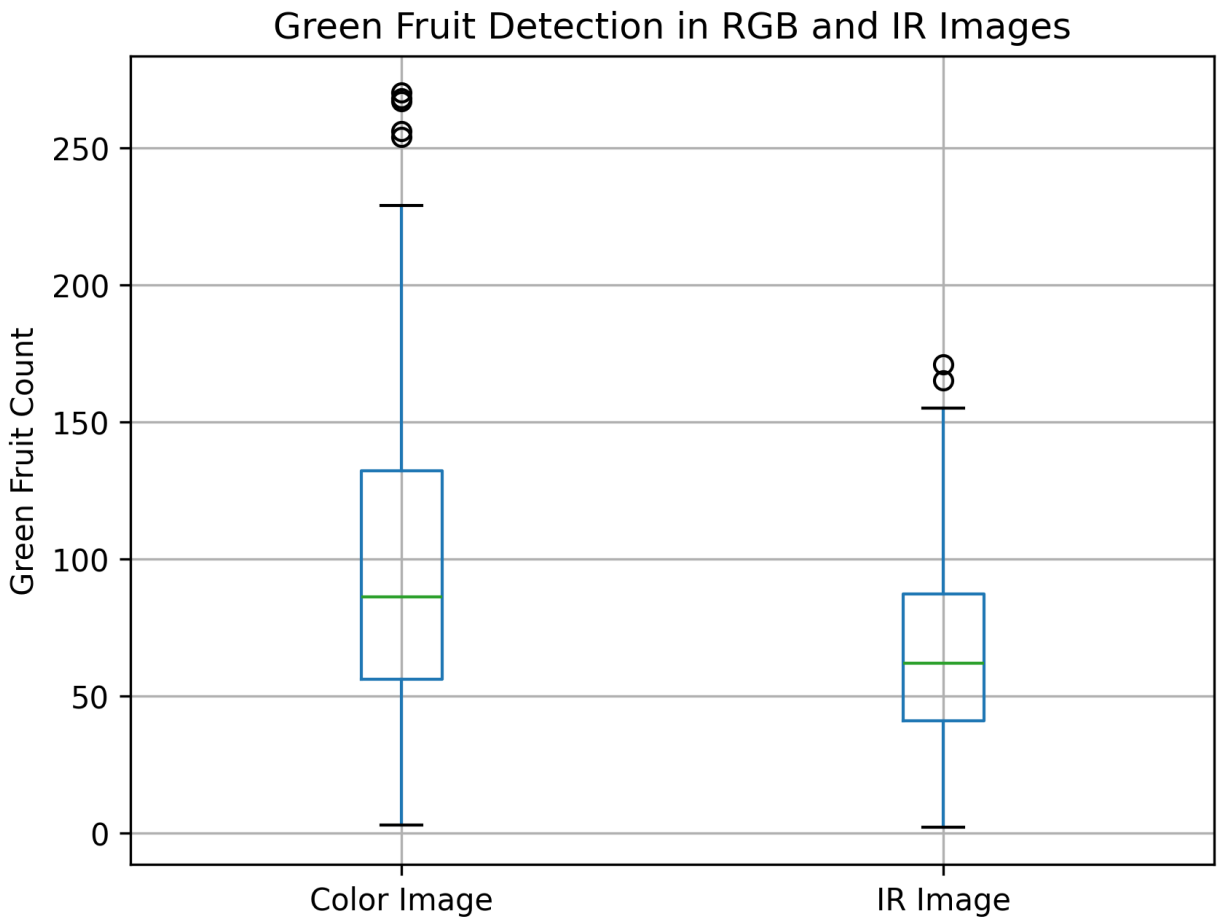


Figure 52: Distribution of average green tomato fruit detected in both color images and IR images.

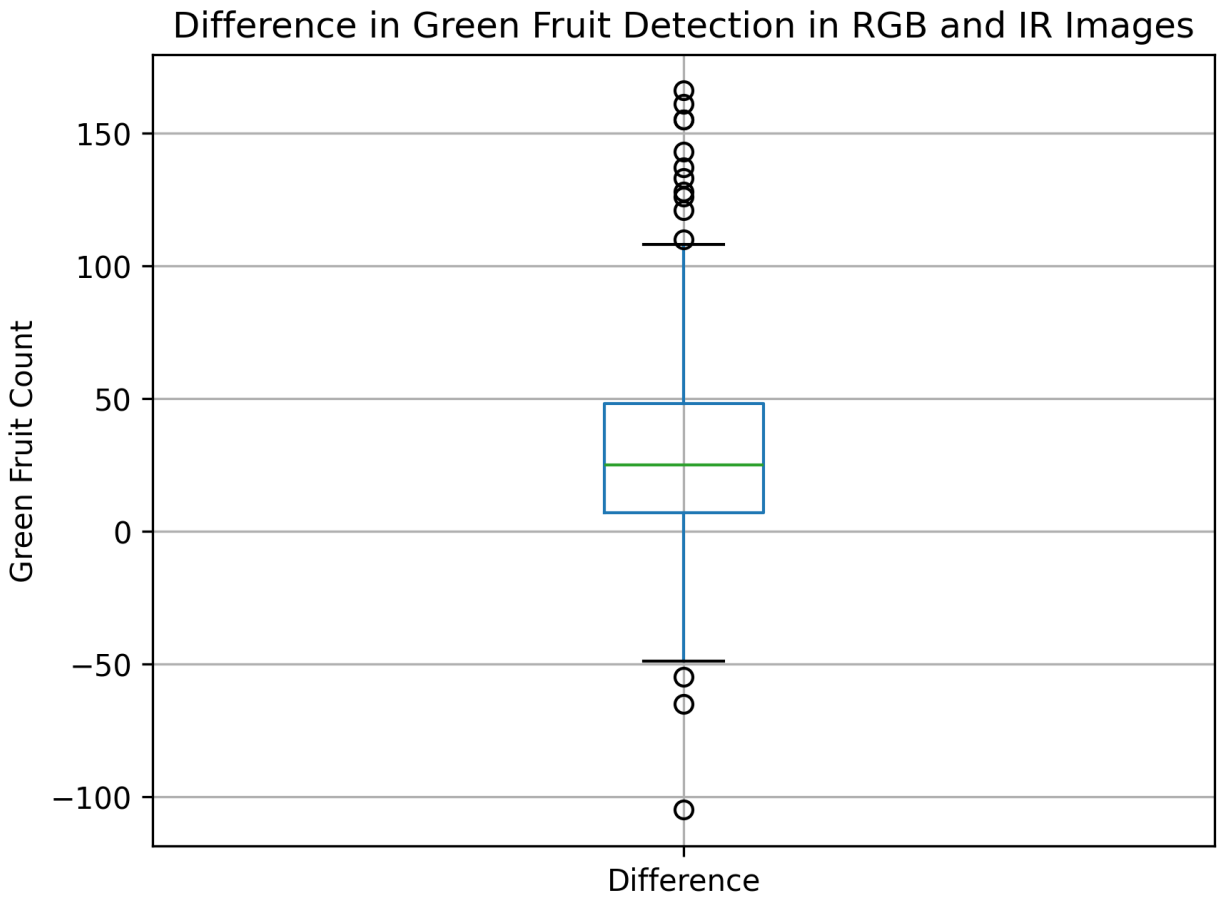


Figure 53: Distribution of difference in green tomato fruit count (Color - IR).

6.4.4. Pepper

6.4.4.1. Pepper Lab Testing

Figure 54(a-e) shows the individual reflectance of the different peppers scanned with the spectrophotometer and. Comparing all of the peppers against each other in Figure 54f we can see there is a lot of variability between different pepper varieties. Figure 55 shows the reflectance of the top and bottom of bell pepper leaves and banana pepper leaves.

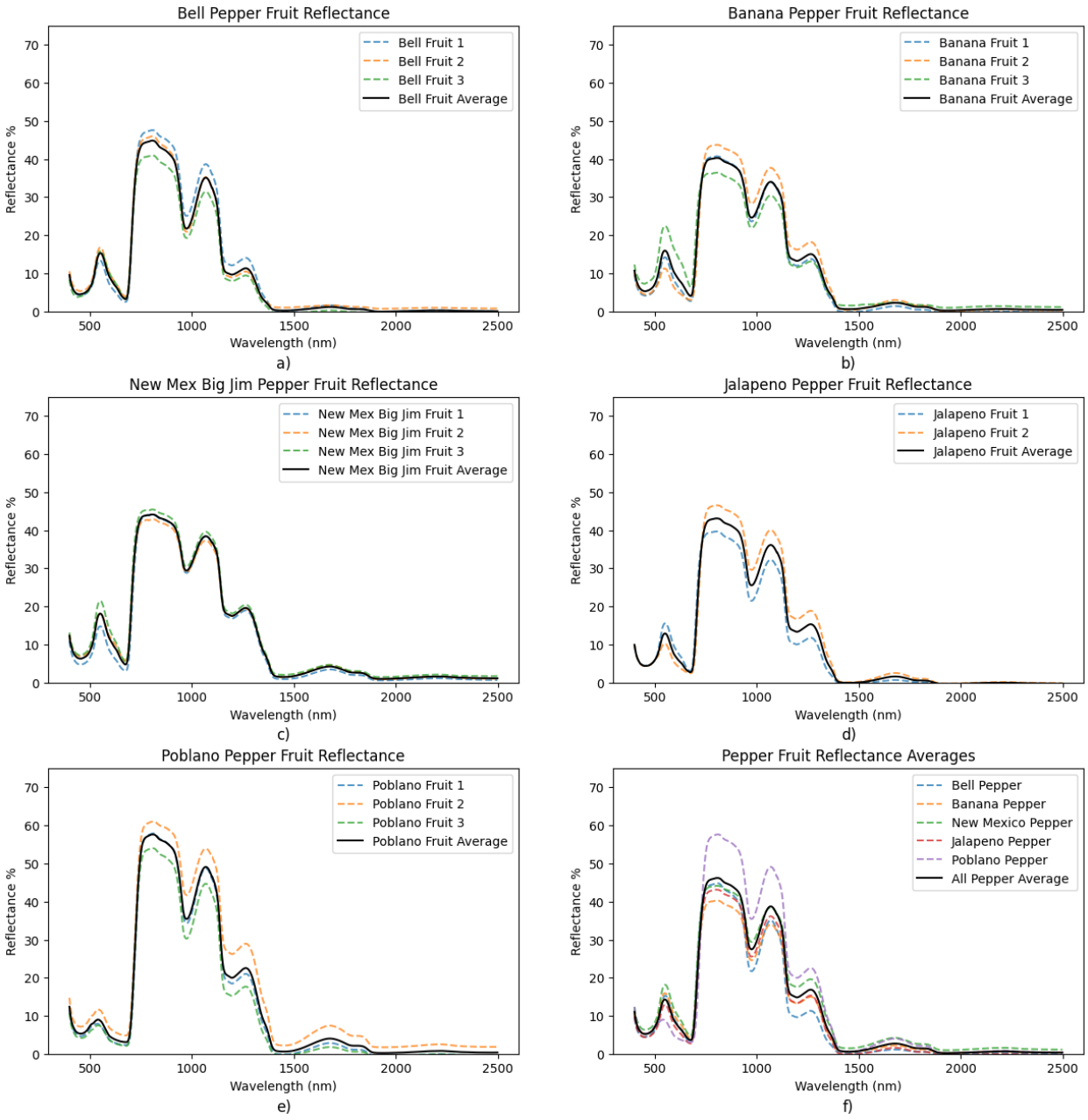


Figure 54: Average reflectance and individual reflectance for Bell Pepper (a), Banana Pepper (b), New Mex Big Jim Pepper (c), Jalapeno Pepper (d), Poblano Pepper (e), and all peppers (f).

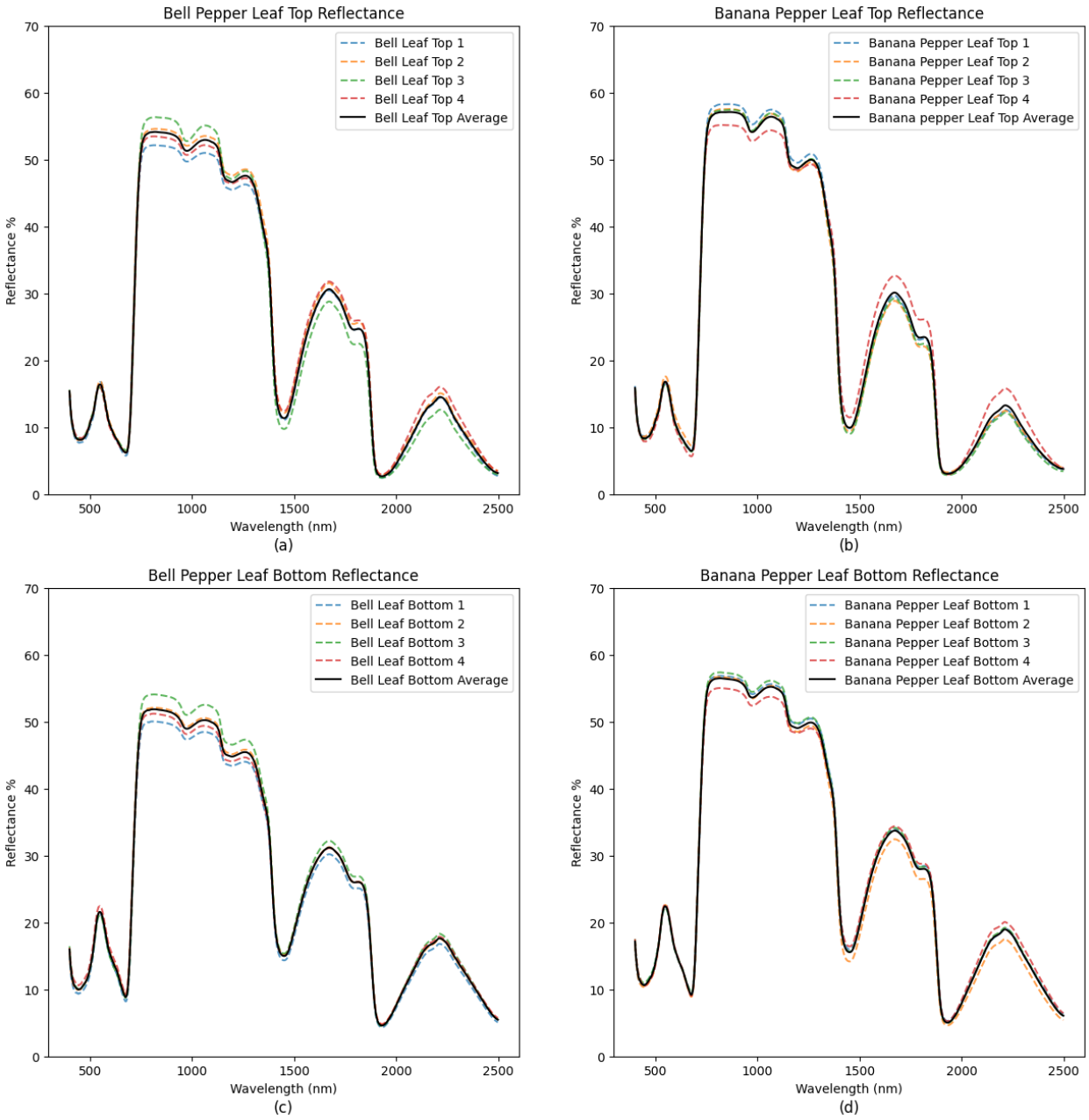


Figure 55: Average reflectance and individual reflectance for Bell Pepper leaf top (a), Banana Pepper Leaf Top (b), Bell Pepper Leaf Bottom (c), Banana Pepper Leaf Bottom (d).

In Figure 56 the fruit reflectance curve has a large error bar due to the differences due to pepper variety. The fruit reflectance error bars overlap with the infrared and near infrared of the leaves. Figure 57 shows the average reflectance curves from Figure 56 for leaf top and leaf bottom for clarity, with the shaded 95% error bars. The error bars of the top and bottom of the leaf completely overlap in the infrared and near infrared regions at 700 – 1000nm. Leaf top has generally lower reflectance compared to the leaf bottom in the visible range, though they follow the same curve, spiking at about 550 – 600 nm. The error bars in the visible range have minimal overlap.

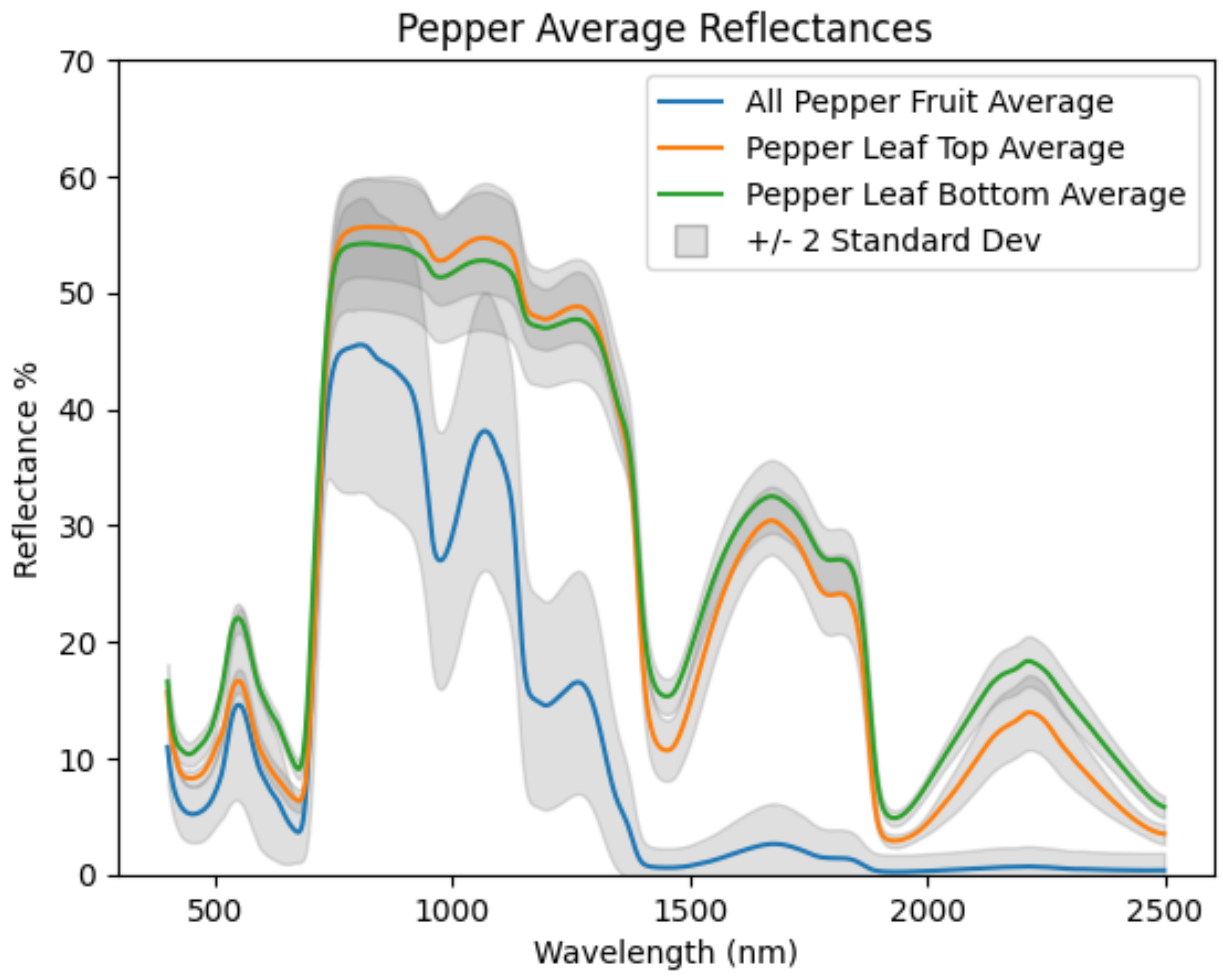


Figure 56: Reflectance data for average reflectance for pepper fruit, top of leaf, and bottom of leaf with 95% error bars.

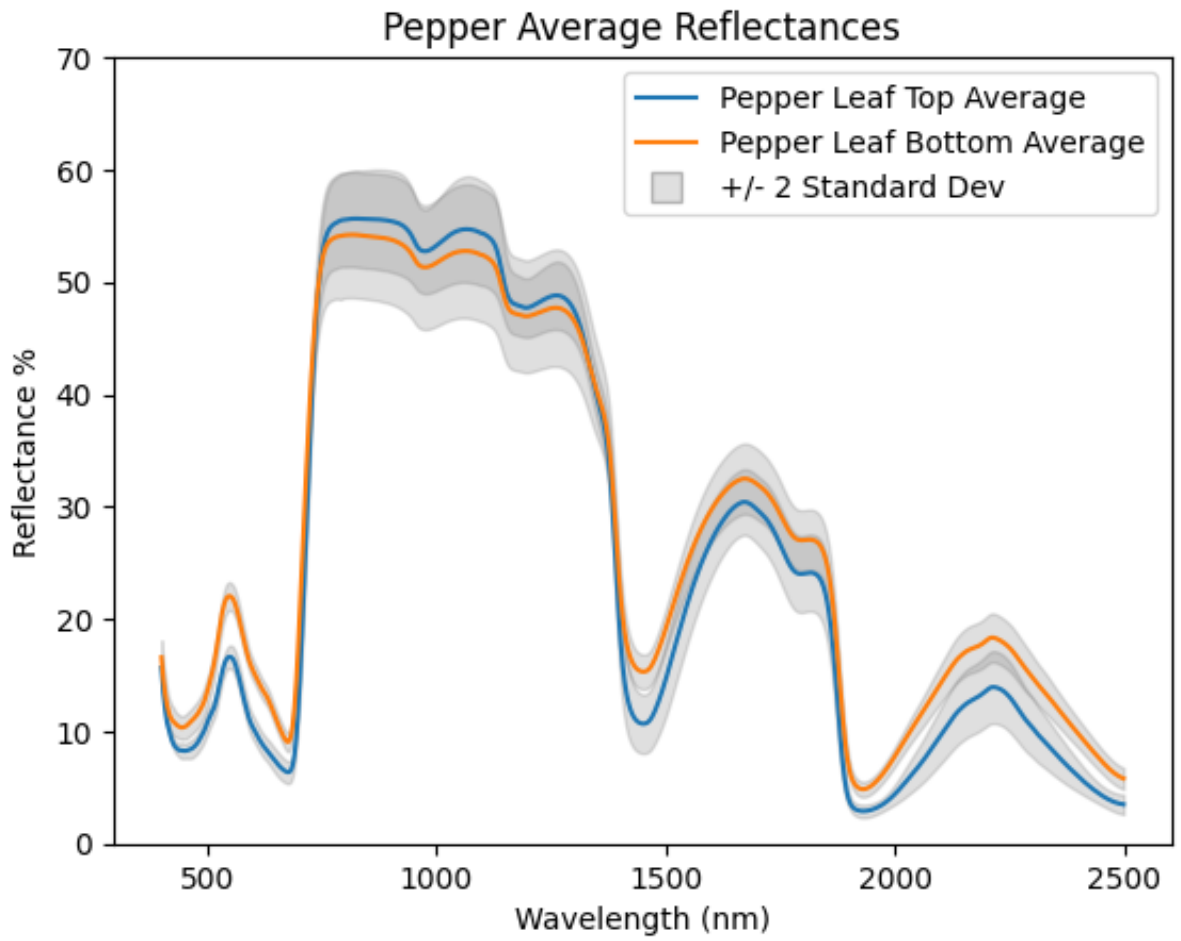


Figure 57: Reflectance data for average reflectance for pepper top of leaf and bottom of leaf with 95% error bars

In the visible range the average difference between pepper fruit and pepper leaf is 2.75069%, the maximum difference is 8.178356 % at 750 nm, and the minimum difference is 0.006598% at 712 nm. In the IR-A range the average difference between pepper fruit and pepper leaf is 14.6078%, the maximum difference is 25.270064% at 974 nm, and the minimum difference is 8.379401% at 752 nm. 970 nm is approximately where water would show in spectroscopy, which is stronger in the peppers than tomatoes. In the IR-B range the average difference between pepper fruit and pepper leaf is 27.35867%, the maximum difference is 34.345667% at 1328 nm, and the minimum difference is 15.962795 % at 1068 nm. Figure 58 shows the average reflectance values of pepper fruit and leaf at each of the 3 ranges with 95% error bars. This indicates that there is better separation in NIR in peppers than tomatoes.

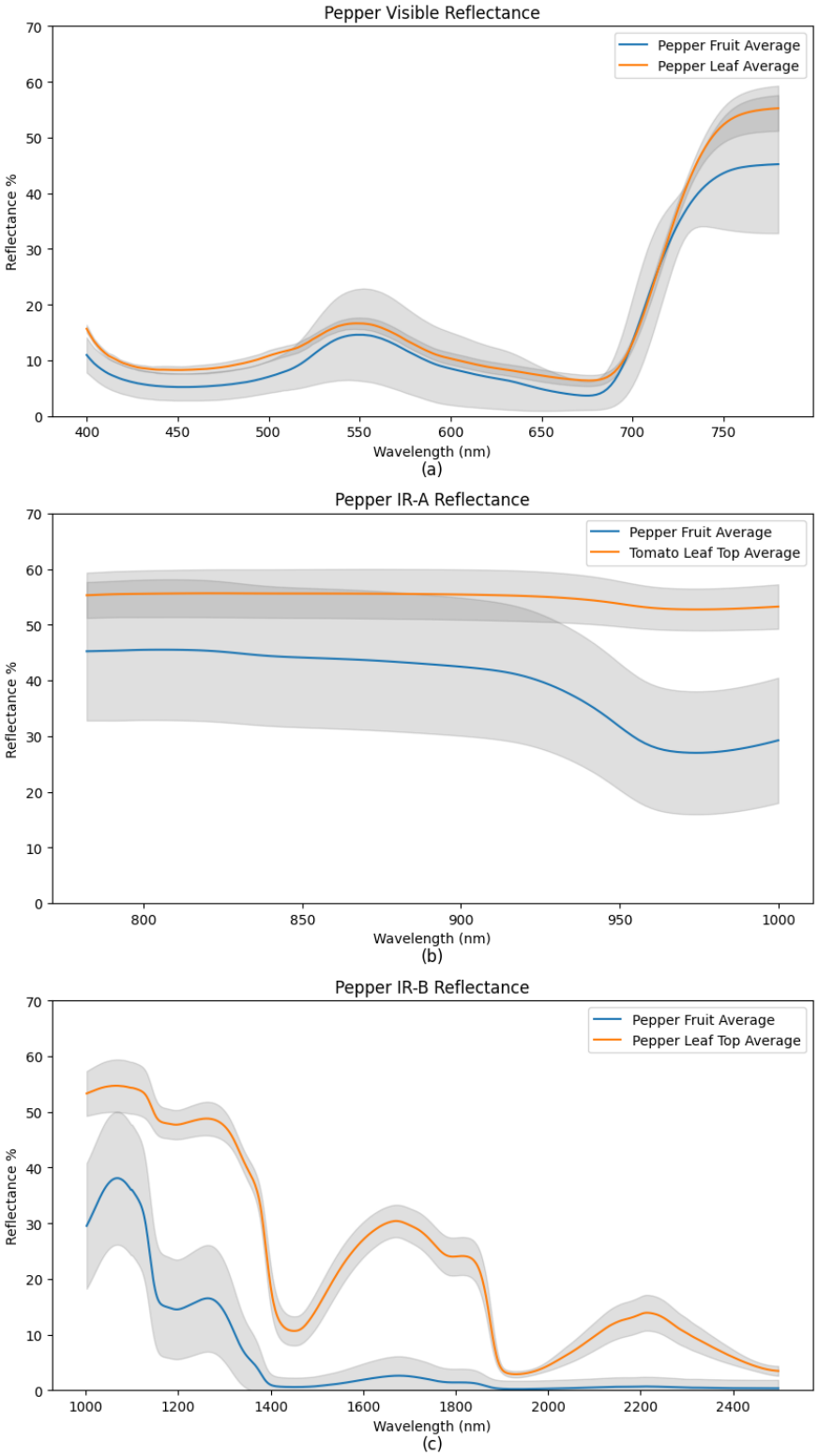


Figure 58: the average reflectance values of the pepper fruit and top of pepper leaf broken down into visible and near IR 380-780nm (a), Infrared-A 782-1000nm (b), and Infrared-B 1000-2498nm (c) ranges.

Table 13: the average, minimum, and maximum absolute difference between pepper fruit and pepper top of leaf reflectance is displayed in the table and split into the 3 wavelength ranges.

	Average diff	Max Diff	Wavelength nm	Min Diff	Wavelength nm
Visible	2.75069	8.178356	750	0.006598	712
Infrared A	14.13678	25.270064	974	8.379401	752
Infrared B	27.35867	34.345667	1328	15.962795	1068

6.4.5. In-Field Tomato Testing

The in-field images show the same plant imaged with a normal color DSLR and a modified infrared DSLR. The imaging was done using the high-throughput phenotyping system described in Paper 1, including using the custom lighting modules to enhance the infrared [64]. The in-field infrared images of bell peppers have dark-orange foliage and orange fruit, and the color images have dark-green foliage and dark-green fruit. ImageJ was used to segment the fruit from the foliage in the HSV color space. Both images segmented fruit from the foliage. The infrared image have a smaller threshold in the hue (14-29) than the color image (44-71). Both the images had foliage and dirt in the segmentation.



Figure 59: Example of the same bell pepper plant in the field captured with a color DSLR (left) and pseudo-infrared DSLR (right). The pseudo infrared camera makes the leaves turn dark orange and the green fruit turn orange.

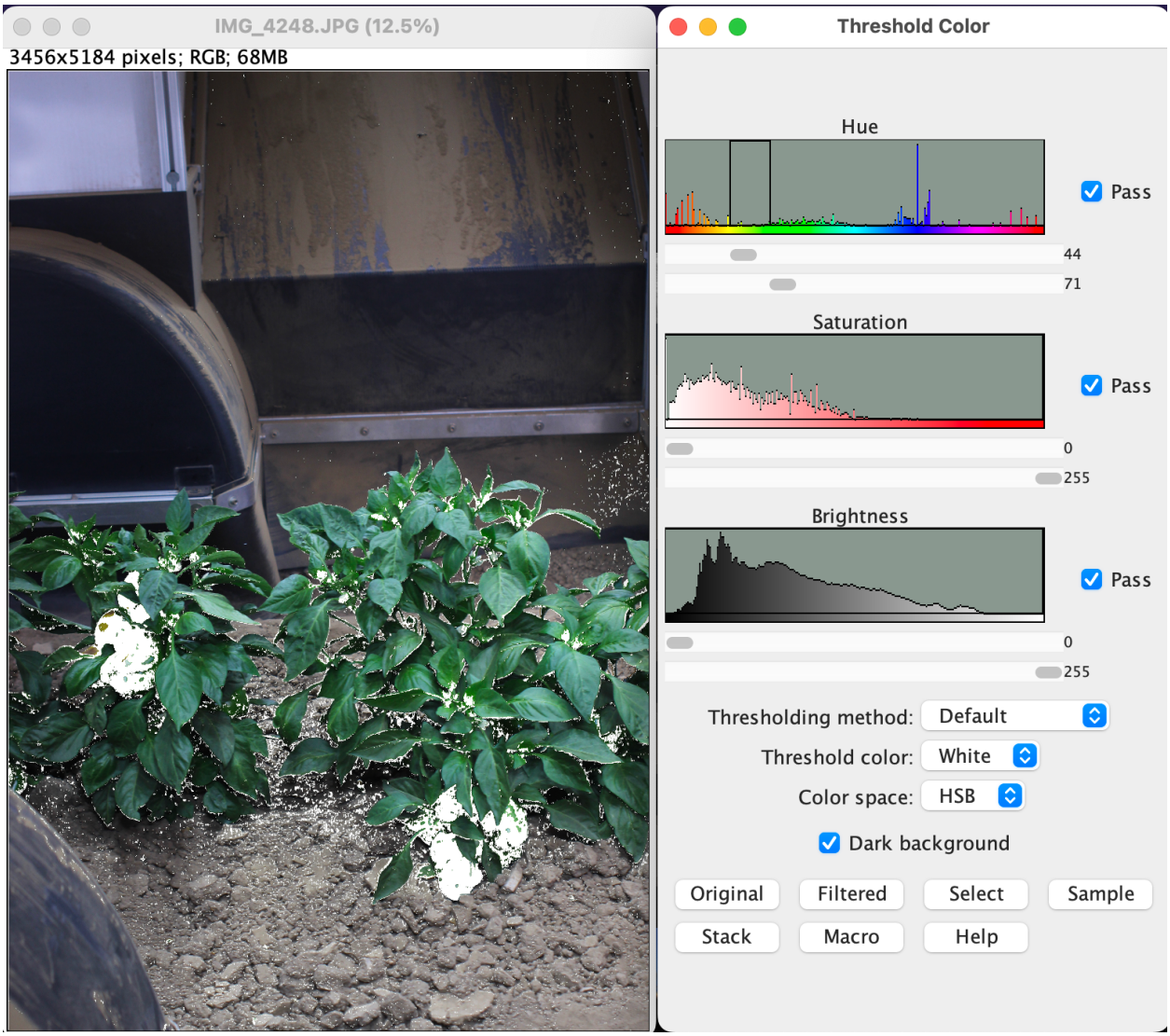


Figure 60: Pixel segmentation of a color image using ImageJ for detecting green bell pepper fruit. The segmentation was done in the Hue/Saturation/Brightness space and pixels that were in the hue range for green fruit the image are highlighted white.

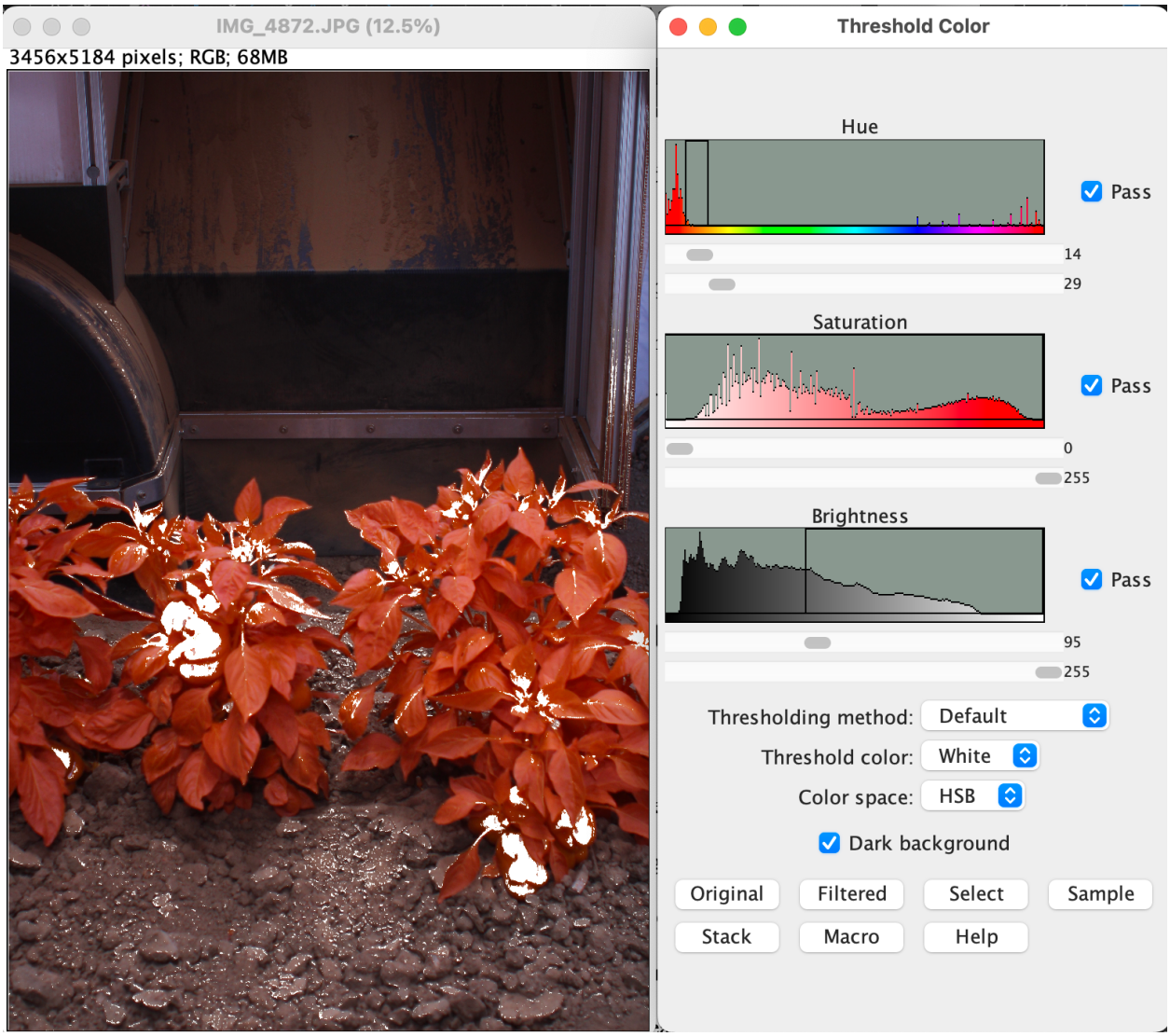


Figure 61: Pixel segmentation of a Pseudo-NDVI image using ImageJ for detecting green bell pepper fruit. The segmentation was done in the Hue/Saturation/Brightness space and pixels that were in the hue range for green fruit in an NDVI image are highlighted white.

6.5.Discussion

Splitting up the wavelengths into visible, infrared A, and infrared B bands at 400-750nm, 750-1400nm, and 1400-3000nm respectively, we can take a closer look. The visible bands, 400-750nm, for leaves and fruit follow the same general pattern. There is a spike of reflectance at around 550 nm and a decrease with the minimum at around 650nm. 650nm is where chlorophyll

shows in spectroscopy. This shows that leaves and fruit both generally reflect green wavelengths more than red wavelengths.

Although there are greater differences between fruit and leaves at wavelengths greater than 1000 nm, the cost of cameras at the time capable of measuring those wavelengths would be too expensive. Looking at infrared and near infrared wavelengths close to the visible wavelengths was more cost effective. The prominent feature is that the water absorbance band at 970 nm is stronger in the fruit for both peppers and tomatoes than in water. The ideal sensor setup for cost, automation, and image quality would be to have two cameras with identical electronics, operating systems, and configuration systems. The difference would be the type of sensor within the camera, that one that can capture visible wavelengths and one that can capture near infrared wavelengths.

6.5.1. Tomato

The tomato leaf spectral signature in Figure 41b followed similar trends to healthy leaves in studies using multispectral data for disease detection in tomato plants [75], [86]. The tomato fruit spectral signature in Figure 41a followed similar trends to the ripe green tomato fruit in previous studies looking for fruit ripeness indicators using multispectral sensors [105]. Figure 43 shows that the top and bottom of the tomato leaf have similar spectral signatures. With error curves of +/- 2 standard deviations, the curves overlap significantly, therefore we can treat the top of the leaf and bottom of the leaf as one unit. For the more in-depth analysis of the spectral data, we will only consider the tomato fruit and top of the tomato leaf.

From Table 12: the average, minimum, and maximum absolute difference between tomato fruit and tomato top of leaf reflectance is displayed in the table and split into the 3 wavelength

ranges., both Infrared A and B have a larger difference in reflectance than the visible, 12.61%, 13.57%, and 10.02% respectively. Meaning using infrared A or Infrared B for distinguishing between green tomato fruit and tomato leaves would likely be more successful than using the visible spectrum.

6.5.2. Pepper

The pepper leaf spectral signature found in this study Figure 55 followed a similar trend to pepper leaves with varying levels of nitrogen treatment [94]. Additionally, the bell pepper fruit scanned in this study follows the NIR spectroscopy study done in assessing the ripening stages and freshness of a bell pepper fruit [95]. Figure 55 shows that the top and bottom of pepper leaves have similar spectral signatures, so for the rest of the study we considered only the tops of the pepper leaves.

From Table 13, both Infrared A and B have a larger difference in reflectance than the visible, 14.14%, 27.36%, and 2.75% respectively. Meaning using infrared A or Infrared B for distinguishing between green pepper fruit and pepper leaves would likely be more successful than using the visible spectrum. This also indicates that NDVI may have more success in pepper than tomato.

Visually examining the infrared images of and bell pepper (Figure 59) plants show that there is not as much visual distinction between green fruit and green foliage in the infrared. The conclusion that can be drawn from this is that in peppers, different wavelengths must be used for enhancing green fruit detection using 2D imaging.

6.5.3. Sensor Selection

Most modern DSLR cameras are equipped with a hot mirror filter. Hot mirror filters reflect near infrared, infrared, and heat generating wavelengths while transmitting visible wavelengths. For a standard digital camera this is necessary because the red section of modern digital camera sensors allow some infrared and near infrared wavelengths through. Without the hot mirror filter the images would have some artifacts and would be affected by temperature. In this case, by removing the hot mirror filter from the DSLR camera it is possible to transmit infrared and near-infrared wavelengths into the digital image. This is a low-cost method of imaging in infrared and near infrared since the digital camera sensors are already sensitive to those wavelengths. There are methods of removing the hot mirror filter and replacing it with a different filter that transmits infrared and near infrared bands. Filter that is used by LifePixel specifically transmits 400-600nm and 700-800nm wavelengths. This blocks the red wavelengths and allows the near infrared wavelengths to go through. The combination of using visible and infrared/near-infrared lights can help make clearer distinctions between green fruit and green leaves, as shown from Table 12 and Table 13.

6.5.4. Pixel Segmentation

The results from segmenting the color vs infrared images in tomato using HSV shows promise for creating classic machine learning and image processing methods to distinguish green fruit from green foliage. Due to the stark contrast of yellow fruit on orange foliage compared to light green fruit on dark green foliage, the infrared images could also be used to simplify total green fruit count. The contrasting colors and images could make it easier for a human to detect green fruit and create manual phenotyping methods that can be turned easily into automated phenotyping. The addition of low-cost NDVI imaging to proximal sensing could enhance the

detection of green fruit on green foliage using classic computer vision techniques. Classic computer vision techniques are generally less computationally intensive than neural networks and machine learning, so this could be an affordable alternative.

6.5.5. Neural Network Performance

The infrared images consistently showed a lower green tomato fruit count than in the color images. This could be explained by the fact that some tomato leaves are similar in shape and color to green tomato fruit. This would mean some of the green fruits that were detected were green leaves, resulting in false positives in the color images. Some of the differences between green fruit and green foliage in the infrared images are minimally different to the human eye, but they may have more distinguishable features that the neural network was able to detect. 85% of plant-plots had more green fruit detected in the color images than in the infrared images. In this small case-study it shows the possibility that the color images results in more double counting than in the infrared images. Future research should include comparing a manual count of green fruit to the green fruit counts from infrared and color images. This would give a more formal conclusion about the effectiveness of infrared images. Additionally, future work should include creating a neural network that fuses both color and infrared images to try to improve green fruit detection.

6.6. Conclusion

The most ideal method for distinguishing between green fruit and green leaves would be to use a broad multispectral camera that can capture images with all visible and non-visible wavelengths. However, broad multispectral cameras are often software configured and triggered, requiring a computer to control it. These are ideal for phenotyping systems that look at only one view and can image a large space in each image, such as a drone. However, for a ground-based platform,

speed is a larger factor. To detect green fruit on green leaves, the most reasonable method is to target specific wavelengths that can distinguish green fruit and leaves.

7. Conclusions and Future Work

The high-throughput phenotyping system developed in this study showed the ability to capture images, make non-contact leaf temperature measurements, and 3D plant architecture in a tomato breeding field. The 2D images captured from the high-throughput phenotyping system could be used to create a neural network for object detection in tomatoes for flowers, green fruit, ripe fruit, and sunburnt fruit. Using high-throughput phenotyping system and neural network throughout the growing season is also able to show the development of the plants. Finally, adding specific non-visible wavelengths to cameras is a cost-effective method that can enhance the detection of green fruit on green foliage. Overall, this study demonstrated the ability to use a ground-based vehicle for non-destructive in-field phenotyping of crops.

Future work should include combining all the sensor data together to create more biological relevant and accurate phenotypes for non-destructive phenotyping. For example, combining ripe fruit count with plant height/width can give a better understanding of how many hidden ripe fruits within the canopy there might be based on the overall plant architecture and structure. This could also give more information on how much occlusion is occurring based on leaf density and canopy volume.

Continuing the development of high-throughput phenotyping (HTP) systems requires close communication and compromise between plant breeders and HTP experts. In many standard plant breeding trials decisions are made on plant distribution and field design for ease of human phenotyping. The width between different plant-plots is minimized for humans to easily and quickly walk an entire field within a day. However, even with high-quality RTK-GPS, a continuously moving vehicle has difficulty rapidly and accurately detecting the GPS coordinates

in real time between small plant-plot spacing. Future plant breeding trials with HTP should consider redesigning plant breeding fields with HTP systems in mind.

Finally, redesigning plant breeding fields to make HTP easier means it may be more difficult for humans to phenotype in the field. Another recommendation for future HTP studies is to redesign ground truth phenotyping data collected manually. Plant breeders should work with HTP experts to redefine phenotypes and use a combination of manual image analysis and manual in-person phenotyping. For example, instead of looking for Day to First Green Fruit in the field, they can use the images collected on the HTP system to find Day to First External Green Fruit. In the field plant breeders can manipulate the plant and look for green fruit hidden within the canopy, but an image can't manipulate the plant and can only see externally available green fruit. Additionally, the use of plant modeling could better predict how many occluded fruit there are on a plant.

8. Works Cited

[1] C. J. Godfray, J. R. Beddington, and I. R. Crute, “Food security: The challenge of the present,” Geoforum, vol. 91, no. February, pp. 73–77, 2018, doi: 10.1016/j.geoforum.2018.02.030.

[2] R. Bernardo, “Molecular markers and selection for complex traits in plants: Learning from the last 20 years,” Crop Sci, vol. 48, no. 5, pp. 1649–1664, 2008, doi: 10.2135/cropsci2008.03.0131.

[3] J. L. Araus and J. E. Cairns, “Field high-throughput phenotyping: The new crop breeding frontier,” Trends Plant Sci, vol. 19, no. 1, pp. 52–61, 2014, doi: 10.1016/j.tplants.2013.09.008.

[4] P. M. Priyadarshan, “PLANT BREEDING: Classical to Modern.”

[5] B. Lenaerts, B. C. Y. Collard, and M. Demont, “Review: Improving global food security through accelerated plant breeding,” Oct. 01, 2019, Elsevier Ireland Ltd. doi: 10.1016/j.plantsci.2019.110207.

[6] B. Lehmann et al., “Steering Committee members.” [Online]. Available: www.fao.org/cfs/cfs-hlpe

[7] The State of Food Security and Nutrition in the World 2024. FAO; IFAD; UNICEF; WFP; WHO;, 2024. doi: 10.4060/cd1254en.

[8] “FSIN Joint analysis for better decisions Food Security Information Network,” 2024. [Online]. Available: https://www.fsinplatform.org/grfc2024

[9] D. Gallegos, A. Eivers, P. Sondergeld, and C. Pattinson, “Food insecurity and child development: A state-of-the-art review,” Sep. 01, 2021, MDPI. doi: 10.3390/ijerph18178990.

[10] United Nations Department of Economic and Social Affairs Population Division, “World Population Prospects 2019: Data Booklet,” pp. 1–25, 2019.

[11] D. K. Ray, N. D. Mueller, P. C. West, and J. A. Foley, “Yield Trends Are Insufficient to Double Global Crop Production by 2050,” PLoS One, vol. 8, no. 6, 2013, doi: 10.1371/journal.pone.0066428.

[12] D. Tilman, C. Balzer, J. Hill, and B. L. Befort, “Global food demand and the sustainable intensification of agriculture,” Proceedings of the National Academy of Sciences, vol. 108, no. 50, pp. 20260–20264, 2011, doi: 10.1073/pnas.1116437108.

[13] C. Lesk, P. Rowhani, and N. Ramankutty, “Influence of extreme weather disasters on global crop production,” Nature, vol. 529, no. 7584, pp. 84–87, 2016, doi: 10.1038/nature16467.

[14] David. S. Battisti and R. L. Naylor, “Historical Warnings of Future Food Insecurity with Unprecedented Seasonal Heat,” vol. 323, no. January, pp. 240–245, 2009.

[15] “California Agricultural Statistics Review 2017-2018,” pp. 1–105, 2018.

[16] T. Hartz, E. V. Specialist, G. Miyao, M. Lestrange, and S. Stoddard, “PROCESSING TOMATO,” 2008.

[17] L. (USDA) Honig, “Vegetables 2018 Summary,” no. March, 2019.

[18] R. Smith et al., “Chile Pepper Production in California,” UC Vegetable Research & Information Center Vegetable Production Series, 2011, doi: 10.3733/ucanr.7244.

[19] W. R. Fehr and J. R. JUSTIN, “Principles of Cultivar Development, vol. 2, Crop Species,” Soil Sci, vol. 145, no. 5, p. 390, 1988, doi: 10.1097/00010694-198805000-00013.

[20] C. Rothan, I. Diouf, and M. Causse, “Trait discovery and editing in tomato,” Jan. 01, 2019, Blackwell Publishing Ltd. doi: 10.1111/tpj.14152.

[21] L. Cong et al., “Multiplex Genome Engineering Using CRISPR/Cas Systems,” vol. 342, no. November, pp. 983–988, 2013.

[22] C. Gao, “The future of CRISPR technologies in agriculture,” Nat Rev Mol Cell Biol, vol. 19, no. 5, pp. 275–276, 2018, doi: 10.1038/nrm.2018.2.

[23] N. Fahlgren, M. A. Gehan, and I. Baxter, “Lights, camera, action: High-throughput plant phenotyping is ready for a close-up,” Curr Opin Plant Biol, vol. 24, pp. 93–99, 2015, doi: 10.1016/j.pbi.2015.02.006.

[24] N. Tilly et al., “Multitemporal crop surface models: accurate plant height measurement and biomass estimation with terrestrial laser scanning in paddy rice,” J Appl Remote Sens, vol. 8, no. 1, p. 083671, 2014, doi: 10.1016/j.cryogenics.2004.10.006.

[25] X. Yin, M. A. McClure, N. Jaja, D. D. Tyler, and R. M. Hayes, “In-season prediction of corn yield using plant height under major production systems,” Agron J, vol. 103, no. 3, pp. 923–929, 2011, doi: 10.2134/agronj2010.0450.

[26] U. Lee, S. Chang, G. A. Putra, H. Kim, and D. H. Kim, “An automated, high-throughput plant phenotyping system using machine learning-based plant segmentation and image analysis,” PLoS One, vol. 13, no. 4, pp. 1–17, 2018, doi: 10.1371/journal.pone.0196615.

[27] J. Christian Rose, S. Paulus, and H. Kuhlmann, “Accuracy analysis of a multi-view stereo approach for phenotyping of tomato plants at the organ level,” Sensors (Switzerland), vol. 15, no. 5, pp. 9651–9665, 2015, doi: 10.3390/s150509651.

[28] N. Kirchgessner et al., “The ETH field phenotyping platform FIP: a cable-suspended multi-sensor system,” Functional Plant Biology, vol. 44, no. 1, pp. 154–168, 2017.

[29] V. Gonzalez-Dugo et al., “Using high resolution UAV thermal imagery to assess the variability in the water status of five fruit tree species within a commercial orchard,” Precis Agric, vol. 14, no. 6, pp. 660–678, 2013, doi: 10.1007/s11119-013-9322-9.

[30] Y. Jiang, C. Li, J. S. Robertson, S. Sun, R. Xu, and A. H. Paterson, “GPhenoVision: A ground mobile system with multi-modal imaging for field-based high throughput phenotyping of cotton,” Sci Rep, vol. 8, no. 1, pp. 1–15, 2018, doi: 10.1038/s41598-018-19142-2.

[31] J. L. Araus, S. C. Kefauver, M. Zaman-Allah, M. S. Olsen, and J. E. Cairns, “Translating High-Throughput Phenotyping into Genetic Gain,” Trends Plant Sci, vol. 23, no. 5, pp. 451–466, 2018, doi: 10.1016/j.tplants.2018.02.001.

[32] D. Luquet et al., “Using multidirectional thermography to characterize water status of cotton,” Remote Sens Environ, vol. 84, no. 3, pp. 411–421, 2003, doi: 10.1016/S0034-4257(02)00131-1.

[33] V. Gonzalez-Dugo et al., “Using high resolution UAV thermal imagery to assess the variability in the water status of five fruit tree species within a commercial orchard,” Precis Agric, vol. 14, no. 6, pp. 660–678, 2013, doi: 10.1007/s11119-013-9322-9.

[34] T. T. Nguyen, D. C. Slaughter, N. Max, J. N. Maloof, and N. Sinha, “Structured light-based 3D reconstruction system for plants,” Sensors (Switzerland), vol. 15, no. 8, pp. 18587–18612, 2015, doi: 10.3390/s150818587.

[35] X. Song, F. Zhong, Y. Wang, and X. Qin, “Estimation of Kinect depth confidence through self-training,” Visual Computer, vol. 30, no. 6–8, pp. 855–865, 2014, doi: 10.1007/s00371-014-0965-y.

[36] T. T. Nguyen, D. C. Slaughter, B. Townsley, L. Carriedo, J. N. Maloof, and N. Sinha, “Comparison of Structure-from-Motion and Stereo Vision Techniques for Full In-Field 3D Reconstruction and Phenotyping of Plants: An Investigation in Sunflower,” 2016 American Society of Agricultural and Biological Engineers Annual International Meeting, ASABE 2016, no. August, 2016, doi: 10.13031/aim.20162444593.

[37] T. T. Nguyen, D. C. Slaughter, N. Max, J. N. Maloof, and N. Sinha, “Structured light-based 3D reconstruction system for plants,” Sensors (Switzerland), vol. 15, no. 8, pp. 18587–18612, 2015, doi: 10.3390/s150818587.

[38] A. G. Olenskyj et al., “End-to-end deep learning for directly estimating grape yield from ground-based imagery,” Comput Electron Agric, vol. 198, Jul. 2022, doi: 10.1016/j.compag.2022.107081.

[39] M. Sheikh, F. Iqra, H. Ambreen, K. A. Pravin, M. Ikra, and Y. S. Chung, “Integrating artificial intelligence and high-throughput phenotyping for crop improvement,” Jun. 01, 2024, Editorial Department of Scientia Agricultura Sinica. doi: 10.1016/j.jia.2023.10.019.

[40] S. H. Kwon et al., “Case study: things to be considered for high-throughput phenotyping in genomic studies,” Plant Biotechnol Rep, vol. 17, no. 3, pp. 415–420, Jun. 2023, doi: 10.1007/s11816-023-00834-9.

[41] V. Vijayakumar, Y. Ampatzidis, and L. Costa, “Tree-level citrus yield prediction utilizing ground and aerial machine vision and machine learning,” Smart Agricultural Technology, vol. 3, Feb. 2023, doi: 10.1016/j.atech.2022.100077.

[42] T. Sritarapipat, P. Rakwatin, and T. Kasetkasem, “Automatic rice crop height measurement using a field server and digital image processing,” Sensors (Switzerland), vol. 14, no. 1, pp. 900–926, 2014, doi: 10.3390/s140100900.

[43] N. Tilly et al., “Multitemporal crop surface models: accurate plant height measurement and biomass estimation with terrestrial laser scanning in paddy rice,” J Appl Remote Sens, vol. 8, no. 1, p. 083671, 2014, doi: 10.1016/j.cryogenics.2004.10.006.

[44] J. E. Spindel et al., “Association mapping by aerial drone reveals 213 genetic associations for Sorghum bicolor biomass traits under drought,” BMC Genomics, vol. 19, no. 1, pp. 1–18, 2018, doi: 10.1186/s12864-018-5055-5.

[45] P. Andrade-Sanchez et al., “Development and evaluation of a field-based high-throughput phenotyping platform,” Functional Plant Biology, vol. 41, no. 1, pp. 68–79, 2014, doi: 10.1071/FP13126.

[46] “World Population Prospects 2024,” 2024. [Online]. Available: www.unpopulation.org.

[47] T. T. Nguyen, D. C. Slaughter, J. N. Maloof, and N. Sinha, “Plant phenotyping using multi-view stereo vision with structured lights,” Autonomous Air and Ground Sensing Systems for Agricultural Optimization and Phenotyping, vol. 9866, no. May 2016, p. 986608, 2016, doi: 10.1117/12.2229513.

[48] T. T. Nguyen, D. C. Slaughter, B. Townsley, L. Carriedo, J. N. Maloof, and N. Sinha, “Comparison of Structure-from-Motion and Stereo Vision Techniques for Full In-Field 3D Reconstruction and Phenotyping of Plants: An Investigation in Sunflower,” 2016 American Society of Agricultural and Biological Engineers Annual International Meeting, ASABE 2016, no. August, 2016, doi: 10.13031/aim.20162444593.

[49] T. T. Nguyen, D. C. Slaughter, B. T. Townsley, L. Carriedo, J. N. Maloof, and N. Sinha, “In-field Plant Phenotyping using Multi-view Reconstruction : An Investigation in Eggplant,” 13th International Conference on Precision Agriculture, no. July, pp. 1–16, 2016.

[50] A. Bannari, D. Morin, F. Bonn, and A. R. Huete, “A review of vegetation indices,” vol. 7257, no. 1995, 2009, doi: 10.1080/02757259509532298.

[51] “Canon DSLR NDVI Conversion.”

[52] C. Roo, “Architectural Phenotype Measurements Utilizing High Throughput Phenotyping in Solanaceae Varieties,” 2021.

[53] H. Sun, D. C. Slaughter, M. P. Ruiz, C. Gliever, S. K. Upadhyaya, and R. F. Smith, “RTK GPS mapping of transplanted row crops,” Comput Electron Agric, vol. 71, no. 1, pp. 32–37, 2010, doi: 10.1016/j.compag.2009.11.006.

[54] S. Gan-Mor, R. L. Clark, and B. L. Upchurch, “Implement lateral position accuracy under RTK-GPS tractor guidance,” Comput Electron Agric, vol. 59, no. 1–2, pp. 31–38, 2007, doi: 10.1016/j.compag.2007.04.008.

[55] M. Pérez-Ruiz, D. C. Slaughter, C. J. Gliever, and S. K. Upadhyaya, “Automatic GPS-based intra-row weed knife control system for transplanted row crops,” Comput Electron Agric, vol. 80, pp. 41–49, 2012, doi: 10.1016/j.compag.2011.10.006.

[56] H. L. Dijksterhuis, L. G. Van Willigenburg, and R. P. Van Zuydam, “Centimetre-precision guidance of moving implements in the open field: A simulation based on GPS measurements,” Comput Electron Agric, vol. 20, no. 3, pp. 185–197, 1998, doi: 10.1016/S0168-1699(98)00016-7.

[57] J. K. Willcox, G. L. Catignani, and S. Lazarus, “Tomatoes and Cardiovascular Health,” Crit Rev Food Sci Nutr, vol. 43, no. 1, pp. 1–18, 2003, doi: 10.1080/10408690390826437.

[58] W. T. (University of C. D. Lanini, J. (AgriDataSensing Inc.) Leboeuf, and Inc.) Rivara, Charles (California Tomato Research Institute, “Crop Profile for Tomatoes (Processing) in California,” 1999.

[59] T. Hartz, E. V. Specialist, G. Miyao, M. Lestrange, and S. Stoddard, “PROCESSING TOMATO,” UC Vegetable Research & Information Center Vegetable Production Series, 2008.

[60] T. Hartz, M. Cantwell, R. Smith, J. Aguiar, and O. Daugovish, “BELL PEPPER PRODUCTION IN CALIFORNIA,” 2008.

[61] R. Smith et al., “Chile Pepper Production in California,” UC Vegetable Research & Information Center Vegetable Production Series, 2011, doi: 10.3733/ucanr.7244.

[62] L. Aguiar et al., “CHILE PEPPER PRODUCTION IN CALIFORNIA University of California,” 2010.

[63] R. Barbosa, Maricela (Department of Botany and Plant Sciences, University of California and R. McGiffen, Milt (Department of Botany and Plant Sciences, University of California, “Crop Profile for Bell Peppers in California,” no. 1, 2000.

[64] V. Vuong, “High-Throughput Phenotyping Methods in Processing Tomatoes,” 2024.

[65] R. Qiu et al., “Sensors for measuring plant phenotyping: A review,” International Journal of Agricultural and Biological Engineering, vol. 11, no. 2, pp. 1–17, 2018, doi: 10.25165/j.ijabe.20181102.2696.

[66] S. P. Moose and R. H. Mumm, “Molecular Plant Breeding as the Foundation for 21st Century Crop Improvement,” Plant Physiol, vol. 147, no. 3, pp. 969–977, 2008, doi: 10.1104/pp.108.118232.

[67] M. Qaim, “Role of New Plant Breeding Technologies for Food Security and Sustainable Agricultural Development,” Appl Econ Perspect Policy, vol. 42, no. 2, pp. 129–150, Jun. 2020, doi: 10.1002/aepp.13044.

[68] V. L. Vuong, D. C. Slaughter, D. St. Clair, P. Bosland, B. Kubond, and A. Kaur, “<i>High-Throughput Phenotyping Methods for Green Fruit</i>,” pp. 2–7, 2018, doi: 10.13031/aim.201800940.

[69] R. Raja et al., “Crop signalling: A novel crop recognition technique for robotic weed control,” Biosyst Eng, vol. 187, 2019, doi: 10.1016/j.biosystemseng.2019.09.011.

[70] “2023 STATE AGRICULTURE OVERVIEW,” 2023.

[71] L. Li, Q. Zhang, and D. Huang, “A review of imaging techniques for plant phenotyping,” Sensors (Switzerland), vol. 14, no. 11, pp. 20078–20111, 2014, doi: 10.3390/s141120078.

[72] A. Walter, F. Liebisch, and A. Hund, “Plant phenotyping: From bean weighing to image analysis,” Plant Methods, vol. 11, no. 1, pp. 1–11, 2015, doi: 10.1186/s13007-015-0056-8.

[73] X. Yin, M. A. McClure, N. Jaja, D. D. Tyler, and R. M. Hayes, “In-season prediction of corn yield using plant height under major production systems,” Agron J, vol. 103, no. 3, pp. 923–929, 2011, doi: 10.2134/agronj2010.0450.

[74] P. Maheswari, P. Raja, and V. T. Hoang, “Intelligent yield estimation for tomato crop using SegNet with VGG19 architecture,” Sci Rep, vol. 12, no. 1, Dec. 2022, doi: 10.1038/s41598-022-17840-6.

[75] J. Lu, R. Ehsani, Y. Shi, A. I. de Castro, and S. Wang, “Detection of multi-tomato leaf diseases (late blight, target and bacterial spots) in different stages by using a spectral-based sensor,” Sci Rep, vol. 8, no. 1, Dec. 2018, doi: 10.1038/s41598-018-21191-6.

[76] D. L. Mangus, A. Sharda, and N. Zhang, “Development and evaluation of thermal infrared imaging system for high spatial and temporal resolution crop water stress monitoring of corn within a greenhouse,” Comput Electron Agric, vol. 121, pp. 149–159, 2016, doi: 10.1016/j.compag.2015.12.007.

[77] G. Van Der Heijden et al., “SPICY: Towards automated phenotyping of large pepper plants in the greenhouse,” Functional Plant Biology, vol. 39, no. 11, pp. 870–877, 2012, doi: 10.1071/FP12019.

[78] K. Yamamoto, W. Guo, Y. Yoshioka, and S. Ninomiya, “On plant detection of intact tomato fruits using image analysis and machine learning methods,” Sensors (Switzerland), vol. 14, no. 7, pp. 12191–12206, Jul. 2014, doi: 10.3390/s140712191.

[79] M. Ecarnot, P. Baogonekczyk, L. Tessarotto, and C. Chervin, “Rapid phenotyping of the tomato fruit model, Micro-Tom, withaportable VIS-NIR spectrometer,” Plant Physiology and Biochemistry, vol. 70, pp. 159–163, 2013, doi: 10.1016/j.plaphy.2013.05.019.

[80] T.-Y. Lin et al., “Microsoft COCO: Common Objects in Context,” May 2014, [Online]. Available: http://arxiv.org/abs/1405.0312

[81] K. He, G. Gkioxari, P. Dollár, and R. Girshick, “Mask R-CNN.”

[82] P. Wan, A. Toudeshki, H. Tan, and R. Ehsani, “A methodology for fresh tomato maturity detection using computer vision,” Comput Electron Agric, vol. 146, pp. 43–50, Mar. 2018, doi: 10.1016/j.compag.2018.01.011.

[83] A. Clément, R. Bacon, S. Sirois, and M. Dorais, “Mature-ripe tomato spectral classification according to lycopene content and fruit type by visible, NIR reflectance and intrinsic fluorescence,” Quality Assurance and Safety of Crops and Foods, vol. 7, no. 5, pp. 747–756, 2015, doi: 10.3920/QAS2014.0521.

[84] J. Christian Rose, S. Paulus, and H. Kuhlmann, “Accuracy analysis of a multi-view stereo approach for phenotyping of tomato plants at the organ level,” Sensors (Switzerland), vol. 15, no. 5, pp. 9651–9665, 2015, doi: 10.3390/s150509651.

[85] R. Kumar, V. Paul, R. Pandey, R. N. Sahoo, and V. K. Gupta, “Reflectance based non-destructive determination of colour and ripeness of tomato fruits,” Physiology and Molecular Biology of Plants, vol. 28, no. 1, pp. 275–288, Jan. 2022, doi: 10.1007/s12298-022-01126-2.

[86] H. R. Xu, Y. B. Ying, X. P. Fu, and S. P. Zhu, “Near-infrared Spectroscopy in detecting Leaf Miner Damage on Tomato Leaf,” Biosyst Eng, vol. 96, no. 4, pp. 447–454, Apr. 2007, doi: 10.1016/j.biosystemseng.2007.01.008.

[87] D. Schwarz, A. J. Thompson, and H. P. Kläring, “Guidelines to use tomato in experiments with a controlled environment,” Front Plant Sci, vol. 5, no. NOV, pp. 1–16, 2014, doi: 10.3389/fpls.2014.00625.

[88] A. N. Nankar, D. Kostova, I. Tringovska, S. Grozeva, and D. Ganeva, “Tomato phenotypic diversity determined by combined approaches of conventional and high-throughput tomato analyzer phenotyping,” Plants, vol. 9, no. 2, Feb. 2020, doi: 10.3390/plants9020197.

[89] D. Ma, “Theory of edge detection,” 1980. [Online]. Available: https://royalsocietypublishing.org/

[90] W. Maldonado and J. C. Barbosa, “Automatic green fruit counting in orange trees using digital images,” Comput Electron Agric, vol. 127, pp. 572–581, Sep. 2016, doi: 10.1016/j.compag.2016.07.023.

[91] S. S. Miller, J. R. Schupp, T. A. Baugher, and S. D. Wolford, “Performance of Mechanical Thinners for Bloom or Green Fruit Thinning in Peaches,” 2011.

[92] I. Sa, Z. Ge, F. Dayoub, B. Upcroft, T. Perez, and C. McCool, “Deepfruits: A fruit detection system using deep neural networks,” Sensors (Switzerland), vol. 16, no. 8, Aug. 2016, doi: 10.3390/s16081222.

[93] H. Gan, W. S. Lee, V. Alchanatis, and A. Abd-Elrahman, “Active thermal imaging for immature citrus fruit detection,” Biosyst Eng, vol. 198, pp. 291–303, Oct. 2020, doi: 10.1016/j.biosystemseng.2020.08.015.

[94] S. Huang, Y. Wu, Q. Wang, J. Liu, Q. Han, and J. Wang, “Estimation of chlorophyll content in pepper leaves using spectral transmittance red-edge parameters,” International Journal of Agricultural and Biological Engineering, vol. 15, no. 5, pp. 85–90, 2022, doi: 10.25165/j.ijabe.20221505.7350.

[95] D. S. Kasampalis, P. Tsouvaltzis, K. Ntouros, A. Gertsis, I. Gitas, and A. S. Siomos, “The use of digital imaging, chlorophyll fluorescence and Vis/NIR spectroscopy in assessing the ripening stage and freshness status of bell pepper fruit,” Comput Electron Agric, vol. 187, Aug. 2021, doi: 10.1016/j.compag.2021.106265.

[96] S.-H. Cho, “Drone-based Vegetation Index Analysis Considering Vegetation Vitality* ·Geun-Sang LEE 2※ ·Jee-Wook HWANG 3 1) 요 약,” Journal of the Korean Association of Geographic Information Studies, vol. 23, no. 2, pp. 21–35, doi: 10.11108/kagis.2020.23.2.021.

[97] J. J. Assmann, I. H. Myers-Smith, J. T. Kerby, A. M. Cunliffe, and G. N. Daskalova, “Drone data reveal heterogeneity in tundra greenness and phenology not captured by satellites,” Environmental Research Letters, vol. 15, no. 12, Dec. 2020, doi: 10.1088/1748-9326/abbf7d.

[98] G. Chandra. Mishra, “Drones for Normalized Difference Vegetation Index (NDVI), to Estimate Crop Health for Precision Agriculture: A Cheaper Alternative for Spatial Satellite Sensors,” Krishi Sanskriti Publications, 2016, p. 80.

[99] S. Harsh, S. Dhiraj, and P. Shraddha, “Efficient and Cost-effective Drone-NDVI system for Precision Farming,” International Journal of New Practices in Management and Engineering, vol. 10, 2021.

[100] Y. Mapping, K. Wang, and Y. Jin, “Citation: Mapping Walnut Water Stress with High Resolution Multispectral UAV Imagery and Machine Learning,” 2024, doi: 10.48550/arXiv.2401.

[101] E. Jacygrad, M. Kelly, S. Hogan, J. E. Preece, D. Golino, and R. Michelmore, “Comparison between Field Measured and UAV-Derived Pistachio Tree Crown Characteristics throughout a Growing Season,” Drones, vol. 6, no. 11, Nov. 2022, doi: 10.3390/drones6110343.

[102] B. Lampinen et al., “Almond Board of California-1-2017,” 2018.

[103] G. Tiwari, D. C. Slaughter, and M. Cantwell, “Nondestructive maturity determination in green tomatoes using a handheld visible and near infrared instrument,” Postharvest Biol Technol, vol. 86, pp. 221–229, Dec. 2013, doi: 10.1016/j.postharvbio.2013.07.009.

[104] G. Polder, G. W. A. M. Van Der Heijden, and I. T. Young, “SPECTRAL IMAGE ANALYSIS FOR MEASURING RIPENESS OF TOMATOES,” Transactions of the ASAE, vol. 45, no. 4, pp. 1155–1161.

[105] R. Kumar, V. Paul, R. Pandey, R. N. Sahoo, and V. K. Gupta, “Reflectance based non-destructive determination of colour and ripeness of tomato fruits,” Physiology and Molecular Biology of Plants, vol. 28, no. 1, pp. 275–288, Jan. 2022, doi: 10.1007/s12298-022-01126-2.